Calhoun: The NPS Institutional Archive

DSpace Repository

Theses and Dissertations | 1. Thesis and Dissertation Collection, all items

1987

Mesoscale applications of high resolution imagery.

Scanlon, Randy J.

http://hdl.handle.net/10945/22352

Downloaded from NPS Archive: Calhoun

http://www.nps.edu/library

Calhoun is the Naval Postgraduate School's public access digital repository for research materials and institutional publications created by the NPS community. Calhoun is named for Professor of Mathematics Guy K. Calhoun, NPS's first appointed -- and published -- scholarly author.

Dudley Knox Library / Naval Postgraduate School
411 Dyer Road / 1 University Circle
Monterey, California USA 93943

NAVAL POSTGRADUATE SCHOOL
MONTEREY, CALIFORNIA 93943-5002

NAVAL POSTGRADUATE SCHOOL
Monterey, California

THESIS

MESOSCALE APPLICATIONS OF
HIGH RESOLUTION IMAGERY

by

Randy J. Scanlon

September 1987

Thesis Advisor: C. H. Wash

Approved for public release; distribution is unlimited

T234397

CURITY CLASSIFICATION OF THIS PAGE

REPORT DOCUMENTATION PAGE

a REPORT SECURITY CLASSIFICATION: UNCLASSIFIED	1b RESTRICTIVE MARKINGS
a SECURITY CLASSIFICATION AUTHORITY	3 DISTRIBUTION / AVAILABILITY OF REPORT: Approved for public release; distribution is unlimited
b DECLASSIFICATION / DOWNGRADING SCHEDULE	
PERFORMING ORGANIZATION REPORT NUMBER(S)	5 MONITORING ORGANIZATION REPORT NUMBER(S)
a NAME OF PERFORMING ORGANIZATION: Naval Postgraduate School; 6b OFFICE SYMBOL (If applicable): 63	7a NAME OF MONITORING ORGANIZATION: Naval Postgraduate School
ADDRESS (City, State, and ZIP Code): Monterey, California 93943-5000	7b ADDRESS (City, State, and ZIP Code): Monterey, California 93943-5000
a NAME OF FUNDING / SPONSORING ORGANIZATION; 8b OFFICE SYMBOL (If applicable)	9 PROCUREMENT INSTRUMENT IDENTIFICATION NUMBER
ADDRESS (City, State, and ZIP Code)	10 SOURCE OF FUNDING NUMBERS: PROGRAM ELEMENT NO; PROJECT NO; TASK NO; WORK UNIT ACCESSION NO

TITLE (Include Security Classification)

MESOSCALE APPLICATIONS OF HIGH RESOLUTION IMAGERY

PERSONAL AUTHOR(S)

Scanlon, Randy J.

a TYPE OF REPORT	13b TIME COVERED	14 DATE OF REPORT (Year, Month, Day)	15 PAGE COUNT
Master's Thesis	FROM ____ TO ____	1987 September	133

SUPPLEMENTARY NOTATION

COSATI CODES			18 SUBJECT TERMS (Continue on reverse if necessary and identify by block number)
FIELD	GROUP	SUB-GROUP	Space shuttle, photography, meteorology, SSEOP, NASA, meteorological satellites, visible imagery, infrared imagery, severe weather, clouds

ABSTRACT (Continue on reverse if necessary and identify by block number)

Analysis of two mesoscale phenomena, a dry slot in stratocumulus over the eastern North Pacific (June 1985) and an enhanced-V cloud formation over the Gulf of Mexico (April 1984) is performed using very-high resolution photographs taken from the Space Transportation System (STS) 41-C and 51-G missions. Collocated meteorological satellite imagery (GOES, NOAA AVHRR, DMSP) and conventional meteorological data are utilized with the shuttle photography to better understand the microscale and mesoscale features of these two events.

DISTRIBUTION / AVAILABILITY OF ABSTRACT: ☒ UNCLASSIFIED/UNLIMITED ☐ SAME AS RPT ☐ DTIC USERS	21 ABSTRACT SECURITY CLASSIFICATION: UNCLASSIFIED
a NAME OF RESPONSIBLE INDIVIDUAL: C. H. Wash	22b TELEPHONE (Include Area Code): (408)-646-2295; 22c OFFICE SYMBOL: 63Wx

D FORM 1473, 84 MAR 83 APR edition may be used until exhausted. All other editions are obsolete.

SECURITY CLASSIFICATION OF THIS PAGE

Approved for public release; distribution is unlimited.

Mesoscale Applications of High Resolution Imagery

by

Randy J. Scanlon
Lieutenant, United States Navy
B.S., U.S. Naval Academy, 1979

Submitted in partial fulfillment of the
requirements for the degree of

MASTER OF SCIENCE IN METEOROLOGY AND OCEANOGRAPHY

from the

NAVAL POSTGRADUATE SCHOOL
September 1987

ABSTRACT

Analysis of two mesoscale phenomena, a dry slot in stratocumulus over the eastern North Pacific (June 1985) and an enhanced-V cloud formation over the Gulf of Mexico (April 1984) is performed using very-high resolution photographs taken from the Space Transportation System (STS) 41-C and 51-G missions. Collocated meteorological satellite imagery (GOES, NOAA AVHRR, DMSP) and conventional meteorological data are utilized with the shuttle photography to better understand the microscale and mesoscale features of these two events.

Thesis
S24245
C.1

TABLE OF CONTENTS

I. INTRODUCTION 11

A. FORECASTING APPLICATIONS 12

B. PREVIOUS STUDIES 13

C. MOTIVATION OF STUDY. 15

II. HIGH RESOLUTION METEOROLOGICAL IMAGERY 17

A. METEOROLOGICAL SATELLITE DEVELOPMENT 17

B. MANNED SPACECRAFT PHOTOGRAPHY. 19

III. DATA DESCRIPTION 22

A. SHUTTLE PHOTOGRAPHY. 22

B. METSAT IMAGERY AND SYNOPTIC DATA 25

C. PHOTOGRAPH AND IMAGE SELECTION 25

IV. PACIFIC DRY SLOT 27

A. INTRODUCTION 27

B. DRY SLOT CHARACTERISTICS 28

C. EVOLUTION AND FORMATION. 31

D. DRY SLOT CONCLUSIONS 36

V. GULF OF MEXICO SQUALL LINE OF 1984 38

A. INTRODUCTION 38

B. BACKGROUND 39

C. SHUTTLE AND SATELLITE IMAGERY. 43

D. SYNOPTIC OVERVIEW. 47

E. CROSS SECTIONS FOR THE ENHANCED-V PATTERN. . .53

F. CONCLUSIONS. 55

VI. SUMMARY AND CONCLUSIONS. 57

A. SUMMARY. 55

B. RECOMMENDATIONS. 59

APPENDIX A: HISTORY OF METEOROLOGICAL SATELLITES. 61

APPENDIX B: GOES 'MB ENHANCEMENT 73

APPENDIX C: TABLES AND FIGURES. 75

LIST OF REFERENCES 126

INITIAL DISTRIBUTION LIST. 131

LIST OF TABLES

1. Mission data for STS 41-C and STS 51-G. 76

2. Shuttle photography and METSAT imagery feature comparison. 77

LIST OF FIGURES

1. Apollo 6 cloud height contouring (Whitehead et al, 1969). 78

2. NASA-modified hand-held Hasselblad 500 EL/M Camera (Nowakowski and Palmer, 1984). 79

3. Location of windows in Shuttle Orbiter (Nowakowski and Palmer, 1984). 80

4. Orbiter inverted position and direction of motion (Snow and Tomlinson, 1987) 81

5. Shuttle photograph (1618 GMT 17 June 1985) of western tip of dry slot (STS 51G-31010). 82

6. Shuttle photograph (1618 GMT 17 June 1985) of west-central section of dry slot and surrounding stratocumulus clouds (STS 51-G-31012). 83

7. Shuttle photograph (1618 GMT 17 June 1985) of central section of dry slot (STS 51-G-31012) 84

8. Shuttle photograph (1619 GMT 17 June 1985) of eastern section of dry slot (STS 51G-31013). 85

9. Shuttle photograph (1619 GMT 17 June 1985) of Guadalupe Island, the Karman vortices, and the new dry slot to the southwest (STS 51G-31014). 86

10. 1632 GMT GOES visible image of 17 June 1985 with dry slot in center of image. 87

11. 2233 GMT NOAA (AVHRR) near-infrared image of 17 June 1985 88

12. 2233 GMT NOAA (AVHRR) channel 4 infrared image of 17 June 1985 89

13. 1415 GMT DMSP visible image of 17 June 1985 with dry slot in center and Guadalupe Island to the north . . .90

14. 1631 GMT GOES visible image of 16 June 1985 with dry slot in early stages 91

15. Evolution of the dry slot from 1630 GMT 16 June to 0000 GMT 19 June 92

16. Surface analysis of eastern Pacific for 1800 GMT 16 June 1985 93

17. Sounding for Guadalupe Island (76151) for 1200 GMT 16 June 1985 94

18. 2330 GMT GOES visible image of 15 June 1985 before dry slot formation 95

19. Shuttle photograph (1338 GMT 9 April 1984) of enhanced-V cloud formation over Florida and the Gulf of Mexico (S13-392008) 96

20. Surface positions of low pressure center across southern states; 1200 GMT 6 April-1200 GMT 10 April. .97

21. 1331 GMT GOES visible image of 9 April 1984 with enhanced-V over Florida and the Gulf of Mexico 98

22. Vertically coupled upper and lower-tropopheric jet front systems and their associated secondary circulations (Shapiro, 1983) 99

23. Schematic features of a severe weather outbreak (Newton, 1967) 100

24. Area of confluence (NO threat) and difluence (threat) in region where the polar and subtropical jets converge and then diverge (Wilderotter, 1981). . . . 101

25. Sketch of the eight features of the enhanced-V . . . 102

26. Shuttle photograph (1338 GMT 9 April 1984) of enhanced-V with 100 mm lens (S13-402134) 103

27. Shuttle photograph (1338 GMT 9 April 1984) of enhanced-V with 250 mm lens (S13-392008) 104

28. 1301 GMT GOES enhanced infrared (MB) of 9 April 1984 105

29. 1331 GMT GOES visible image full resolution (1 km) of 9 April 1984 106

30. 1338 GMT GOES enhanced infrared image (original colored) of 9 April 1984 107

31. 1336 GMT NOAA (AVHRR) near infrared (channel 2) image of 9 April 1984. 108

32. 1336 GMT NOAA (AVHRR) enhanced infrared (channel 4) image of 9 April 1984. 109

33. 1336 GMT NOAA (AVHRR) visivle (channel 1) image of 9 April 1984 110

34. 1336 GMT NOAA (AVHRR) enhanced infrared (original colored) image of 9 April 1984 111

35. 2330 GMT GOES infrared image of 7 April 1984 with enhanced-V over eastern Texas. 112

36. NMC Surface Analysis, 0000 GMT 8 April 1984. 113

37. NMC Radar Summary, 0035 GMT 8 April 1984 114

38. NMC 850 mb Analysis with Heights/Temperature 0000 GMT 8 April 1984 115

39. NMC 500 mb Analysis with Heights/Temperature 0000 GMT 8 April 1984 116

40. FNOC 300 mb Analysis with Heights/Tmeperature/Winds 0000 GMT 8 APRIL 1984. 117

41. NMC Surface Analysis, 1200 GMT 9 April 1984. 118

42. NMC 500 mb Analysis with Heights/Temperature 1200 GMT 9 April 1984 119

43. FNOC 200 mb Analysis with Heights/Winds 1200 GMT 9 April 1984 120

44. NMC Radar Summary for 1200 GMT 9 April 1984. 121

45. Plot of sounding cross-sections over the southern U.S 122

46. North-South cross-section of isentropes/isotachs 0000 GMT 8 April 1984 for Omaha, NE (OMA) to Vera Cruz, Mexico (VER). 123

47. North-south cross-section of isentropes/isotachs 1200 GMT 9 April 1984 for Monet, MO (UMN) to Bahamas (YNN). 124

48. Examples of the boundaries that define the enhanced-V 125

ACKNOWLEDGEMENTS

I thank Dr. C.H. Wash, my thesis advisor, for his discussions, support and expert advice throughout this study. I also thank Dr. P.A. Durkee for his careful review, sound scientific guidance and literary criticism. I am indebted to AG1 Danielson and AG2 Davis of the Naval Environmental Prediction Research Facility (NEPRF) for their efforts in supplying the synoptic dataset. A special thanks is extended to Mr. Mike McDermet for his constant support and advice. The members of the Meteorology Department of San Jose State University, Satellite Data Services Division of NOAA/NESDIS, and World Data Center at the University of Colorado are thanked for providing the METSAT imagery for this study. Mr. E. Daghir of the National Weather Service Office, Redwood City, CA is also thanked for providing satellite imagery. Finally, my love and heart-felt thanks to my wife and typist, Greta, whose support, patience, and understanding were invaluable during the thesis process and my graduate studies.

I. INTRODUCTION

Meteorological information obtained from high resolution satellite imagery has shown significant value in the analysis of various categories of mesoscale (2-2000 km) and microscale (0-2 km) weather elements. Through continued improvement of interactive meteorological display devices, high resolution information will allow the research meteorologist, and eventually the field forecaster, to better understand the complex mesoscale atmospheric processes.

The World Meteorological Organization (Johnson and Vetlov, 1977) defines "high resolution" imagery as those images with horizontal ground or cloud resolution of approximately 1.0 km with extremely-high (very-high) resolution at approximately .1 km. Medium resolution is defined as 3-5 km and low resolution as 8 km and greater. Today there are numerous sources of high resolution imagery available from standard meteorological satellites (METSATs): the Geostationary Operational Environmental Satellite (GOES), the National Oceanic and Atmospheric Administration's (NOAA's) satellites, and the Defense Meteorological Satellite Program (DMSP) polar-orbiting satellites and numerous foreign satellites.

The more recent addition of high resolution photography from the National Aeronautics and Space Administration's (NASA) manned Skylab and Space Shuttle projects has added a new source and dimension of high resolution imagery research that could ultimately enhance our understanding of mesoscale and microscale processes. The incorporation of medium resolution imagery into daily weather analysis has increased analysis and forecast accuracy on the synoptic scale (2000-5000 km) over the last twenty years. In time, the use of higher resolution data will lead to a better understanding of the behavior of mesoscale and microscale phenomena and its improved prediction.

A. FORECASTING APPLICATIONS

The short-term forecasting of mesoscale phenomena, or "nowcasting", is one of the most challenging problems in meteorology today. The reason for this is that some mesoscale phenomena remains ill-defined and relatively unobserved. Satellite imagery is the only true mesoscale data source that covers a substantial region. Some improvements in nowcasting will certainly be achieved through the incorporation of empirical knowledge into new procedures or guidelines developed for various nowcast situations as derived from high resolution imagery studies. Some of these procedures can also be extended and applied to longer term forecast situations. High resolution imagery

from the present satellite systems (i.e. GOES) complemented by very-high resolution imagery from the space shuttle is one avenue to achieving a better understanding of mesoscale weather development.

The Navy and Air Force meteorologist must understand not only the synoptic but also mesoscale processes and must make accurate forecasts and nowcasts, both underway at-sea and ashore. Underway, operations often include areas with little conventional data available, so high resolution imagery is utilized when available. Regional forecast guidelines and forecast rules have proven to be helpful for the Battle Group Commander when it is necessary, for example, to remain under cloud cover to transit point-to-point secretly, or when a nowcast is necessary to know if flight operations are feasible for a certain window in a given transit region. High resolution satellite imagery is available to the military meteorologist ashore and is becoming more readily available to the afloat forecaster, so applications of forecasting or nowcasting guidelines are necessary throughout the meteorological community.

B. PREVIOUS STUDIES

Several previous studies have investigated high resolution imagery and space shuttle photography. Markley (1986) investigated mesoscale island barrier effects as observed in satellite imagery and in photographs from manned

spaceflight missions. Five types of island barrier effects were examined: a) von Karman vortices, b) single plumes, c) transitions from vortices to plumes, d) calm sea streaks, and e) ship wake-like cloud patterns. Markley's results from 23 cases indicated a strong relationship between inversion height and type of barrier effect phenomena. He noted the importance of high resolution satellite imagery to meteorologists and a knowledge of island barrier effects that could contribute to operational use in nowcasting and forecasting.

Svetz (1985) analyzed three atmospheric phenomena utilizing high resolution photography from NASA's Space Shuttle Challenger: a) a squall line over the Gulf of Mexico, b) Hurricane Kamisy in the Indian Ocean and c) a smoke plume from the Mauna Loa volcano. Comparisons were made to collocated METSAT imagery and conventional meteorological data to illustrate the advantages and deficiencies of high resolution photographic data.

Fisher (1986) analyzed a series of sun glint images taken from the Space Shuttle Challenger and compared them to NOAA-7 AVHRR (Advanced Very High resolution Radiometer) infrared imagery. This study focused on a persistent oceanographic feature east of the Alboran Basin in the Mediterranean Ocean and the efficacy of using sunglint images for location of acoustically important oceanographic features.

Fett and Mitchell (1977) produced a comprehensive handbook relating high resolution cloud imagery to meteorological features in the first volume of the Naval Tactical Applications Guide (NTAG) issued by Naval Environmental Prediction Research Facility (NEPERF). Various aspects of sunglint patterns and DMSP imagery are illustrated and described for determining low-level wind direction and sea state. Anomalous gray shade patterns, island and land barrier effects are thoroughly explored, also, with examples of each specific cause. In volume two of the NTAG series, Fett and Bohan (1979) cover large- and local-scale atmospheric phenomena detected in visible and infrared imagery including illustrations and correlations with conventional surface and upper air data.

NASA (1977) reviewed manned space flight high resolution imagery, specifically from Skylab photography. Various experts qualitatively and quantitatively analyzed mesoscale cloud features, mesoscale wake clouds, tropical storm structure, and atmospheric pollution phenomena.

C. MOTIVATION OF STUDY

Most of the studies completed in the past on high resolution imagery have either covered a specific case and compared space shuttle photography to METSAT imagery, or have illustrated and analyzed numerous space shuttle cloud photographs but not compared them to collocated METSAT

images. Therefore, the motivation for this thesis is to combine these ideas and to qualitatively and quantitatively compare space shuttle and METSAT imagery in two separate cases.

The goals of this thesis are:

1) Accurately interpret synoptic, mesoscale, and microscale meteorological phenomena in space shuttle photography.

2) Correlate meteorological phenomena in space shuttle photographs to high resolution METSAT imagery.

3) Determine the value of very-high resolution imagery for mesoscale studies.

This thesis begins with a meteorological satellite development and the progress of manned spacecraft photography. Chapter III provides a brief description of the data used for the case studies. The data described includes the shuttle photography, METSAT imagery and synoptic data necessary for each case. The Pacific dry slot stratocumulus cloud formation is described in detail in Chapter IV including its characteristics and formation. Chapter V discusses a detailed description and analysis of the enhanced-V cloud formation over the Gulf of Mexico and southern United States in April 1984. The thesis concludes with a summary of the results and the recommendations in Chapter VI.

II. HIGH RESOLUTION METEOROLOGICAL IMAGERY

A. METEOROLOGICAL SATELLITE DEVELOPMENT

After the end of World War II, long range rocketry progressed as a significant new technology after the first meteorological rocket launch in 1946. The resolution of resulting cloud photographs was very low, but it was a successful first step towards satellite meteorology. In 1954, a Navy rocket system returned photographs of the southwestern United States with a tropical storm in the Gulf of Mexico. The resolution and method of image delivery were slowly improving. March 1958 brought the important creation of the National Aeronautics and Space Administration, NASA, and renewed push for a meteorological satellite program. Finally, on 1 April 1960, TIROS I was successfully launched into orbit 730 km above earth with the primary objective of observing cloud cover by means of television camera. An important tool for the meteorological community had finally become reality, and synoptic weather forecasting advanced significantly from the new observational continuity.

The TIROS satellites were designed to give pictures at 10 to 30 second intervals with horizontal resolution as good as 3.6 km at subsatellite point. The later TIROS satellites used improved lenses which increased resolution to as good as 2.75 km. The goal of daily high resolution, worldwide

weather observation was close at hand. TIROS IX, launched in January 1965 expanded the capability of meteorological satellites to attain that goal (Schnapf, 1982).

The 1970's brought an improved NIMBUS system and the first night-time cloud observations. The Improved TIROS Operational Satellite or ITOS was a satellite series which, by means of scanning radiometers, provided day-and-night weather observation of the entire planet (Schnapf, 1985). This led to the development of the TIROS-N (NOAA) satellites and the Advanced Very-High Resolution Radiometer (AVHRR) with full resolution of 1.0 km. The age of high and very-high resolution satellites had arrived. With the two satellite GOES system (1 km resolution) and the addition of DMSP (1 km) polar-orbiting system, the United States had developed a number of very-high resolution meteorological satellites. Further details on the development of meteorological satellites are presented in Appendix A.

Progress of the unmanned satellites continues as GOES-NEXT is being built for launch in the early 1990's. Also, the NOAA-NEXT series of satellites is now under development with introduction expected in 1990. A Block 6 series is now under development for DMSP with early 1990s operation possible. The continued improvement of the meteorological satellites is certain, and with the addition of very-high resolution manned spacecraft photography, the future of meteorological remote sensing is bright.

B. MANNED SPACECRAFT PHOTOGRAPHY

Observing the Earth and atmosphere was an important part of crew activities during Project Mercury and Gemini manned space programs, and many spectacular photographs of the land, oceans, and atmosphere were obtained (NASA, 1977). With the exception of the photographic experiments on Apollo 7 and 9, observations were made and photographs were taken at the discretion of the individual crew members. A large number of very high resolution cloud photographs were processed during the Apollo missions and used in meaningful atmospheric research. Manned orbiting spacecraft have provided very-high resolution photography which has allowed an almost perfect two-dimensional (horizontal) view of the clouds from above (Shenk et al, 1975). The vertical dimension can be added if the photographs overlap sufficiently to permit stereographic analysis. Such cloud photographs offered significant information to meteorologists because of their very fine detail during the Apollo flights, where some shots were taken automatically from mounted cameras, but most were taken manually from varied positions. Apollo spacecraft achieved orbits with average altitudes of 200 km with resulting estimates of spatial resolution of 30-50 m (Shenk and Holab, 1975). Some photograph pairs were subjected to stereoscopic photogrammetry to determine the heights of cloud bases and the tops of convective clouds. The detail within the

photographs allowed for contouring of cloudtop heights within mesoscale systems with accuracy of heights estimated to be ±250 m (Whitehead et al, 1969). Figure 1 illustrates the stereographic cloud height contouring possible with the astronaut photographs.

The launch of Skylab in May 1973 again enabled man to observe and study the atmosphere from low orbit. During three different missions in 1973-74, Skylab crews spent 171 days in orbit approximately 435 km above the Earth's surface taking thousands of photographs. Of the many meteorological phenomena photographed, there was a focus on those features unresolvable in meteorological satellite images. Those features were particularly important for understanding the relationship to weather conditions and predictions (NASA, 1977). A study of Karman vortices downwind of large islands was conducted utilizing the Skylab photographs. Important observations and photographs were made of persistent convective overshoot regions, concentric waves in developing tropical storms, and the examination of outward-tilting eyewall clouds. Cloud and surface spatial resolutions better than 100 m made studies of the mesoscale meteorological phenomena very rewarding. NASA's pre-flight training of the crews by 19 different discipline scientists provided the astronauts with an insight into the scientific significance of the features.

A new era in space travel and meteorological research began in 1980 with the launch of the first Space Shuttle or Space Transportation System (STS). The orbiting space shuttle served as another manned platform from which high resolution photographs of various cloud scenes were taken. Many projects have been flown on the Shuttle to photograph meteorological phenomena. The Orbiter Camera Payload System (OCPS) utilized a 24 cm large format camera mounted onboard the Shuttle. The CLOUDS experiment flew on 3 missions and consisted of a single hand-held camera with film which was sensitive throughout the visible range (Snow and Tomlinson, 1987). CLOUDS II was a follow-on experiment that used two identical cameras, fastened together and synchronized to give enhanced cloud photos with resolutions as good as 25 m. The Space Shuttle Earth Observations Project (SSEOP) was another program created to support the acquisition of earth and atmosphere observation photography by Shuttle astronauts (NASA, 1984). NASA formed earth science investigative teams to aid in the definition of photographic requirements. Project personnel coordinated and provided crew training in the earth sciences, provide real-time support during missions, and disseminate data. It was under the SSEOP program that photography was obtained for this thesis.

III. DATA DESCRIPTION

A. SHUTTLE PHOTOGRAPHY

Space Shuttle photographic images available for these cases present a unique view of mesoscale and microscale meteorological phenomena because of their very-high resolution. These images of mesoscale cloud structure can enhance our understanding of mesoscale phenomena. A total of 60 photographs were considered from three space shuttle missions between February 1984 and June 1985. The space shuttle photograph format was 8x10 inch color prints and one inch color slides.

The space shuttle is a part of NASA's Space Transportation System (STS) and has given scientists an abundance of very-high resolution photographs. The photographic images are a product of the Space Shuttle Earth Observations Project (SSEOP) of NASA. The entire photographic project relied on the cooperation and enthusiasm of the shuttle crews to utilize any available time within the strictly-formatted schedule (Svetz, 1985). The shuttle crews were trained in the fields of geology, meteorology, and oceanography and are familiar with the results of previous SSEOP photography. In addition, they have the advantage of being able to consult with scientists on the ground at Mission Control during flight for timely decision

making (Nelson, 1986). The scientists did periodically make real-time input to the crew to direct the astronauts' attention to areas of interest on each orbit. Features particularly sought for photographic study included hurricanes, major storms, floods, volcanoes, ice areas, and unusual mesoscale meteorological events. After completion of a shuttle flight, the mission films were processed and catalogued by NASA into a concise format for easy research utilization (Nelson, 1986).

The shuttle orbits the earth at an altitude of 183-550 km, considered low Earth orbit, thus giving the possibility of very-high resolution photography. This compares to the altitudes of orbits for geostationary and polar orbiting satellites of 800 - 40,000 km. The shuttle photographs used in this study were from the the STS-41C mission (squall line case) and the STS-51G mission (Pacific dry slot case). The shuttle orbited at an altitude of 492 km for STS-41C and 351 km for the STS 51-G mission. Shuttle velocity during orbit is 6.625 $km\text{-}sec^{-1}$ over the ground. Data on the three STS missions is contained in Table 1.

The camera equipment used on the missions included two hand held NASA-modified Hasselblad 500 EL/M 70 mm cameras (Figure 2), equipped with a Zeiss 50 mm Distagon C4.0 lens, a 100 mm Planar C3.5 lens and a Sonnar 250 mm C5.6 lens (Nelson, 1986). These shuttle photographs were taken using

the 50 mm lens for the Pacific dry slot case, the 100 mm and 250 mm lens for the Gulf of Mexico squall line. Two Kodak natural color films, Ektachrome 64 Professional types 5017 and 6017, were used in the cameras (Nowakowski and Palmer, 1984). The 8 x 10 inch color photographs had resulting ground coverage per side of between 54.5 km and 586.8 km depending on lens size. Horizontal resolution varied between 25 m for the 250 mm lens and 214 m for the 50 mm lens, depending on altitude as shown in Table 2.

The photographs taken during the three STS missions were mostly obtained through the overhead windows (Fig. 3) while the shuttle was in an inverted position, orbiting to the east relative to the Earth (Fig. 4). There were some limitations to taking photographs through the shuttle's windows. The orbiter's windows were ten inches thick and not perfectly flat, so some distortion is expected. Reflections in the windows from the cockpit control panels were another possible problem, but photographs used in this study had minimum distortion and reflection.

There were some limitations on accurately analyzing some of the shuttle photographs. On missions STS 41-B and STS 41-C an accurate system had not been installed to record the precise time on each photograph, so most photograph times were approximate to within 30 seconds utilizing the shuttle's ground track and identifiable landmarks. Given the shuttle's complex ground track across the Earth, unless

identifiable landmarks were noted in the photograph, a precise location could not be established for a meteorological feature (Maul and McCaslin, 1977). Some photographs with no landmarks visible also caused problems identifying the image orientation.

B. METSAT IMAGERY AND SYNOPTIC DATA

METSAT imagery, used to compare and contrast to the shuttle very-high resolution photography, included GOES (1-8 km), NOAA AVHRR (1-4 km), and DMSP (2.7 km) visible and infrared imagery. Supporting synoptic data consisted of the National Meteorological Center's (NMC) analyses for the surface, 850 mb, 700 mb, 500 mb, and 200 mb in addition to the surface radar summary, The Fleet Numerical Oceanography Center's (FNOC's) surface analyses, 300 mb analysis, radar soundings, surface station 3-hourly observations, and ship observations. These products provided all the synoptic data necessary to analyze of the atmospheric structure in each case.

C. PHOTOGRAPH AND IMAGE SELECTION

One of the purposes of this study was to correlate meteorological phenomena seen in space shuttle photographs to high resolution METSAT imagery. For this reason, only shuttle photographs which were positively identified in time and position were utilized. Shuttle photographs which were

within 20 minutes of an applicable METSAT image were analyzed and compared. Hundreds of METSAT images were collected in support of the study, and all those which helped identify or describe formation of the meteorological phenomena were utilized. Some of the more timely digital GOES imagery was processed through the computer systems of the Meteorology Department (NPS) "IDEA lab" and enhanced appropriately.

IV. PACIFIC DRY SLOT

A. INTRODUCTION

On 17 June 1985, the crew of Space Shuttle Mission STS 51-G (Discovery), photographed an unusual cloud-related phenomena, best described as a "dry slot", southwest of Guadalupe Island, Mexico in the eastern North Pacific Ocean (29.2^{o}N 118.3^{o}W). Four 100mm photographs of this slot taken during orbit 4 are presented in Figures 5-8. The photographs show the dry slot to be a long, thin, partly-cloudy (2/8 covered) line surrounded by a large area of stratocumulus cloud cover. These four photographs, along with two others that showed Karman vortices to the south of Guadalupe Island, initiated a detailed study of the this boundary layer phenomena. There were three general questions that served as goals for this case:

1) What were the characteristics and structure of the dry slot?

2) What was the evolution of the dry slot?

3) How and why did the dry slot form?

To properly answer these questions an in-depth study of shuttle photographs, METSAT imagery, synoptic data, surface observations, and upper-air data was completed.

The shuttle photography provided the initial information on structure, characteristics, evolution and formation of the dry slot. All four photographs show the partly-cloudy

character of the inner dry slot with some thicker stratocumulus along the slot edge. The long, thin structure of the dry slot was obvious in the photographs, but length and width were difficult to estimate due to the absence of a reference landmass. A more educated guess of the formation process was made possible by the fifth picture (Fig. 9) since Guadalupe Island, the Karman vortices, and a "new slot" were visible. The "new slot" was a smaller dry slot located 36 km to the west (point A - Fig. 9) of the line of Karman vortices south of Guadalupe and was approximately 183 km (100 nm) long by 27 km (15 nm) wide. It formed similarly to the larger dry slot but did so twelve hours later.

B. DRY SLOT CHARACTERISTICS

1. METSAT Imagery

Several sources of METSAT imagery were studied for this time period. The initial question posed was how did the METSAT imagery reflect this dry slot phenomenon? The closest imagery to the shuttle photographs was a GOES visible image of 17 June at 1632 GMT (4 km) (Fig. 10) which occured within 14 minutes of the shuttle photography. It provided a complete synoptic view of the dry slot as it began to interact with Tropical Storm Blanca ($18^{o}N$ - $126^{o}W$) to the south. The stratocumulus cloud region during this period extended from south of the dry slot east to the Baja

Mexico coast, north to the Oregon coast, and west-northwest to 130°W.

The GOES image illustrates the dry slot as a thin, partly cloudy area 878 km (480 nm) long and oriented nearly east-west. Another (new) small dry slot, previously discussed, formed to the south of Guadalupe Island with the island showing as a dark point through the low cloud deck. Karman vortices (shown in Fig. 9) were barely visible in the GOES imagery to the south-southeast of Guadalupe. There was some enhancement of the stratocumulus cloud deck around the edges of the dry slot apparent in this image.

A second METSAT view of the slot is provided in the NOAA-9 polar orbiting satellite imagery. Information through near-infrared (channel 2) and infrared (channel 4) images at 1 km resolution from the AVHRR are presented for later in the day on the 17th (Fig. 11 and 12). The near-infrared image illustrated the thickening edges of the dry slot, the Karman vortices, the new dry slot, and its relationship with the tropical storm. The infrared image emphasized the clear area around Guadalupe along with the thicker stratocumulus outlining the slot. It was noted that the higher cloud tops along the slot edge had colder temperatures of 282°K vice surrounding cloud temperatures of 283°K and internal slot temperatures of 284°K. Both images clearly showed that the slot was not clear but partly cloudy with stratocumulus and cumulus. The DMSP visual image

(Fig. 13) of 1415 GMT 17 June produced another view of the dry slot area with excellent detail even though resolution was only 2.7 km and the sun's angle was very low. Many details seen in the shuttle photography two hours later could be viewed in this image. The nearly-vertical position of the DMSP satellite over the slot also helped in resolving the details of the phenomenon. The Karman vortices, however, were not seen in the image due to the coarse resolution. The surrounding stratocumulus deck appeared as a smooth, milky layer of clouds vice the bumpy definition of the clouds seen in the shuttle photographs. Detail of the structure of the eastern half of the dry slot was noted in the image, with the variations of edge easily seen and comparable to the shuttle picture (Fig. 8). In all, the dry slot was illustrated with a sharp outer boundary with some enhancement (brighter) outside the edge, and a length of considerable distance.

2. Conventional Data

Data in and around the dry slot was limited during the 15-20 June period, but with some ship reports, numerous Guadalupe surface and upper-air reports, and satellite imagery, the characteristics of the dry slot were fairly clear. Surface ship reports showed the boundary layer to be very moist with wet and dry bulb temperature spreads of 1-2^{o}C and relative humidities of 85-95%. The stratus and stratocumulus cloud deck was near 100% overcast at 200 to

500 meters across the entire area over the five days, with about 25% cloud cover of stratocumulus and cumulus in the dry slot itself. The three ship reports within the dry slot over the period showed no significant difference in atmospheric data from reports outside the dry slot. Surface winds were anywhere from 340^{o}-040^{o} in direction at 5-15 knots over the area of interest with gradual changes over the period.

C. EVOLUTION AND FORMATION

The evolution of the dry slot is described well by the sequence of GOES imagery from 16-19 June. The GOES visible image of 1631 GMT 16 June (Fig. 14) was the first good full view of the dry slot after development earlier on that day. The dry slot was 695 km long and an average of 91 km wide during this time. The evolution of the dry slot from formation on 16 June to collapse on 19 June is illustrated in Fig. 15. The dry slot thinned and lengthened over its 65 hour life a maximum length noted of 951 km and width of 64 kmat 1700 GMT 17 June. Change in formation of the dry slot was influenced by the synoptic flow of the northerly low-level winds and the influence of the tropical system with its northeasterly and then easterly winds. Plots of the tropical storm position are shown with the slot positions in Fig. 15. The dry slot began to collapse on 18 June and showed its last broken form in GOES visible

imagery at 2330 GMT 18 June. Final collapse took place at 0200 GMT 19 June, resulting in a total dry slot duration of 65 hours.

The final analysis objective is the study of the dry slot formation. Where did the phenomena form and when was it first seen in METSAT images? The following hypotheses guide the investigation of the formation:

1. Formed from island barrier effect off Guadalupe Island or Baja California.
2. Formed from ship track mechanisms.
3. Formed from oceanographic features.
4. Formed locally from boundary layer wind field (difluence).
5. Formed from the tropical storm's wake.

An in-depth study of available data and imagery allowed for an elimination of some formation possibilities. After all ship surface observations were plotted in and 500 km around the dry slot for 15-20 June, and after all infrared imagery was studied, no connection to oceanographic features seemed likely. Ship reports of sea surface temperature from within the dry slot illustrated no significant difference from the temperatures outside the slot or from climatology.

There was the possibility of the dry slot formation caused by ship-induced phenomena as noted by Fett (1979) in the Naval Tactical Applications Guide (NTAG) Volume 2. In this type of situation, a transiting ship, its hot stack gasses containing effluent, combines with a shallow, moist

marine layer capped by a strong inversion to produce anomalous cloud lines or slots. There are microscale circulations with these cloud lines that produce upward and downward motions that also produce clear slots adjacent to the cloud lines. It was considered that a variation on this phenomena caused the dry slot situation. However, in studying all the recorded ship reports in that area during the 15-16 June period, there were no ships to correlate to the dry slot formation. In addition, ship tracks are usually slow to form and lengthen as the ship transits, wheras this dry slot was quite large at formation and only lengthened when stretched by low-level flow.

Consideration of barrier effect formation of the dry slot phenomena was the primary task in this case since the slot was first observed only 45 km off the southwest coast of Guadalupe Island. Markley (1986) investigated five types of island barrier effects including Karman vortices, single cloud plumes, transition vortices to plumes, wake effects, and calm sea streaks, but did not provide any typical guidelines for a dry slot phenomena. One possible explanation for the dry slot formation was from the residual dry slot associated with Karman vortices due to turbulence in the boundary layer and that formed at angles up to 38^{o} from the line of vortices (Fujita and Tecson, 1977). As seen in Fig. 9, one of the later shuttle photographs over Guadalupe, vortices were being formed to the south of the

island during all five days with a dry slot, in this case, within the 38° angle. Normally, there is a dry slot at 38° on each side of a cloud plume, but other cases have shown that often one dry slot is obliterated by the cloud plume or by boundary layer turbulence. METSAT imagery (NOAA and GOES) also showed this vortex to dry slot formation relation on 17 June. However, the dry slot formation on the 15-16 June period seemed to be formed approximately 50° to the west of the southern line of vortices.

A southern line of Karman vortices formed in the stratocumulus cloud deck as noted both in shuttle and METSAT imagery. In retrospect, this should have been expected from observing the eastern North Pacific meteorological situation. There was a large subtropical high pressure area to the northwest of Guadalupe and the associated northerly flow over the Guadalupe area (Fig. 16). Tropical Storm Blanca was to the southwest in dissipating stages moving west, but influencing the low-level flow around the cyclone, and thus the movement of the dry slot to the south and west. The sounding for the formation period (Fig. 17) showed a strong subsidence inversion with a base at 935 mb (750 m), a thickness of 35 mb, a strong inversion strength in a moist boundary layer, and a lifting condensation level of 967 mb (960 m). The 850 mb level was at 1508 meters with winds of 250° at 5 m/s (10 knots). This boundary layer situation related clearly to formation of Karman vortices, and it was

possible that the dry slot was a by-product of the turbulence in the boundary layer from the vortex formation. In addition, there have been dry slot cases since (14 May 1987 and 28 Jun 1987) which have shown possible barrier effect formation in METSAT imagery based on first observations. However, the initial large size of the slot on 16 June would not be expected with a barrier formation of this type.

The fourth possibility of dry slot formation was from locally produced boundary layer flow which was very difluent over the Guadalupe area during the 15-17 June formation period. The surface chart (Fig. 16) shows this strong difluence in the northerly flow shifting to westerly flow to northwest flow. It was possible that this very strong difluent flow "pulled apart" the low-level deck of stratus and stratocumulus clouds along pre-existing inhomogeneities. GOES imagery from 2330 GMT 15 June (Fig. 18) shows the lighter and darker bands of stratus and stratocumulus and related to cloud layer thickness. The northeast-southwest orientation of the bands also lined up with the eventual formation position of the dry slot. It was sometime within the next 12 hours after the 2330 GMT GOES image that the dry slot formed.

The final possibility of dry slot formation was from the wake of Tropical Storm Blanca and the slot she could have produced. Rosenthal and Lee (1984) noted that tropical

storms leave a wake of disturbed stratocumulus and a band of mostly clear skies as they traverse the southern edge of subsidence-capped low cloud field during summer in the eastern North Pacific. They also noted that the clear signature is often persistant, lasting two or more days, and is very narrow (55 km) but very long (up to 2200 km). The three cases Rosenthal and Lee illustrate do not resemble this dry slot case, however. Their cases show jagged, clear streaks that are clearly associated with the tropical storm flow, whereas, this dry slot formed well north of the storm and was pushed down into it by synoptic flow. The dry slot was also much more distinct during its 65 hour lifespan than the Rosenthal and Lee (1984) slot cases.

E. DRY SLOT CONCLUSIONS

It was clear that the shuttle photography of 17 June was the tipoff to a remarkable mesoscale feature, the dry slot, in the eastern North Pacific on 16-19 June 1985. The dry slot was a distinct dry zone in a low-level stratus and stratocumulus cloud deck which lasted for approximately 65 hours and showed evidence of a microscale circulation which maintained the distinct shape of the formation. Unfortunately, few ship reports were available in and around the dry slot to give a more accurate description of the formation period. Formation of the dry slot phenomenon was related to a combination of island barrier effect processes

and the boundary layer difluence that existed in the area during the period. It is possible, that, by monitoring meteorological conditions across the eastern North Pacific, and noting the first signs of dry slot formation, one can predict where these operationally important transitions in ceiling and visibility may occur.

V. GULF OF MEXICO SQUALL LINE OF 1984

A. INTRODUCTION

On 9 April, the crew of Space Shuttle Mission STS 41-C (Challenger) extensively photographed a very-well developed squall line over Florida and the Gulf of Mexico (Fig. 19). This squall line was the product of three days of development, dissipation and reorganization of a strong cyclone and frontal system that formed over eastern New Mexico on 6 April 1984. Over four days the system tracked over the southern United States to Florida (Fig. 20), with a total of 71 reported cases of severe weather reported (Storm Data, 1984). These severe weather events included; 19 tornadoes, 8 funnel clouds, 24 hailstorms, 4 thunderstorms with damaging lightning, and 16 strong damaging wind thunderstorms. These events caused one death, 10 injuries and over $103 million in property damage. The damaging weather was restricted primarily to the series of squall lines which moved through the states of Texas, Oklahoma, Arkansas, Louisiana, Mississippi, Georgia, and Florida during the period 6-10 April 1984. Both the shuttle photographs and METSAT (GOES, DMSP, NOAA) imagery captured the distinct signature of the "enhanced-V" squall line cloud formation associated with this severe weather over Florida and Gulf of Mexico (Fig. 21) on 9 April and over Texas on

7 April. The most severe of the reported storms occurred in conjunction with this enhanced-V phenomenon. These two areas were studied closely for this case.

The two objectives established for this case are:

1) To document which mesoscale squall line features noted in the space shuttle photography (Fig. 19) could also be seen in METSAT imagery. These squall line features include cumulonimbus tops, cloud deck notches, cirrus blowoff, gravity waves and the frontal rope cloud.

2) To explain the existence of the enhanced-V cloud formation and its characteristic details including the distinct tip of the V, the front and back boundaries of the V, and their relation to key synoptic features such as the low-level jet, the upper-level jet, and the frontal position.

B. BACKGROUND

The enhanced-V, also known as the "squall-line V" or "White Tornado" cloud formation, was noted by Brandli (1976) as the satellite-observed cloud pattern in the shape of a tilted wedge associated with a cold front or squall line. This distinctive type of squall line, which is observed in visible, infrared, and water vapor imagery, is a composite cloud formation composed of a series of thunderstorm cells characterized by overshooting tops that penetrate the

tropopause (Fett, 1986). The V-shape of the cloud pattern has been partially explained by various studies, but no source seems to have a fully-adequate explanation for the unique signature. In most of the literature on the subject, the enhanced-V refers to the infrared (IR) signature, but for this study, the term will define the squall line cloud wedge formation rather than the cloud top temperature signature.

The enhanced-V in terms of the signature that appears in enhanced infrared (GOES MB scale - see Appendix B) satellite imagery has been described by McCann (1983) and others. That signature is caused by a cold temperature area adjacent to a warm spot, which may depict a collapsing cumulonimbus cloud initiated by a downburst (McCann, 1983). McCann suggested that the shape is caused by the strong upper-level winds that are diverted around a strong updraft which forms the core of the central thunderstorm cell, much as horizontal flow would be forced around the sides of an upright cylinder. A study of the signature being used as a good indicator of severe weather showed that 69% of observed (884 cases) enhanced-V storms are associated with severe weather events within 60 minutes afterwards (McCann, 1983).

Other research in this area has also been completed by Whitney (1976), Fett (1986), and Shapiro (1983). The enhanced-V squall formation and severe convective storm systems also seem to be related to the intersecting and

coupling of the upper-level and low-level jets (Shapiro, 1983). Whitney (1976) noted that the area of the most severe weather associated with an enhanced-V squall line situation is north of the subtropical jet, ahead of the cold front, under the exit region of the upper-level jet, and near the maximum of the low-level jet. The low-level jet, in this case, runs parallel to the established cold front, and the upper-level jet (subtropical jet) runs across the front as shown in Fig. 22a. Uccellini and Johnson (1979) illustrated how this pattern of the upper and lower-level jet streams is the classical configuration for triggering the release of convective and potential instability. Figure 22b shows that the upper and lower circulations are vertically aligned, producing a deep, narrow plume of ascending motion near the leading edge of the surface front (Shapiro, 1983). The ascent is located within a layer of convective instability as the differential motion between the upper and lower front results in a substantial destabilization of the thermal lapse rate. The destabilization aloft coupled with the decrease in moisture above the low-level jet are the thermodynamic components of the potential instability with the dynamic trigger for its release being the vertical alignment of the upper and lower-level geostrophic deformations (Shapiro, 1983).

The importance of the low-level jet to convective weather was noted by Bonner's (1968) summary which

illustrated the large number of low-level jet streaks that develop in the Great Plains, Midwest, Texas and the Gulf of Mexico coast during the spring and summer months. The low-level jet is defined as the "significant wind maximum" within the first 1.5 km above the ground. Some of the low-level jets (Great Plains) are characterized by diurnal oscillation, but others have shown minimal diurnal oscillation. The low-level jet for the convective systems along the Gulf of Mexico coast show development anywhere from the surface to the 700 mb level, however, most exist from above the planetary boundary layer to the 850 mb level (Uccellini and Johnson, 1979). Speeds for the low-level jet range from 25-60 knots and only define the jet when surrounding winds are noticeably reduced (Bonner, 1968).

The interaction between the upper and lower-level jets is the important factor in the development of these organized severe convective storm systems. While the low-level jet rapidly transports heat and moisture northward (Fig. 23), the upper-level jet advects cool, dry air eastward within the middle and upper troposphere (Uccellini and Johnson, 1979). Furthermore, these upper-level jets are frequently associcated with strong upper-level divergence which can trigger the convection.

Another feature which is noted for enhancing convective areas is an upper-tropospheric region where the polar and subtropical jets converge and then diverge (Fett, 1986).

This phenomena produces a region of strong difluence and probable divergence aloft (Fig. 24) which encourages vigorous, deep convection and an increased threat of severe weather underneath the difluence. Skaggs (1967) showed that tornadoes are statistically more closely associated with both the polar and subtropical jet streams than with either jet alone. When the jets were located well apart the most severe storms developed under the direct influence of the subtropical jet and most often in the left exit region of the jet (Whitney, 1986).

C. SHUTTLE AND SATELLITE IMAGERY

Shuttle photography was taken of the enhanced-V squall line during three orbits (46-48) on 9 April 1984. However, only photographs taken during orbit 47, at 1338 GMT, were used to compare with METSAT imagery in this case. The comparison of photography and imagery was made for eight cloud features of the squall line and surrounding region. Figure 25 is a sketch of shuttle photograph 40-2134 (Fig. 26), a near-vertical view of the enhanced-V cloud formation, with labels of the eight compared features. These features are:

1. Individual lower level cumulus cells behind or well ahead of the front
2. Low-level stratus cloud deck behind the front including wave structure in the stratus
3. Shadow of the higher level cumulonimbus on the lower stratus deck

4. Towering cumulonimbus cells or convective turrets of various sizes in the V

5. Notches in the western edge of the enhanced-V cloud wedge

6. Upper-level cirrus blowoff from the towering cumulonimbus and the distinct difference between the blowoff and cumulonimbus tops.

7. Rope cloud line of convective cumulus to the south of the wedge

8. Gravity waves in the cloud deck of the wedge primarily downwind of large turretts.

Table 2 summarizes the shuttle and METSAT data used in the comparisions. Listed in Table 2 are three shuttle views (Figs. 19, 26 and 27), four GOES images (Figs. 21, 28, 29 and 30), four NOAA-7 images (Figs. 31, 32, 33, and 34) and one DMSP image (not shown). Table 2 shows also the comparison of the very high resolution shuttle photography to the high and normal resolution METSAT imagery.

Greater resolution is generally available with shuttle photography than with METSAT imagery. Shuttle photographs taken with the 250 mm lens (Fig. 27) are estimated to have approximately 43 meter resolution for nadir views and showed very-fine cloud detail. Shuttle photographs taken with the 100 mm lens have approximately 110 meter resolution and provide better area coverage (Fig. 19). The photograph resolution is less for oblique views. The nadir resolution of the METSAT data is summarized in Table 2.

The first feature clearly more visible in shuttle photographs was the individual low-level cells of cumulus in

the cold air behind the front and in the inflow area ahead of the enhanced-V formation. The small cumulus clouds were only resolved well by images with 1 km resolution or better. A feature which was illustrated well by the shuttle photographs and was clearly visible (CV) by most METSAT images was the low-level stratus cloud deck. The very-high resolution images could separate the different cloud layers from the highest cumulonimbus/cirrus deck, to the lower-level stratocumulus/ cumulus deck, to the lowest stratus deck behind the front. Only the GOES (Fig. 29) and NOAA-7 (Fig. 33) visible 1 km images were entirely successful in resolving the various cloud levels.

The two notable convective turrets (cumulonimbus tops) were very detailed in the shuttle photographs and extremely visible in most the METSAT images. However, the shuttle view gave more of a 3-D impression to the turrets since the oblique sun angle provided ideal shadows that outlined the circular, stepwise intrusions the thunderstorms made into the tropopause. The DMSP image illustrated the entire squall line as a solid white cloud mass with only a faint shadow near the cumulonimbus tops, thus providing the poorest view of the feature. The NOAA-7 (Fig. 34) and GOES (Fig. 30) color enhanced infrared images provided views of the two turrets with cloud top temperature colder than $-60^{o}C$. There were also many smaller turretts visible on the western edge of the V in the shuttle photos (Figs. 19, 26

and 27). The 1 km visual and 1 km AVHRR IR resolution METSAT imagery were able to resolve most of these small turretts (Figs. 29 and 33). A typical problem with most of the operational visual METSAT data was an oversaturation of the Cumulonimbus top view due to its brightness. Digital satellite displays (e.g. Fig. 34) reveal more detail by avoiding this problem.

All the shuttle photographs and METSAT imagery illustrated the notches in the northwest side of the enhanced-V. The notches were located to the southwest of the turrets which indicated that they were formed by the induced subsidence around the deep convection. The specific cloud detail was visible within the shadows of the notch in the shuttle photographs (Fig. 26 and 27) but was not distinguishable in the satellite images. The cirrus blowoff streaming east of the squall line was another feature extremely visible in all imagery. Again, the enhanced infrared imagery showed the cirrus deck as a warmer temperature from the other cloud types (Figs. 28, 30, 32 and 34). These warmer temperaturew in the IR are misleading in that the shuttle photographs show the Cirrus canopy at the same level has the Cumulonimbus tops.

The final feature noted was the propagating gravity waves between the two largest convective turrets and around the southernmost turret (Fig. 25). The wave pattern was identifiable in all the shuttle photographs but was best

illustrated in the photograph taken with the 250 mm lens (Fig. 27). The gravity waves were barely visible in the AVHRR image (Fig. 33) and GOES visible image (Fig. 29). Svetz (1985) noted these wave patterns propagating along the stable tropopause with an approximate wavelength of 1 to 2 km, thus making it difficult to see the waves without at least a 1 km sensor.

Of the METSAT imagery, the NOAA-7 AVHRR visible image (Fig. 33) provided 1 km resolution, excellent cloud detail, and an excellent view of all features except the gravity waves. The GOES full resolution visible image (Fig. 29) also provided 1 km resolution and excellent detail of all features except the gravity waves. It was a much better view, however, than the normal 2 km GOES images. The DMSP visible image illustrated the least amount of feature detail with only 2.7 km resolution.

D. SYNOPTIC OVERVIEW

The shuttle photographs and METSAT imagery of the enhanced-V illustrated numerous interesting meteorological features in addition to the V cloud formation itself. To better understand the reasons of formation of the enhanced-V signature and its mesoscale features, an overview of the synoptic conditions is now presented.

At 1800 GMT 6 April 1984, a surface low pressure center of 1000 mb was located over northeastern New Mexico with

some middle and high level cloudiness and no precipitation. Over the next 6 hours, the low had remained stationary but had deepened to 997 mb by 0000 GMT 7 April with more organized cloudiness and the subtropical jet (STJ) located to the south of the system by 500 km. The STJ maximum at 200 mb was located over Baja California and was slowly migrating eastward. Some precipitation in the form of showers and thundershowers commenced at 0000 GMT over northern New Mexico and southern Colorado as a steady low-level southerly flow started advecting moisture into the system.

By 1200 GMT 7 April, the low (997 mb) moved to northwest Texas, and the first signs of a front were noted from the Texas panhandle southward to northern Mexico. Rain, showers and thunderstorms were noted from Oklahoma through southwestern Texas with hail reported widespread in both states (Storm Data, 1984). Numerous funnel clouds and two tornados were reported during this period in northern Texas and widespread 60 knot winds were also noted. Maximum cloud top heights were estimated at 11,000 m over Texas. The 850 mb, 500 mb, and 200 mb level charts (not shown) indicated a closed low to 850 mb located over eastern New Mexico, with a trough to the west over Arizona at 500 mb and 200 mb. The STJ and polar jet (PJ) started to converge by this time over central Texas with a 150 knot (STJ) jet streak. The GOES infrared image at 1101 GMT indicated

growth of the convective cloudiness over Texas and surrounding states, and the first signs of cirrus blowoff to the east over Arkansas and Louisiana with the jet.

The GOES infrared image of 1800 GMT 7 April illustrated the overall cloud-cover expanding north to the Canadian border, east to Georgia, and south over half of the Gulf of Mexico. Also shown was a thin squall line formed along 100°W longitude through Texas which correlated to the frontal position. The cloud mass and squall line started to develop into the wedge or enhanced-V shape for the first time also.

The GOES infrared image from 2330 GMT 7 April showed the distinct V cloud formation (Fig. 35). By 0000 GMT 8 April, the surface low pressure center (996 mb) was situated over the Texas panhandle (Fig. 36). A cold front stretched from the Texas-Oklahoma border southward to northern Mexico with a warm front from Oklahoma to northern Mississippi. Showers, thundershowers, hail and lightning were noted in Texas along with one tornado during the period (Fig. 37). Maximum cloud tops were building and estimated at 12,800 m along the squall line. The 0000 GMT significant precipitation covered a larger area from Minnesota to Mexico, with tornado watch areas designated in Texas.

The 850 mb level chart showed a closed low over northern Texas with a trough over southeastern Texas (Fig. 38). Southerly winds up to 45 knots were observed to the east of

the front coinciding with the low-level jet and the east edge of the cloud wedge. At 500 mb (Fig. 39), a closed low was present over the Texas panhandle only slightly northwest of the surface low. At 300 mb, the trough was located over the panhandle also showing the maturity of the system (Fig. 40). The STJ at 200 mb was approximately aligned with the lower tip of the evolving enhanced-V cloud band with a jet maximum of 120 knots. The distinct shape of the wedge-shaped squall line at 0000 GMT 8 April is closely correlated to the locations of the STJ, low-level jet and surface front.

Twelve hours later at 1200 GMT 8 April, the surface low (1003 mb) was located in eastern Oklahoma with a stronger cold front trailing down into Gulf of Mexico and a warm front stretching from Oklahoma to Alabama. The radar summary showed a wide band of showers and the V shape of the southernmost cells into Gulf of Mexico. Maximum heights of cloud tops were 13,100 m over the Gulf coast of Louisiana. Only one case of severe weather was reported during the period, a tornado in eastern Texas. The convective activity subsided during the night, and the enhanced-V area seemed to disorganize. The STJ and PJ diverged over the area of the front and V with a maximum 200 mb wind speed of 110 knots. The STJ had started to migrate south during the period but still remained orthogonal to the cold front.

At 0000 GMT 9 April the low pressure system and associated cold front began to show signs of re-intensifying as the vertical alignment of lows tilted drastically to the northwest with height. The STJ at 100 knots was at a maximum over southern Louisiana and the low-level jet began to strengthen again (40 knots) at the 850 mb level just ahead of the cold front and orthogonal to the STJ. Severe weather was again well documented over Louisiana and Mississippi during the period. By 0830 GMT 9 April, 5 hours before the shuttle photography, the wedge shape of the enhanced-V had become visible in the GOES imagery as the severe weather increased over Florida and the Gulf of Mexico.

The synoptic situation at 1200 GMT 9 April again supported the onset of severe weather in the Florida area. The surface chart (Fig. 41) showed the double low (1005 mb) over the south with the associated cold front over Alabama, Florida and Gulf of Mexico. The southerly winds ahead of the front were at 25 knots (30 knots at 850 mb) forming the low-level jet, forcing warm, moist tropical air over Florida to converge with the cooler, drier northwesterly flow behind the front. A warm front stretched from western Florida across Georgia east over the Atlantic.

A comparison of radiosonde soundings from either side of the front, at Boothville, Louisiana and Tampa Bay, Florida, by Svetz (1985) further defined the air mass

differences. Boothville sounding showed dry, stable continental air mass west of the front, while Tampa Bay data showed near saturated warm air mass with dry air above 3660 meters. The Showalter stability index had a value of -4.5 at Tampa Bay, illustrating the convective storm potential of the air mass. The Tampa Bay sounding also exhibited a low-level jet (35 knots - 900 mb) and a noticeable inversion with large wind shear near the 650 mb level.

The 500 mb (Fig. 42), 300 mb, 200 mb (Fig. 43) and 100 mb upper-air analyses indicated definite height falls over the area. The analyses also indicated two important contributors to the squall line development and maintenance. First, there was the area of strong difluence produced by the divergence of the polar jet and subtropical jet over Florida at or near the 200 mb level. Secondly, there was evidence of the orthogonal orientation of the low-level jet (south at 25 knots) and the subtropical jet (west at 95 knots) supporting a narrow, deep layer of strong convection as theorized (Fig. 22) by Shapiro (1983). Consideration of the surface land heating provided by local sunrise should also be noted for this period. Finally, Figure 44 illustrates the precipitation which developed off Florida in Gulf of Mexico during the morning of 9 April. At this point maximum cloud tops were only up to 10,950 m, but by mid-afternoon the cumulonimbus tops built to 16,150 m.

The low pressure continued to move east and off the coast of southern Georgia (Fig. 20) with the cold front trailing across Florida and off the coast by 1800 GMT 10 April. The most severe weather created by this system occurred in Georgia and Florida between 1100 and 1800 GMT 9 April in association with enhanced-V cloud formation. In Georgia, there were four funnel cloud sightings, four damaging hailstorms, and one damaging wind case reported. In Florida, there were four tornadoes, one hail storm, and four damaging thunderstorms reported.

E. CROSS SECTIONS FOR THE ENHANCED-V PATTERN

There were two periods during the life cycle of the low pressure system and front that best illustrated the enhanced-V phenomenon, 0000 GMT 8 April Texas and 1200 GMT 9 April over Florida and the Gulf of Mexico. For these key periods, cross-sections both north/south and east/west (Fig. 45) of available radiosonde data were analyzed to produce isentropes and isotachs. The cross-section information expands the previous synoptic analyses in study of the boundaries of the enhanced-V.

A cross-section was produced 0000 GMT 8 April from Omaha Nebraska (OMA) to Vera Cruz, Mexico (VER) using seven stations (Fig. 46). The cross-section indicated the warm front, which was near Oklahoma City (OKC), in both the isentropes and isotachs especially at the 1000-700 mb level.

The close proximity of the subtropical jet with 110 knots at 170 mb, and the polar jet with 110 knots at 240 mb was very obvious and illustrated the converging jets (Fig. 44) over Texas. The low-level jet was not so obvious in the same cross-section since the program plotted wind speed components perpendicular to the line of stations, therefore, a speed of zero indicated a southerly wind/speed. The low-level wind was verified southerly at 35-45 knots ahead of the cold front at 850 mb in eastern Texas and western Louisiana. The enhanced-V cloud formation during this period was defined by the cold front position (west edge of V), the centerline of the subtropical jet (Southern tip of V), and centerline of the low-level jet (eastern edge of V).

The best defined enhanced-V formation was over Florida and Gulf of Mexico starting at 1200 GMT 9 April. The V was oriented southwest-northeast so the cross-section from Monet, Missouri (UMN) to the Bahamas (YNN) was utilized (Fig. 47). The plot showed the subtropical jet over Tampa (TPA) at 60 knots/180 mb and the polar jet over Panama City, Florida (AQQ) at 60 knots/220 mb. Actual speeds of the subtropical and polar jets were 94 and 72 knots, respectively. The low-level jet was not quite as organized as earlier, but 20-25 knot reports were noted at the surface and 850 mb. The enhanced-V boundaries were defined, again as noted, except that the low-level jet did not seem to define any specific boundary.

F. CONCLUSIONS

The comparison of METSAT imagery to shuttle photography showed that high resolution METSAT images provided an excellent view of many mesoscale squall line features. The notches, stratus deck, and cirrus blowoff were features seen well in operational imagery. However, the rope cloud, small cumulus cells and gravity waves were not shown as well by METSAT.

A close study of the enhanced-V signature and synoptic conditions give some guidelines which describe the boundaries of the V (Fig. 48). First, the back (west) side of the cloud mass coincides with the cold front position. Secondly, the southern-most tip of the V is defined by the centerline of the subtropical jet axis. Even though the front may continue further to the south, the upper-level jet axis determines the limit of cumulonimbus cloud growth. Finally, the right (east) edge of the V is usually the eastern limit of the cirrus cloud deck, but, at times the east edge is determined by the eastern limit of the low-level jet. Depending on the time of year and synoptic conditions, the enhanced-V can last as a distinct feature for several days. Diurnal growth and decay of severe convective systems may often depress or destroy the enhanced-V formation. In this case, shuttle photography served as a valuable tool in the analysis of this mesoscale severe weather cases.

It is important that the forecaster has mesoscale imagery and data to analyze severe weather events. These mesoscale features evolve rapidly, so the forecaster/ nowcaster may have only 20 to 60 minutes to warn the public of severe weather. This case, as well as previous studies, demonstrates the severe weather potential of the enhanced-V wedge cloud pattern. The presence of the favorable synoptic patterns and/or the satellite observations of enhanced-V development should alert the forecaster for a possible severe weather situation.

VI. SUMMARY AND CONCLUSIONS

A. SUMMARY

In the two cases presented in this study, synoptic and mesoscale features, observed by very-high resolution shuttle photography and high resolution METSAT imagery, were analyzed to study the formation and evaluation of interesting mesoscale phenomena. Investigation of the phenomena was completed through use of the imagery and photography in addition to the conventional data available for case periods. Detailed imagery comparisons were made for both a Pacific dry slot and Gulf of Mexico enhanced-V utilizing the various types of METSAT imagery and shuttle photography. Through these comparisons and the synoptic investigation of the events, the value of very-high resolution imagery in resolving the cloud structure of mesoscale circulations was demonstrated.

The Pacific dry slot feature illustrated evidence of mesoscale circulation which maintained the distinct shape of the formation within the thick stratocumulus cloud deck. The dry slot also exhibited unusual endurance as it remained detectable for approximately 65 hours in the very stable North Pacific environment. The formation of the dry slot still was not entirely understood but was probably a combination of the difluence in the region and island

barrier effects from Guadalupe Island. Further study of the region showed that the phenomena was fairly frequent during the summer months.

The Gulf of Mexico enhanced-V phenomena of April 1984 utilized very-high resolution shuttle photographs to compare with GOES, NOAA (AVHRR) AND DMSP imagery. Eight different microscale and mesoscale features within the enhanced-V synoptic feature were analyzed and compared with METSAT data. Only some of the smallest features seen in the shuttle photography, such as gravity waves and individual cumulus elements, were not resolvable in the majority of the METSAT images. The boundaries of the enhanced-V, well-defined during two 12 hour periods of the study, were correlated to specific synoptic mechanisms in the conventional data. The west side of the cloud wedge coincided with the cold front position, the southern-most tip of the V was defined by the centerline of the subtropical jet axis, and the east edge of the wedge was often times defined by the the low-level jet.

In these cases, the very-high resolution space shuttle photography has demonstrated its value as a research tool. The photographs aided the detailed analysis of unique phenomena that are difficult to understand and explain. The photography does illustrate the potential, however, of very-high resolution imagery in assisting a forecaster or nowcaster in a real time situation. It provides a

convincing argument for the use of continuous very-high resolution imagery at forecast centers. It is through this improved understanding of mesoscale events that the field meteorologist would be able to make more accurate local forecasts.

B. RECOMMENDATIONS

This thesis only considered two cases of many unique features that are seen in very high-resolution imagery and impact in some way normal operations. More of these cases, specifically the dry slot and enhanced-V, should be studied to refine the results of this thesis. In-situ data from aircraft and ships, not available in the operational data base, would greatly assist in answering the outstanding questions of characteristics and formation. Project FIRE (The First ISCCP Regional Experiment) (Cox et al, 1987) is one such project being conducted to study such phenomena. It focuses on the marine stratocumulus of the west coast of the United States and high-altitude cirrus.

The Space Shuttle Earth Observations Project (SSEOP) should continue to assist in meteorology photography in conjunction with other shuttle operations. Additional ground to shuttle coordination could improve on the quality of photographs for significant meteorological features. An automated camera system in the cargo bay controlled on the ground could also enhance the earth photography. The space

shuttle should also be considered for experimentation of higher resolution sensors for meteorological imagery. This might be a more cost-effective test platform for such equipment than individual satellites.

Forecasters at major centers are working with 1 km imagery, at best, in real time. This satisfies most of today's forecasting requirements. In order to improve forecasting or nowcasting and better understand mesoscale phenomena, higher resolution imagery is needed initially for research purposes and eventually in real time for the forecaster.

APPENDIX A

HISTORY OF METEOROLOGICAL SATELLITES

1. HISTORY OF U.S. SATELLITES

The most spectacular and significant of the new technologies brought about by World War II benefitting meteorological research and forecasting was long range rocketry. After the U. S. Weather Bureau had first proposed work on the remote sensing rockets in 1920, Dr. Robert H. Goddard did some preliminary work in the field. It was not until after the war that significant progress toward high altitude remote sensing of clouds took place (Vaeth, 1965).

The German-developed V-2 missile, spare parts and experts were available to the United States at war's end. This provided scientists the opportunity to commence vertical soundings and atmospheric research. A series of scientifically instrumented V-2 launches began at the Army's White Sands Proving Ground in New Mexico during 1946 and continued into late 1952 (Vaeth, 1965). In March 1947, a V-2 rocket launched at the Proving Ground, took the first successful photographs of the earth's cloud cover, from altitudes of 110 to 165 km, with composite pictures of over 300,000 km^2 over the southwestern United States. This was the first time there was a relatively large and complete cloud picture of an area where it was possible to correlate

the visible meteorological phenomena with atmospheric structure measured by conventional means (Crowson, 1949). A total of about fifty V-2s were launched during the period 1947 to 1952, each with more improved meteorological instrumentation than the previous. As high-altitude meteorological photography and atmospheric sounding were becoming more routine, only proper guidance from opportunistic meteorologists would ensure growth of the high-altitude programs.

The late 1940s brought the Viking rocket system that carried advanced high-altitude cloud-photography experiments which led to the first serious proposal for meteorological satellites (NASA, 1966). During the summer of 1948, sets of pictures were obtained from a V-2 and a Navy Aerobee rocket launched twelve hours apart. The areas covered by those high resolution photographs included the southwestern United States once again (Crowson, 1949). The Department of Defense and the General Electric Company participated in the White Sands launches of the 1940s and early 1950s for purposes of a wide range of upper-air research programs. The research also included experiments for weather forecasting. This was a step forward from the limited observations and research conducted from airplane and balloon during the 1930s.

The first photographs of clouds from a rocket were published by Captain D. Crowson in January (1949). It was a

first analysis of rocket meteorology but did not take the additional step to point out the potential of satellite imagery. Meteorologists were impressed by the photographs and encouraged since they knew that the secret of understanding synoptic and mesoscale weather systems was to see the large scale cloud systems from above. The Rand Corporation was contracted by DOD in 1951 to start investigating the concept of orbiting satellites, and specifically how satellites could be used as weather reconnaissance vehicles. Project RAND by the Rand Corporation and RCA utilized the best scientists and meteorologists available including Dr. Harry Wexler (1954), S.M. Greenfield (1956), W.W. Kellog (1982), and Dr. J. Bjerknes (1951), the expert of synoptic meteorology of that period. Bjerknes (1951) showed great support for the idea of doing detailed analysis of synoptic conditions from satellite (rocket) photographs. This support in conjunction with several case-studies he conducted helped convince many meteorologists that the development of meteorological satellites would revolutionize research and forecasting.

In 1954, a Navy Aerobee rocket system of the Naval Research Lab returned pictures over the southwestern United States that showed a tropical storm, unnoticed by conventional means, that passed onto land from the Gulf of Mexico. The case emphasized the utility of deploying meteorological satellites by the ability to show the storm's

position and extent. This led, in 1955, to the first official steps toward actually putting a satellite into orbit. An Army-Navy project designated **Orbiter** was established and then superceded by Vanguard (Vaeth, 1965) under the sole direction of the Naval Research Laboratory.

Sputnik I, the first successful earth satellite, was launched by the Soviet Union on 4 October 1957 and intensified the pace of the U.S. satellite program. President Eisenhower announced the creation of NASA, the National Aeronautics and Space Administration, in March 1958, and DOD continued to push for launch of a meteorological satellite. The first meteorological satellite launched was Vanguard II (February, 1959) which contained very simple scanning radiometers. Balance problems caused uncontrollable rotation of the satellite, and, therefore, no acceptable pictures were obtained (Kellogg, 1982). Explorer VI was launched in August, 1959 with a cloud mapping and television system adapted from earlier probes. Pictures were obtained and transmitted to earth, but the quality was unsatisfactory.

The TIROS (Television and Infrared Observational Satellite) program was turned over to NASA in early 1959 as the meteorological satellite program for the United States. On 1 April 1960, TIROS I was successfully launched into orbit 730 km above earth, with the primary objective of observing cloud cover by means of slow-scan television

cameras on a spin-stabilized satellite. Pictures were received from space during the first orbit clearly demonstrating the feasibility of such a system (Schnapf, 1985). An important tool for the meteorological community had finally become reality, and synoptic forecasting would advance significantly from the new observational continuity. With the success of TIROS-1, there followed an orderly growth and evolution of the TIROS family of meteorological satellites over the 1960s and 1970s. Figure 1 illustrates the chronology of the TIROS meteorological satellites (Schnapf, 1982). The TIROS satellites were designed to give pictures at 10 to 30 second intervals with approximately 50 percent overlap. Surprisingly, pictures were programmed to have resolution as good as 3.6 km at subsatellite point. The later TIROS satellites had medium-angle and narrow-angle lens which produced pictures with potential resolution as good as 2.75 km with .2 km for television (Barrett, 1967). The actual photographs had resolution twice the television resolution (5.50 km) since contrast and brightness was so poor. TIROS VIII, launched in December 1963, utilized both a 1/2 inch standard satellite camera and a 1 inch automatic picture transmission (APT) camera. This was the first in-space use of the APT system which allowed direct, real-time television picture transmission to a series of APT ground stations around the world.

TIROS IX was launched in January 1965, and expanded the capability of meteorological satellites to provide complete global weather observation on a daily basis. Two television cameras were mounted on the satellite, and it was injected into a higher inclination orbit to allow complete global coverage. Daily observations were increased by four times as preparations were made for deploying a truly operational meteorological satellite after TIROS X was launched. TIROS X was the last of the research and development series of TIROS satellites and was launched in July 1965 to provide hurricane observations (Schnapf, 1982). The TIROS satellites from 1960 to 1967 provided over 500,000 usable pictures and vital information for issuance of over 3000 storm advisories (Anderson et al, 1966).

To provide continued daily routine worldwide cloud observations the Environmental Science Services Administration (ESSA) introduced the TIROS Operational System (TOS) in February 1966 by launching the ESSA-1 satellite into a 732 km near-polar sun-synchronous orbit. The ESSA-2 satellite was also launched in February of that year into a 1372 km sun-synchronous orbit to complement ESSA-1 and to fulfill a U.S. commitment to provide an operational meteorological satellite system in the first quarter of 1966 (Schnapf, 1982). The horizontal resolution was improved slightly with the ESSA-3 launch as the advanced

vidicon camera system (AVCS) was utilized. The ESSA series of satellites were operational through 1971.

At the same time as the ESSA operational satellites were being deployed, a new generation of experimental satellites (NIMBUS) was testing new meteorological sensors. The first NIMBUS satellite was launched in August 1964 into a near-polar orbit. NIMBUS was conceived as a meteorological test bed satellite concerned primarily with providing research data for improved weather forecasting. Through the addition of more sophisticated sensing devices on each succeeding vehicle, this research observatory program grew significantly in capability and performance. A total of seven successful launches were completed, concluding in 1978 (NASA, 1982). The horizontal resolution for cloud observations did not improve upon that of previous systems with a resolution of 3.7-9.2 km was the norm. NIMBUS was notable for night-time cloud observation. The series of satellites was concluded with the launch of NIMBUS 7 in October 1978. NIMBUS was also the lead-in for the series of LANDSAT environmental satellites.

A third generation of TIROS satellites, TIROS-M or ITOS (Improved TIROS Operational Satellites), was placed into orbit in December 1970. This series of satellites, by means of infrared scanning radiometers and television cameras, provided day-and-night observation of the entire planet (Schnapf, 1985). Each ITOS satellite was capable of

observing world-wide every 12 hours at resolutions similar to the earlier TIROS satellites. A total of six ITOS/NOAA satellites were placed in orbit between 1970 and 1976.

The fourth meteorological satellite generation, TIROS-N (NOAA) was introduced in October 1978 with a successful launch of NOAA-6 in June 1979 (NASA, 1982). This satellite class utilized the Advanced Very High resolution Radiometer (AVHRR) which increased radiometric information for improved day-and-night imaging in the visible and infrared bands. Other instruments were added to these satellites, but none that affected cloud detection. The NOAA-7 satellite was the last of this group of operational craft as NOAA-8 was developed as an advanced TIROS-N/NOAA satellite. This current series includes NOAA-8, 9, and 10 (operational) and the future NOAA 11 and 12 satellites with deployments in 1988 and 1989, respectively, The advanced NOAA craft have been designed for larger payloads to fly new instruments to further enhance the TIROS Operational System (NASA, 1982). The NOAA-NEXT class of satellites is now under development with introduction expected in 1990.

In 1966, the launch of NASA's ATS-1 (Applications Technology Satellite) provided, for the time, the use of the time domain in the analysis and interpretation of meteorological satellite data (Greaves and Shenk, 1985). It was also the first time that nearly continuous observations of the same area of the U.S. could be made. A new era of

meteorological research had begun. The ATS-1 satellite's spin-scan cloud camera (SSCC) system provided black and white images at a spatial resolution of 3.2 km. Three experimental ATS craft were deployed through 1974 in preparation for an operational series of geostationary satellites. Two operational prototype satellites, designated Synchronous Meteorological Satellites (SMS), were launched in 1974 and 1975. The fully operational GOES (Goestationary Operational Environmental Satellite) satellites commenced with GOES-1 in October, 1975 by GOES-2 and 3 in 1977 and 1978. The five SMS and GOES satellites were identical in design and very successful. Beginning with GOES-4 in 1980, a new contractor and new design were utilized which included the VISSR (Visible/Infrared Spin-Scan Radiometer) Atmospheric Sounder (VAS). The VAS was a radiometer with 8 visible channel detectors and 6 thermal detectors that could detect infrared radiation in 12 spectral bands. The spatial resolution was .9 km in the visible and 7 km in the infrared range (Greaves and Shenk, 1985). Currently GOES-6 and 7 are active "West and "East" geostationary satellites covering the U.S. and adjoining Atlantic and Pacific waters. The GOES system is the primary tool for meteorologists to observe cloud motions, severe storm formation and other mesoscale phenomena. The improved GOES system GOES-NEXT, is in the development stages, and the first launch is scheduled for late 1989.

Another polar-orbiting satellite system currently in use is the Defense Meteorological Satellite Program (DMSP) with a primary mission of providing high-quality meteorological data in a timely fashion to the Armed Forces of the United States. The DMSP evolution has paralleled that of the civilian polar-orbiting satellites, but DMSP has its own mission objectives which require unique sensor payloads and nodal cross times (Gomberg and McElroy, 1985). In 1965 the first DMSP satellite was deployed in the Block IV series with cloud coverage obtained by high resolution television cameras at 2.4 km resolution. Over the years the needs for DMSP changed and so its mission. The design and hardware changed regularly to keep pace with technological change and mission update. Block 5 lasted from 1970 to 1977 with minor changes instituted in Block 5A, 5B, and 5C. A Block 5C significant change included the addition of a high resolution infrared channel with resolution equal to the visible channel at .5 km. This feature allowed DMSP to detect small cloud elements both day and night, and, with normalization of cloud reflectivity, allowed excellent cloud coverage across the terminator (Meyer, 1985). A Block 5D change of the imaging radiometer allowed for preservation of the ground resolution of the image from spacecraft nadir to the edge of scan. Block 5D-2 upgrades are now in place on DMSP to improve its lifetime and reliability while maintaining very high resolution images. A Block 6 is now

under development for DMSP and should be operational by the early 1990s.

2. THE FOREIGN SATELLITES

The European Space Agency (ESA) currently operates a geostationary satellite, METEOSAT-2, which has a satellite subpoint at 0^{o}E, 0^{o}N. This gives METEOSAT an areal coverage from Antarctica to Greenland and from Saudi Arabia to Brazil (Fett et al, 1983). The European region is covered for imagery every half-hour while the entire METEOSAT field-of-view is covered every 3 hours. There are two visible sensors onboard which give a spatial resolution of 2.9 km and the three infrared sensors give a resolution of 5.8 km. The METEOSAT Operational Program expects to launch three more satellites in August 1987, mid-1988, and 1990, with their subsequent exploitation until 1995 (Honvault, 1985).

The Japan Meteorological Agency (JMA) and the National Space Development Agency (NASDA) launched GMS-3 (Geostationary Meteorological Satellite) in August, 1984 and placed it 36,000 km above the equator at 140^{o}E longitude. It is the third in a series of Japan's meteorological satellites contributing to the weather watch program over Japan and the West Pacific (Homma et al, 1985). The GMS satellites deployed since 1977 have mission objectives similar to those of the U.S. GOES system. The resolution for visible spectrum is 1.25 km and is 5 km for the

infrared. The VISSR is utilized to obtain the visible and infrared spectrum mappings of the Earth and its cloud cover.

The French government decided in 1978 to undertake, with Belgium and Sweden, the development of the "Systeme Probatoire d'Observation de la Terre" or SPOT (Courtois and Weill, 1985). The satellite was launched in 1986 into a circular, sun-synchronous orbit at 832 km altitude. The resolution at satellite subpoint is 20 m with the high resolution visible-range instruments (HRV). SPOT 2 is near completion and should be deployed in late 1987 with SPOT 3 and 4 to launch by the 1990s.

Other countries have developed satellite systems in the 1970s and 1980s that are capable of producing high resolution cloud images. Japan's Marine Observation Satellite (MOS-1) is a polar-orbiting land, ocean, and atmosphere observing satellite with resolution as good as 50 m. India has deployed the Indian National Satellite (INSAT) into a geostationary orbit at 74^{o}E with a VHRR and resolutions of 2.75 km for the visible band and 11.5 km for the infrared band. The Soviet Union has two distinct meteorological satellites, METEOR and GOMS. The METEOR series satellites have television-type scanning equipment with resolution of 250-600 m in the nadir.

APPENDIX B

ENHANCEMENT MB

GENERAL DESCRIPTION

Segments 1, 2, and 3 are extracted directly from the old Z curve: This steeper slope will give better definition to the low and mid clouds. Segments 4 through 7 contours convective areas. Segment 8 slopes with a factor greater than zero from -63° C to -80° C which allows for good definitions of very cold domes. Although specific temperatures cannot be obtained--it better isolates the coldest tops by gradually going to white rather than producing a complete white-out at all temperatures colder than -65° C. This curve is utilized for rainfall estimates.

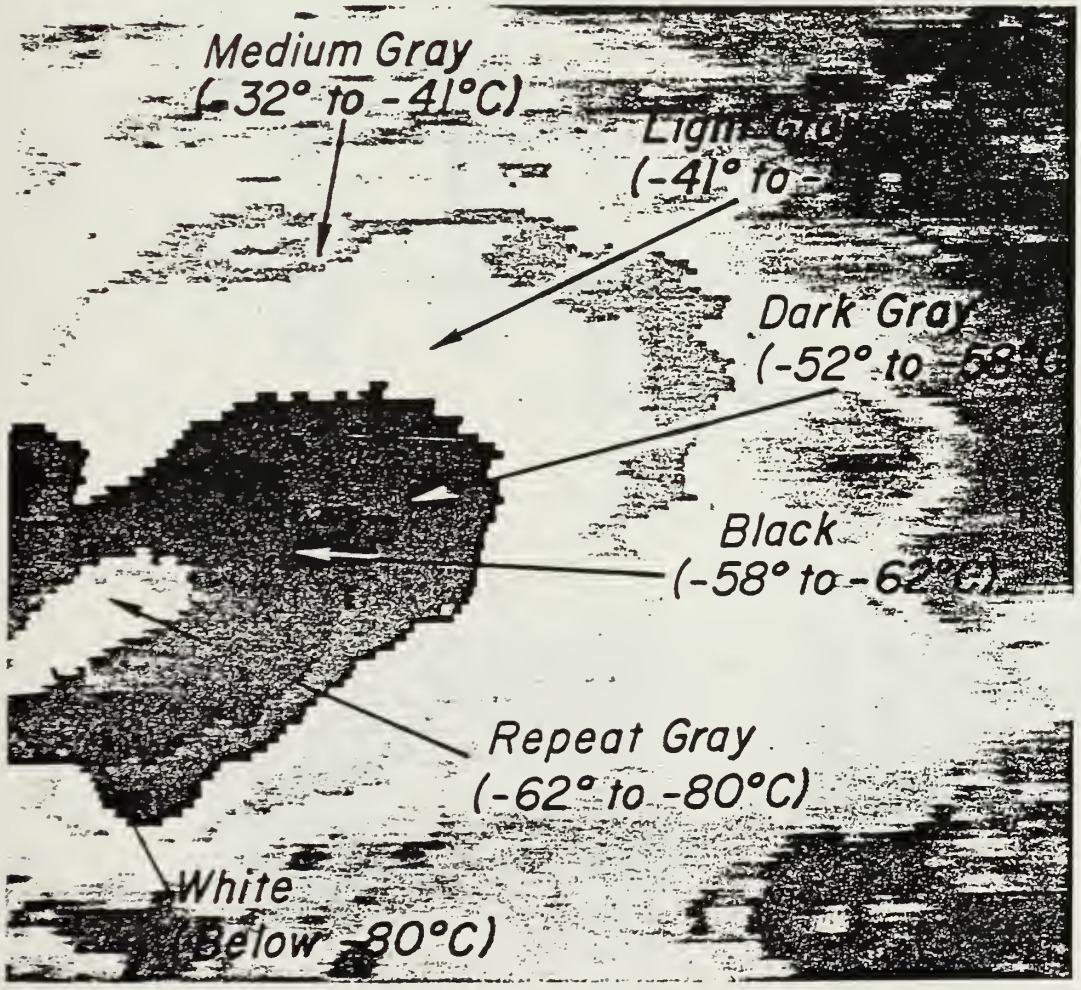

ENHANCEMENT MB

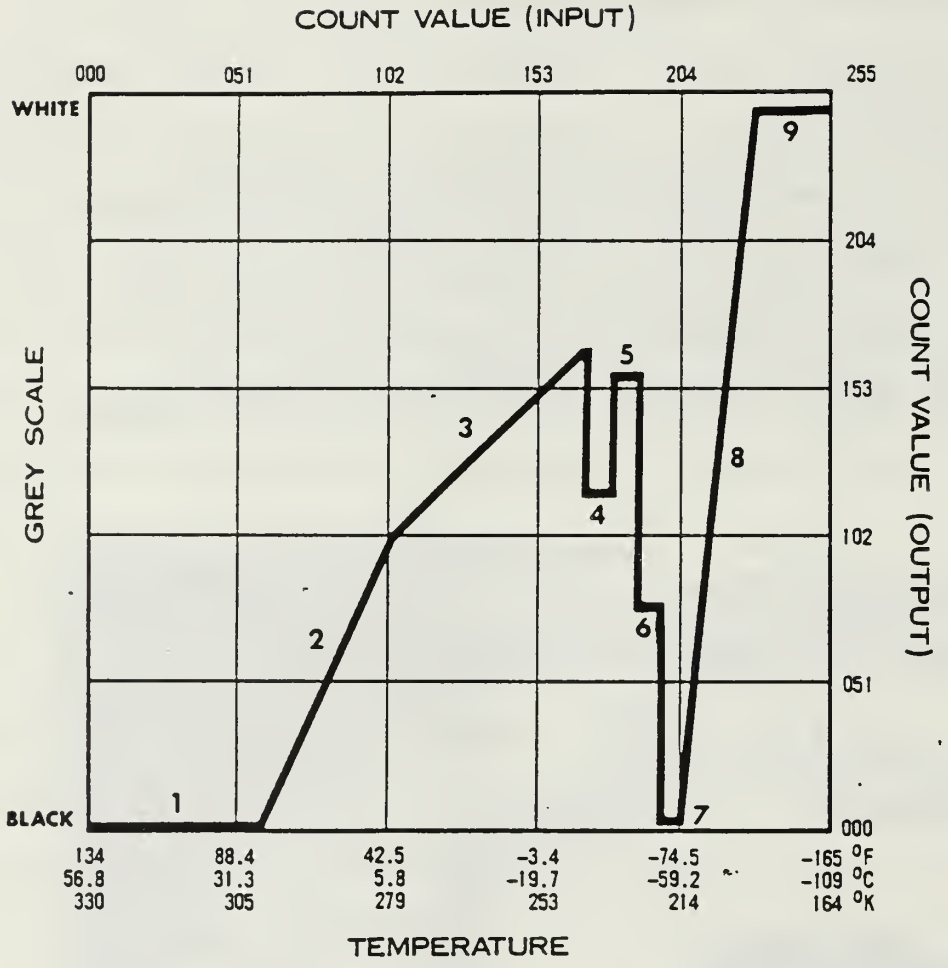

SEGMENT NUMBER	°C TEMPERATURE	COMMENTS
1	58.8 to 29.3	Little or no useful Met Data (Black)
2	28.8 to 6.8	Low Level/Sea Surface Difference
3	6.3 to -31.2	Middle Level - No Enhancement
4	-32.2 to -42.2	First Level Contour (Med Gray)
5	-43.2 to -53.2	(Light Gray)
6	-54.2 to -59.2	Thunderstorm (Dark Gray)
7	-60.2 to -63.2	Enhancement (Black)
8	-64.2 to -80.2	Overshooting Tops Enhancement
9	-81.2 to -110.2	(White)

APPENDIX C

TABLES AND FIGURES

The following tables and figures are provided to highlight the text of this thesis. The space shuttle photography has lost some resolution due to black and white reproduction of color originals.

TABLE 1
MISSION DATA FOR STS 41-C AND STS 51-G

STS 41-C

Launch: April 6, 1984, 8:58 a.m. EST
from Kennedy Space Center, Florida

Landing: April 13, 1984, 8:38 a.m. EST
at Edwards Air Force Base, California

Orbits: 107

Vehicle: Challenger (OV-099)

Orbit Altitude: 269 nm

Inclination: 28.5°

Crew: Commander, Capt. Robert L. Crippen, USN
Pilot, Mr. Francis R. Scobee
Mission Specialists
Mr. Terry J. Hart
Dr. George D. Nelson
Dr. James D. van Hoften

STS 51-G

Launch: June 17, 1985, 7:34 a.m. EST
from Kennedy Space Center, Florida

Landing: June 24, 1985, 6:12 a.m. EST
at Edwards Air Force Base, California

Orbits: 112

Vehicle: Discovery (OV-103)

Orbit Altitude: 190 nm

Inclination: 28.5°

Crew: Commander, Capt. Daniel C. Brandenstein, USN
Pilot, Cdr. John O. Creighton, USN
Mission Specialists
Lt. Col. Steven R. Nagel, USAF
Col. John M. Fabian, USAF
Dr. Shannon W. Lucid
Payload Specialists
Prince Sultan Salman Al-Saud
Lt. Col. Patrick Baudry, FAF

TABLE 2
SHUTTLE PHOTOGRAPHY AND METSAT IMAGERY FEATURE COMPARISON

PLATFORM (FIG.NO)	IMAGE TYPE	RES (KM)	TIME (GMT)	FEATURES 1	2	3	4	5	6	7	8
SHUTTLE (19)	VIS	.11	1338	CV	CV	CV	CV	CV	CV	CV	CV
SHUTTLE (26)	VIS	.11	1338	CV	CV	CV	CV	CV	CV	CV	CV
SHUTTLE (27)	VIS	.04	1338	CV	CV	CV	CV	CV	CV	CV	CV
GOES (21)	VIS	2.0	1331	BV	CV	CV	BV	CV	CV	CV	NV
GOES (28)	EIR	2.0	1301	NV	BV	NV	BV	CV	CV	BV	NV
GOES (29)	VIS	1.0	1331	CV	CV	CV	CV	CV	CV	CV	BV
NOAA-7 (31)	VIS	1.0	1336	BV	CV	CV	BV	CV	CV	CV	NV
NOAA-7 (32)	EIR	1.0	1336	BV	CV	NV	CV	CV	CV	CV	NV
NOAA-7 (33)	VIS	1.0	1336	CV	CV	CV	CV	CV	CV	NA	BV
DMSP (--)	VIS	2.7	1521	BV	CV	BV	BV	CV	CV	BV	NV
NOAA-7 (34)	EIR	1.0	1336	BV	CV	NV	CV	CV	CV	BV	NV
GOES (30)	EIR	8.0	1338	NV	BV	NV	CV	CV	CV	BV	NV

LEGEND

FEATURES
1: Cumulus cells
2: Stratus cloud deck
3: Shadow on stratus deck
4: Convective Cb Turrets
5: Notches
6: Cirrus blowoff
7: Rope cloud
8: Gravity Waves

FEATURE DESCRIPTION
CV: Clearly Visible
BV: Barely Visible
NV: Not Visible
NA: Area not covered

ACRONYMS
RES: Resolution
VIS: Visible channel
IR: Infrared channel
EIR: Enhanced Infrared

Fig. 1. Apollo 6 cloud height contouring (Whitehead et al, 1969)

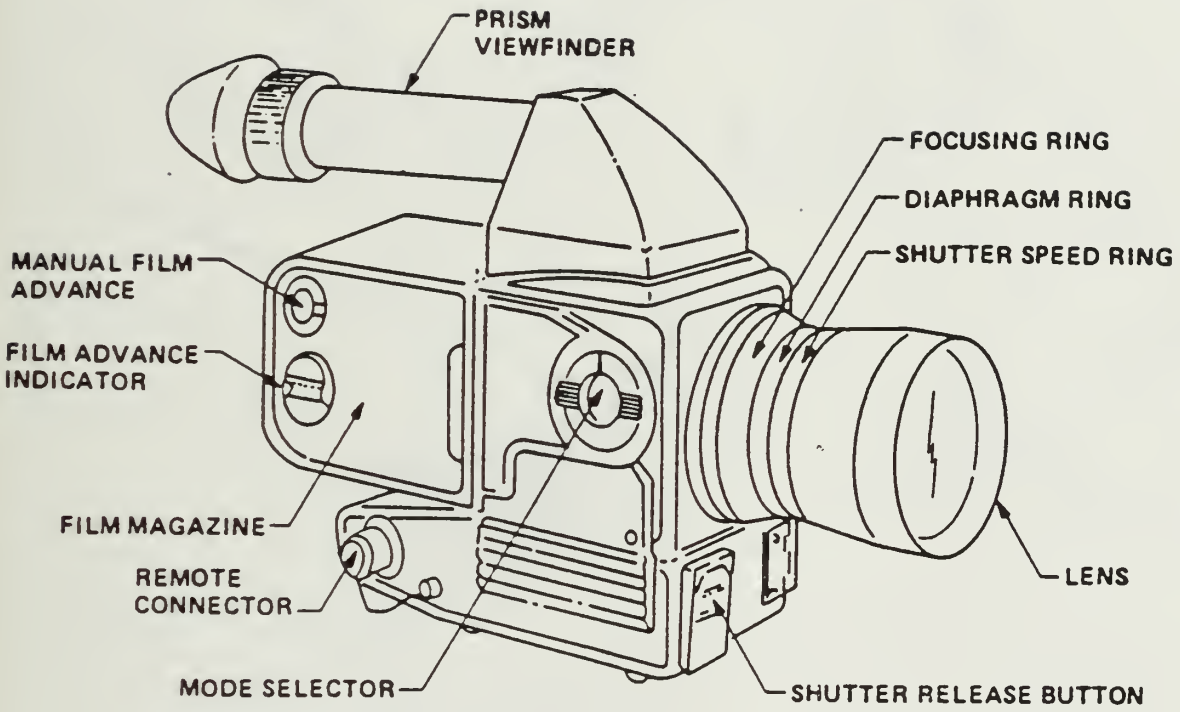

Fig. 2. NASA-modified hand-held Hasselblad 500 EL/M Camera (Nowakowski and Palmer, 1984)

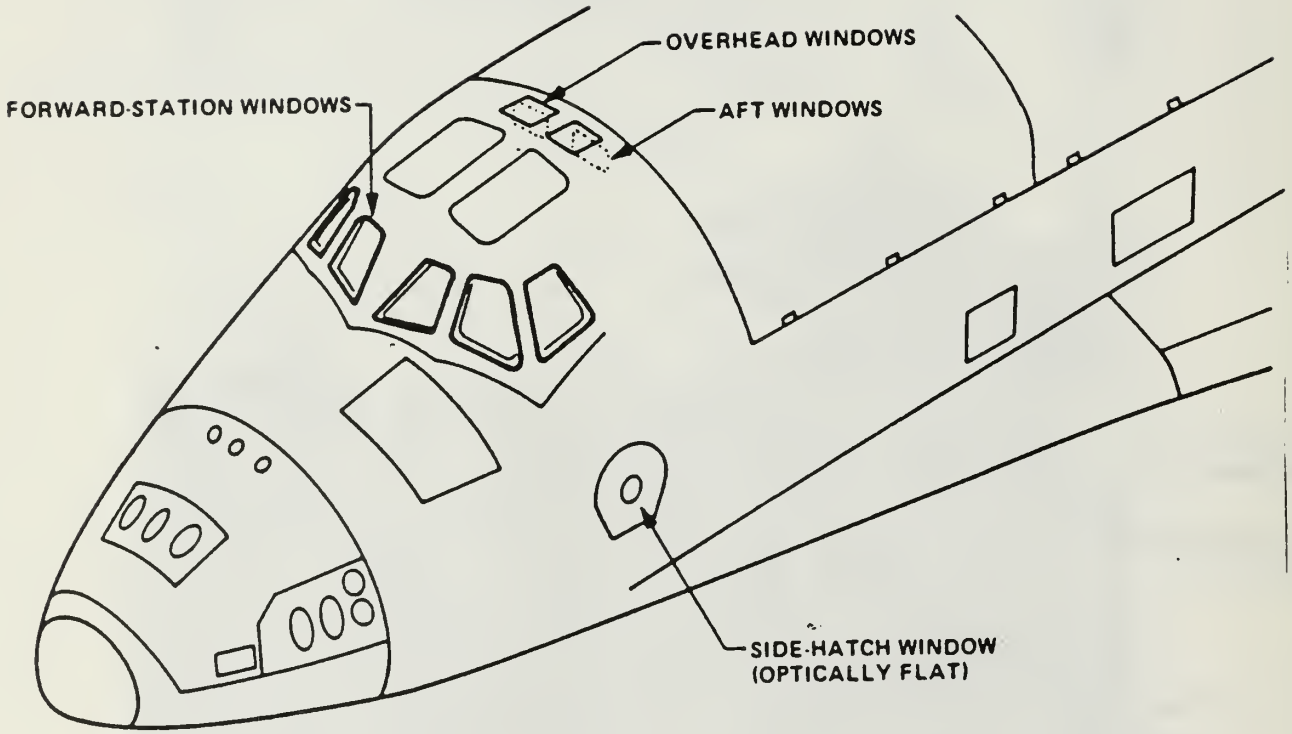

Fig. 3. Location of windows in Shuttle Orbiter (Nowakowski and Palmer, 1984)

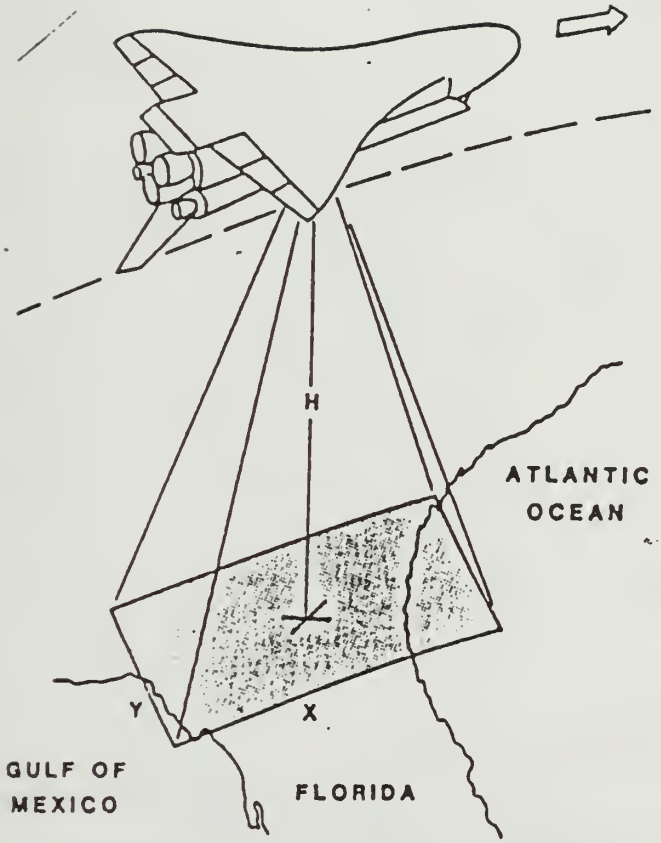

Fig. 4. Orbiter inverted position and direction of motion (Snow and Tomlinson, 1987)

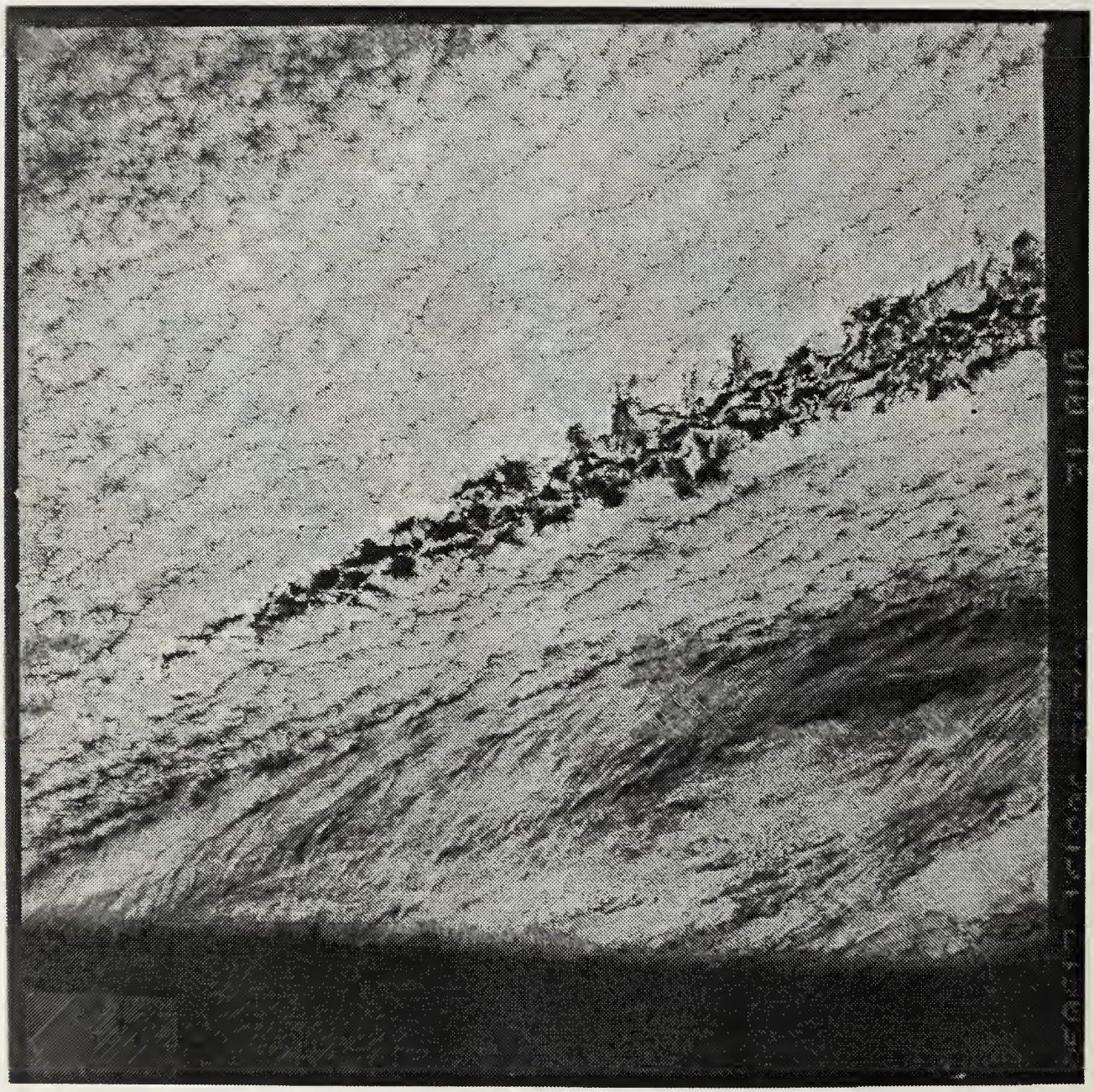

Fig. 5. Shuttle photograph (1618 GMT 17 June 1985) of western tip of dry slot (STS 51G-31010)

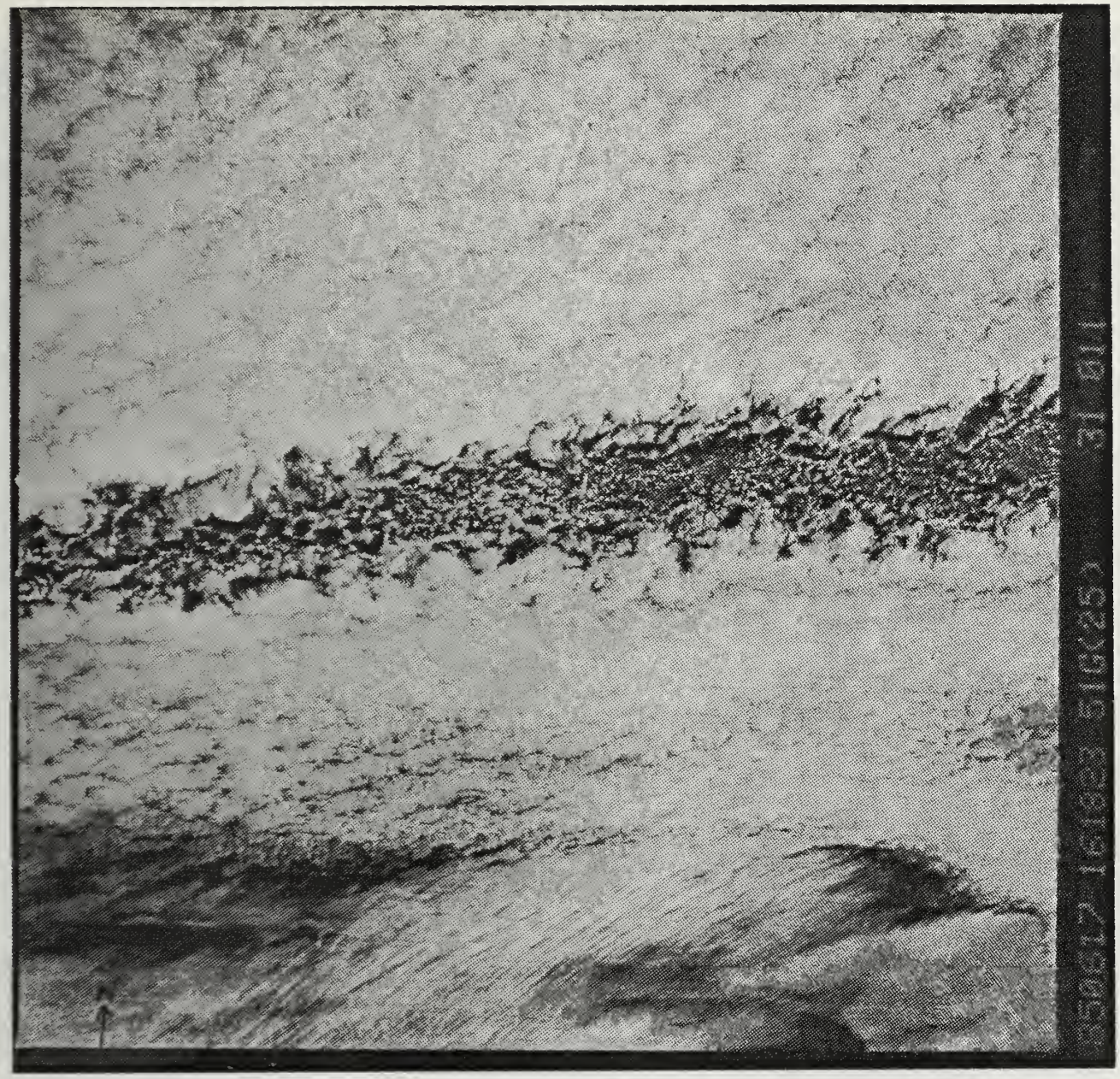

Fig. 6. Shuttle photograph (1618 GMT 17 June 1985) of west-central section of dry slot and surrounding stratocumulus clouds (STS 51G-31012)

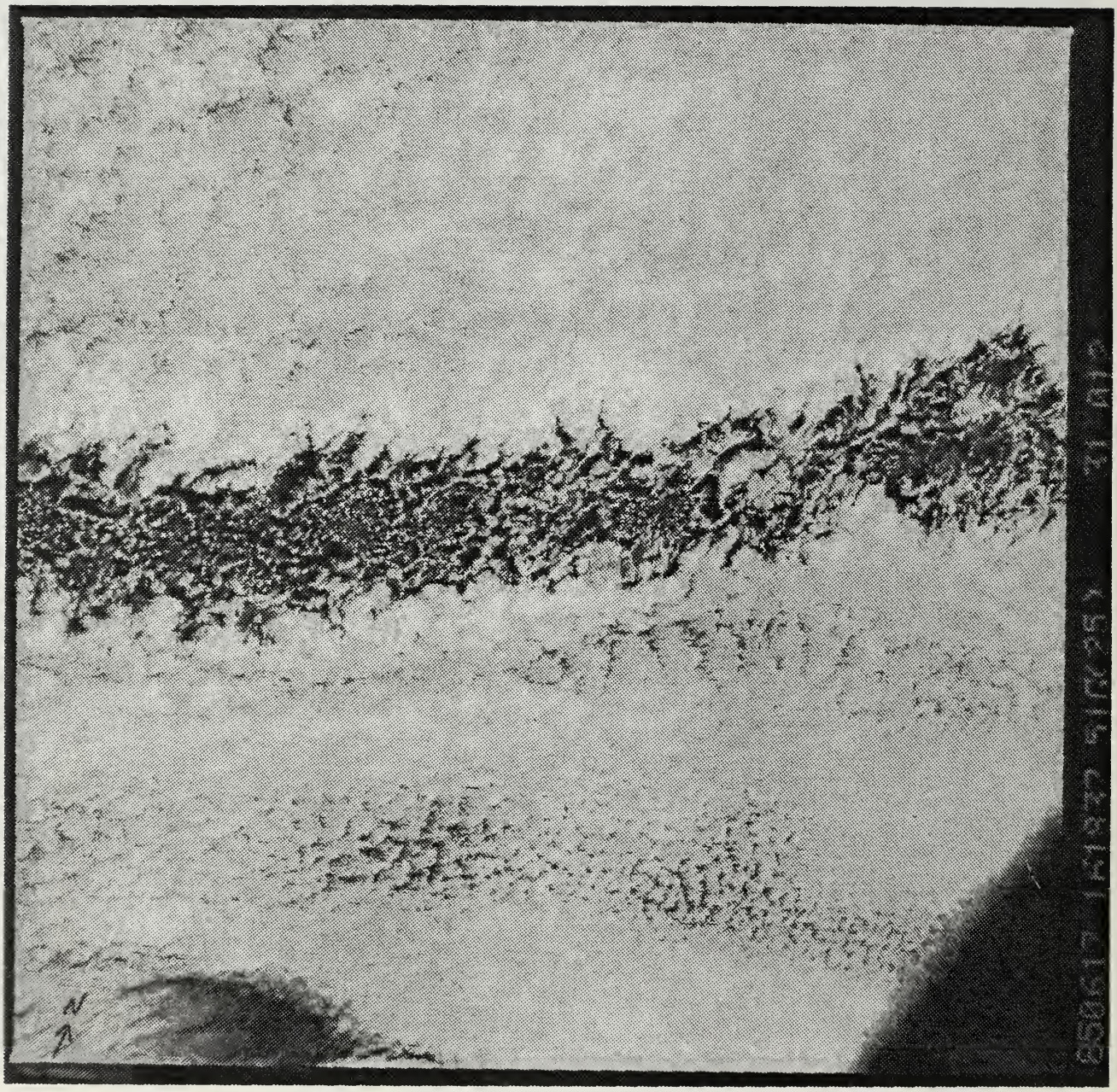

Fig. 7. Shuttle photograph (1618 GMT 17 June 1985) of central section of dry slot (STS 51G-31012)

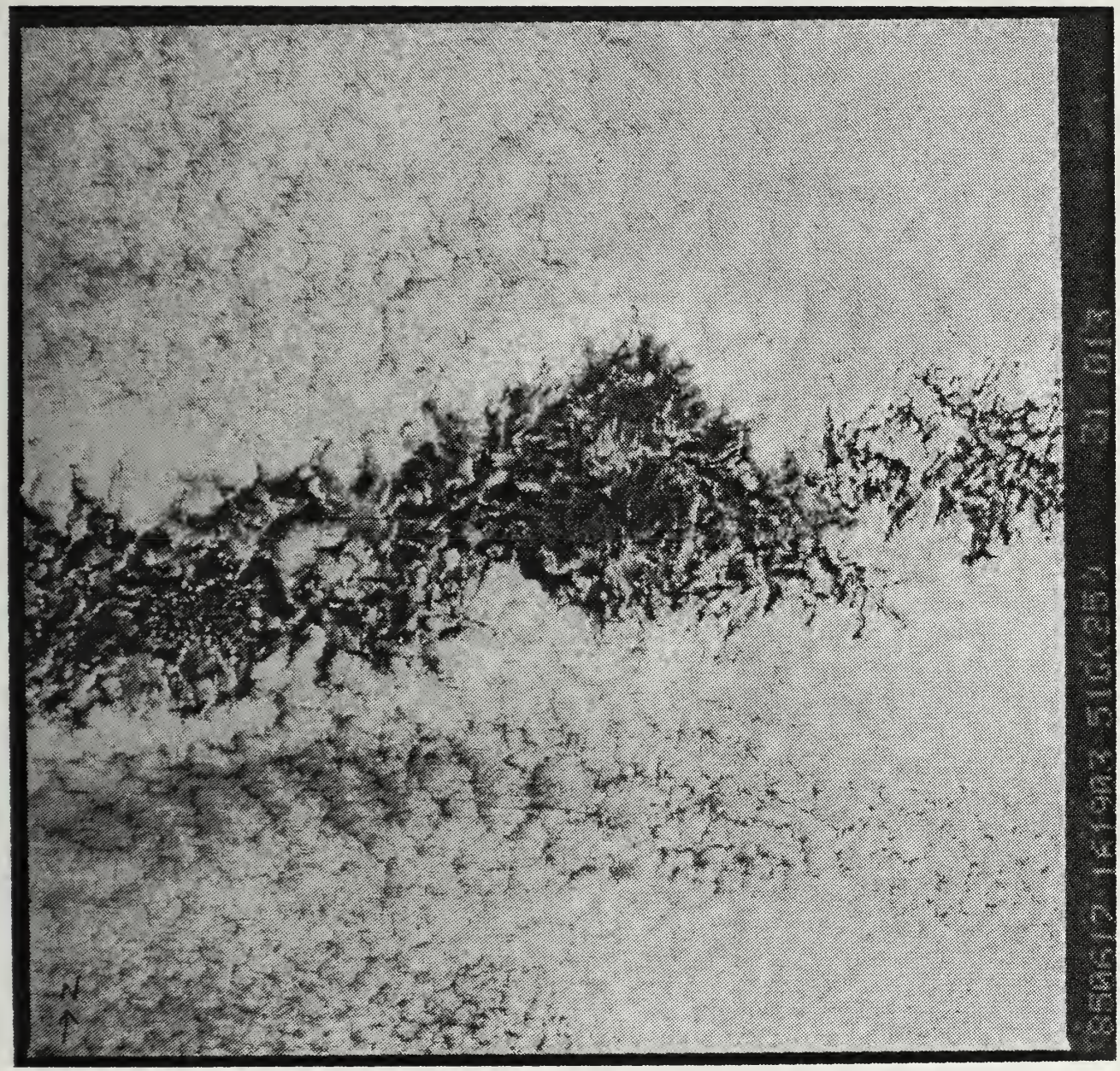

Fig. 8. Shuttle photograph (1619 GMT 17 June 1985) of eastern section of dry slot (STS 51G-31013)

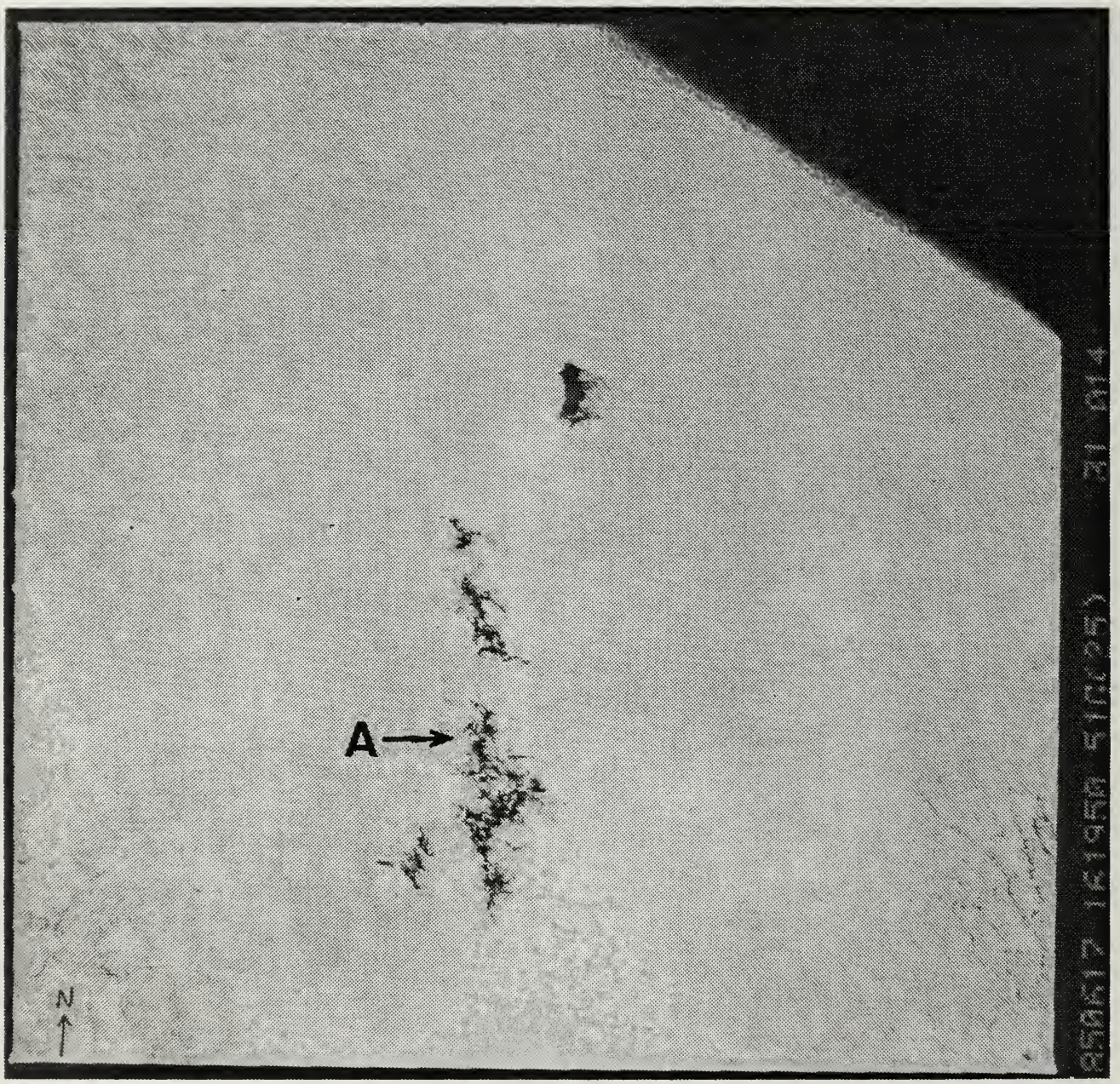

Fig. 9. Shuttle photograph (1619 GMT 17 June 1985) of Guadalupe Island, the Karman vortices, and the new dry slot to the southwest (STS 51G-31014)

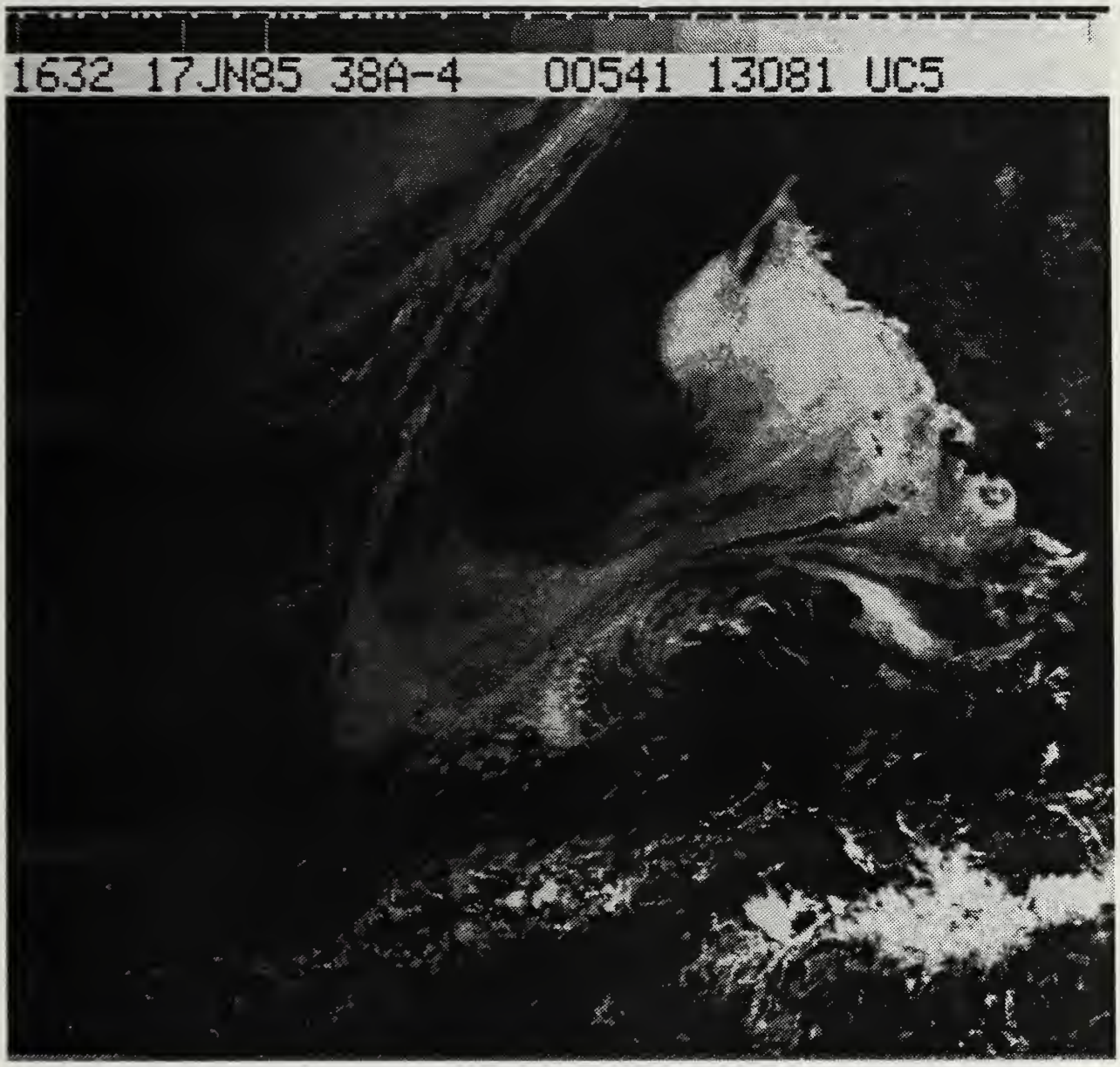

Fig. 10. 1632 GMT GOES visible image of 17 June 1985 with dry slot in center of image

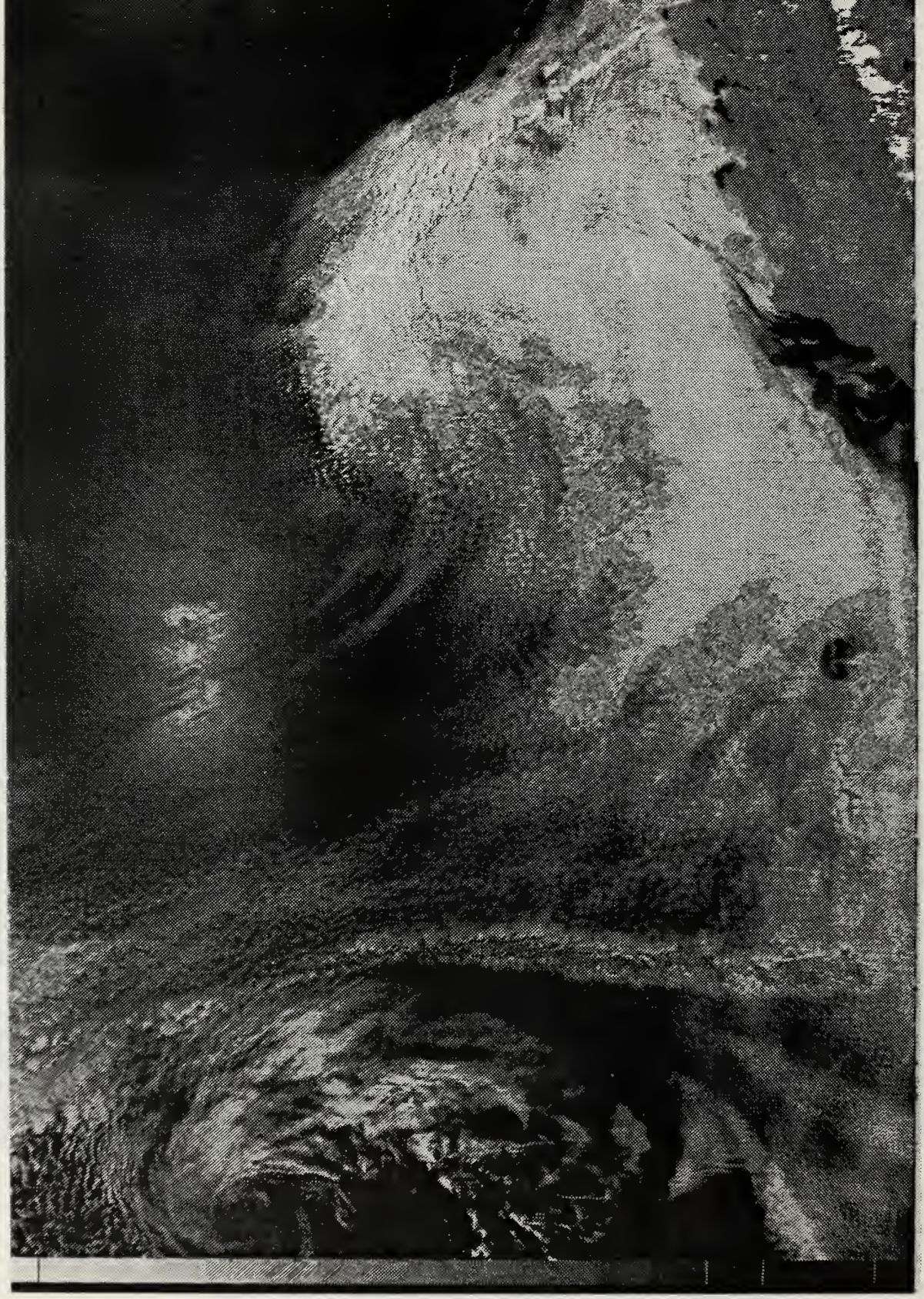

Fig. 11. 2233 GMT NOAA (AVHRR) near-infrared image of 17 June 1985

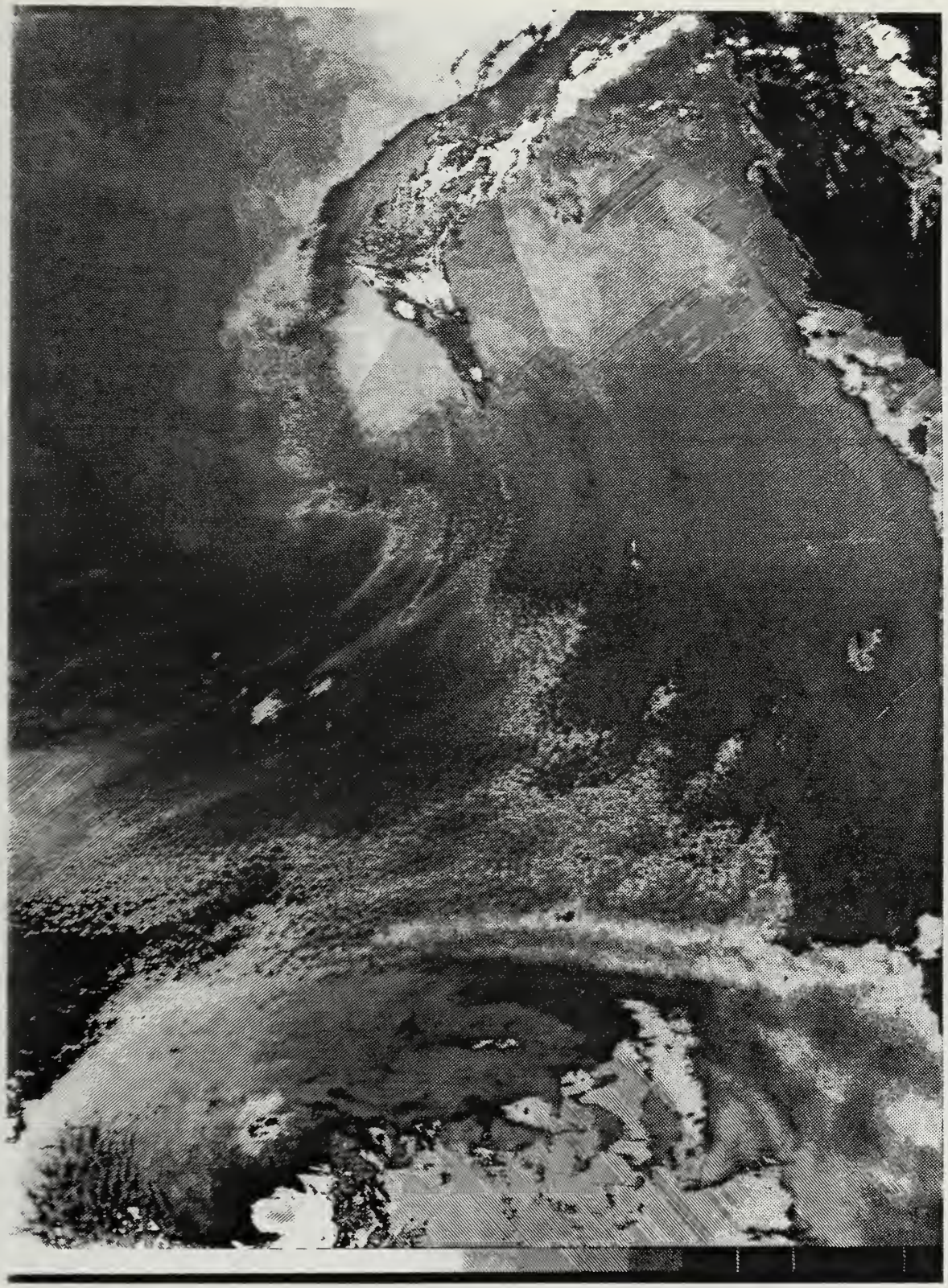

Fig. 12. 2233 GMT NOAA (AVHRR) channel 4 infrared image of 17 June 1985

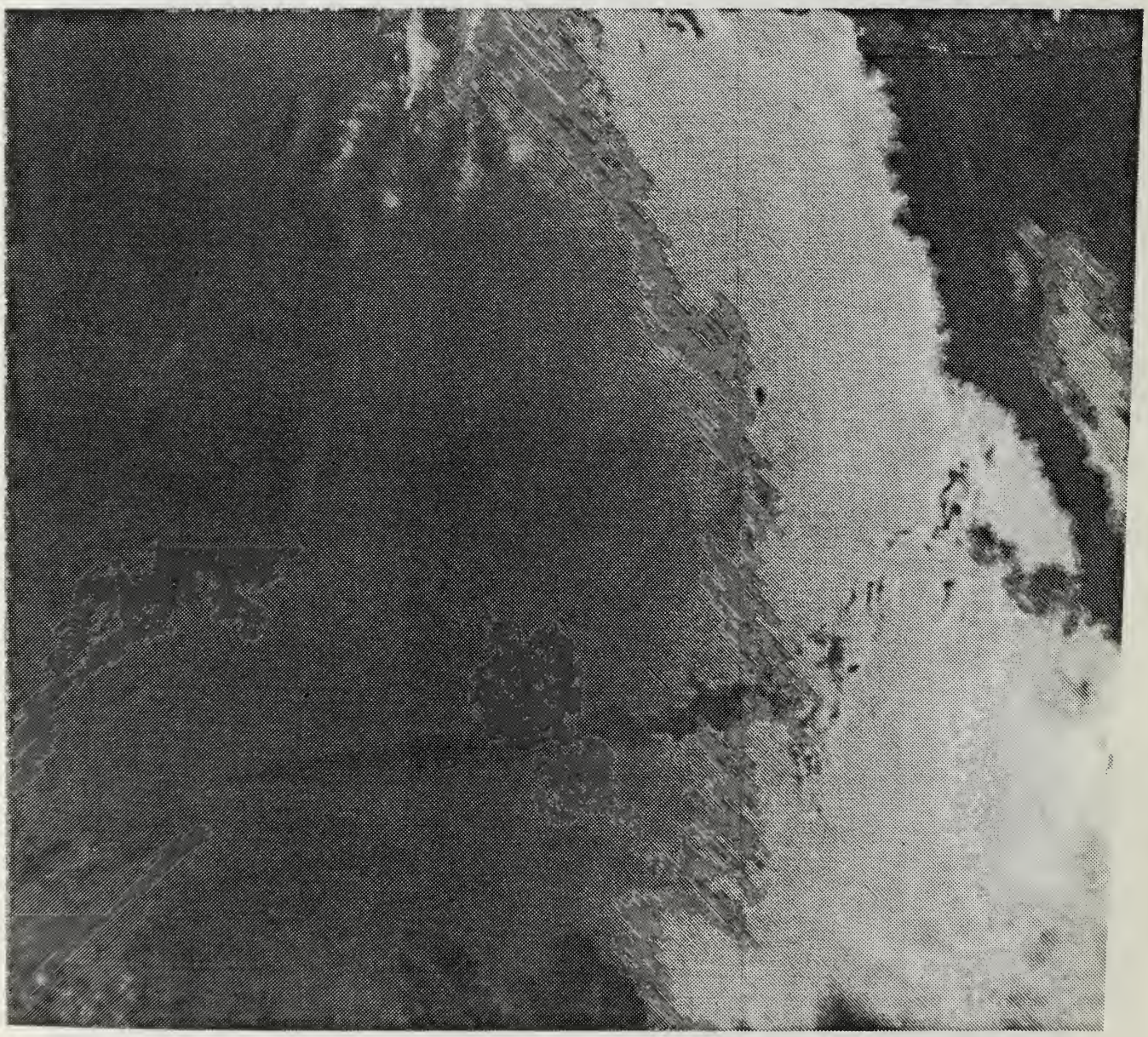

Fig. 13. 1415 GMT DMSP visible image of 17 June 1985 with dry slot in center and Guadalupe Island to the north

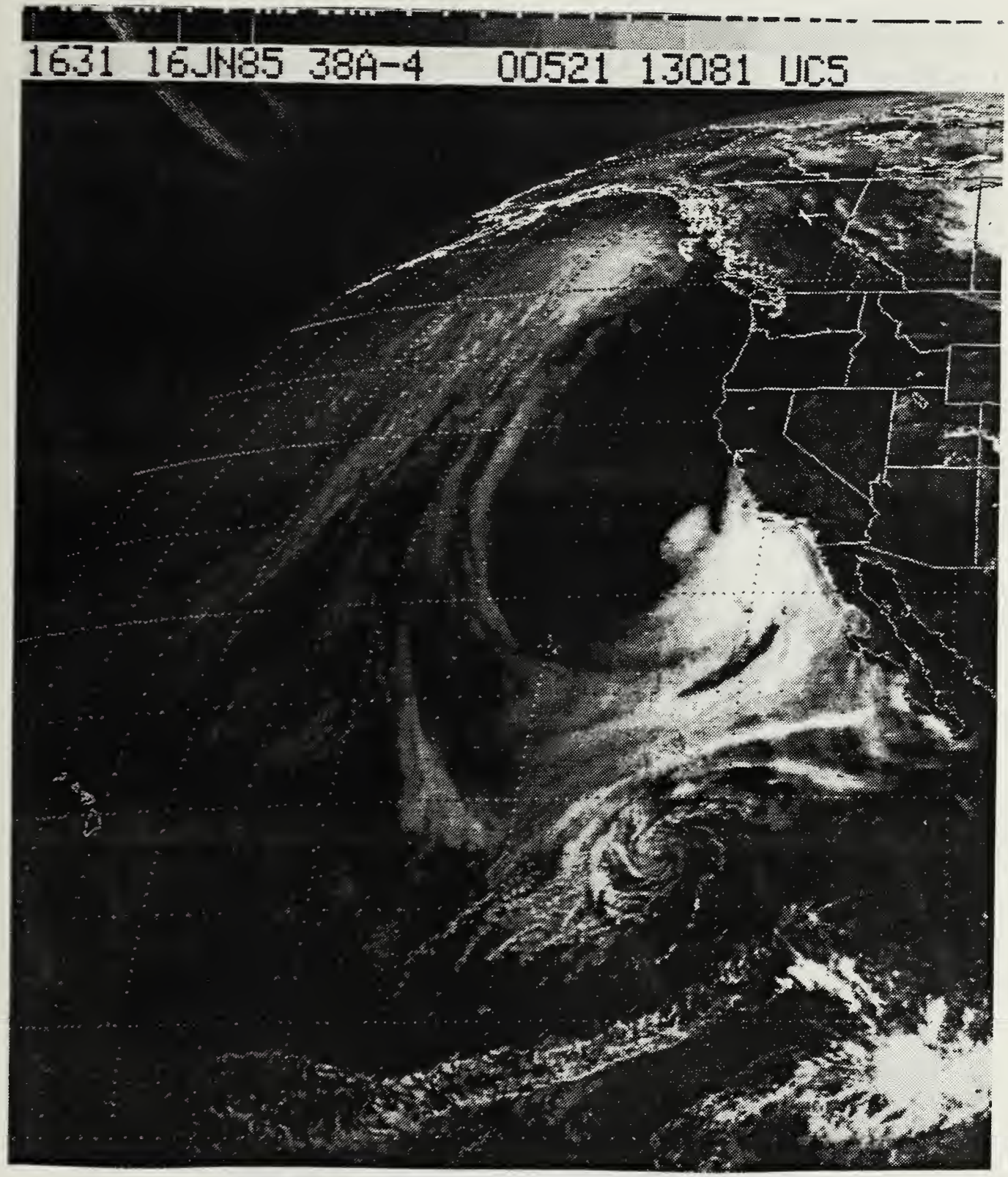

Fig. 14. 1631 GMT GOES visible image of 16 June 1985 with dry slot in early stages

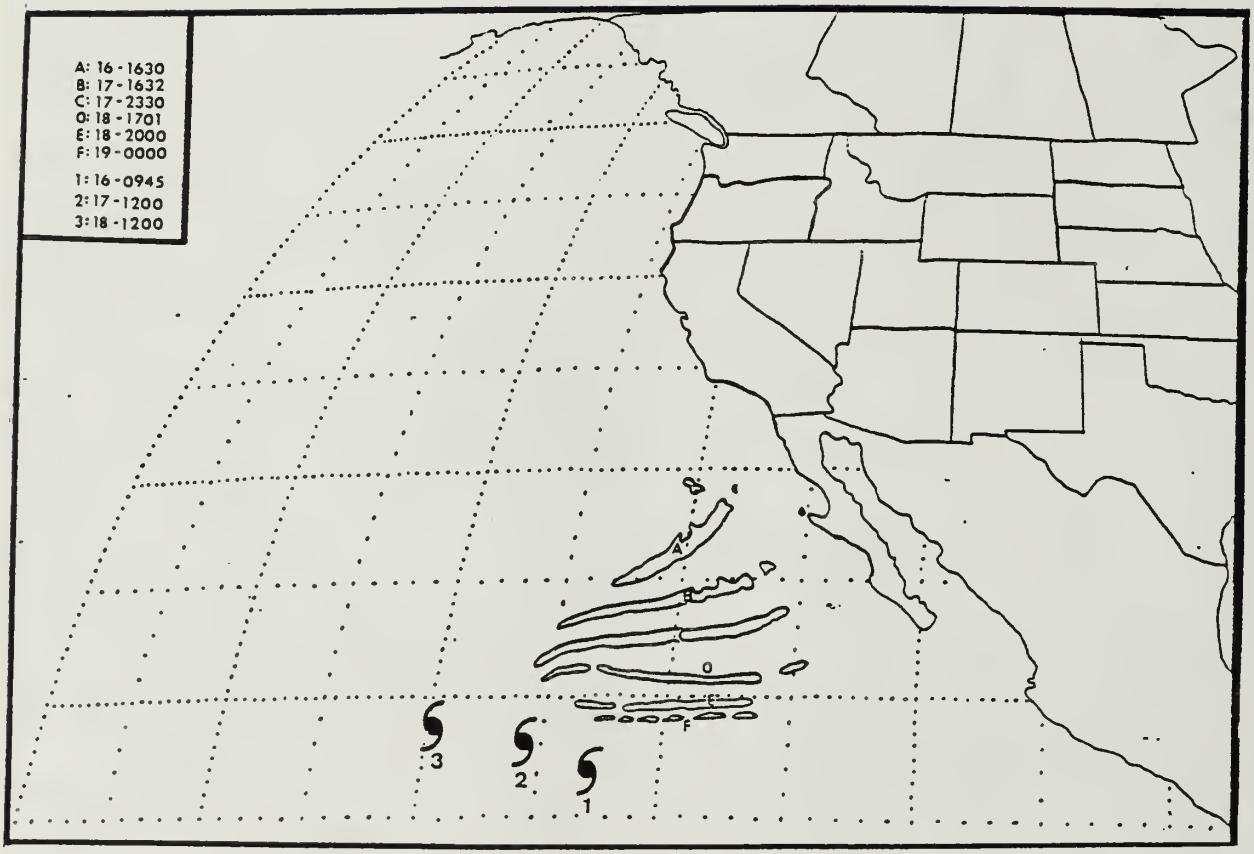

Fig. 15. Evolution of the dry slot from 1630 GMT 16 June to 0000 GMT 19 June

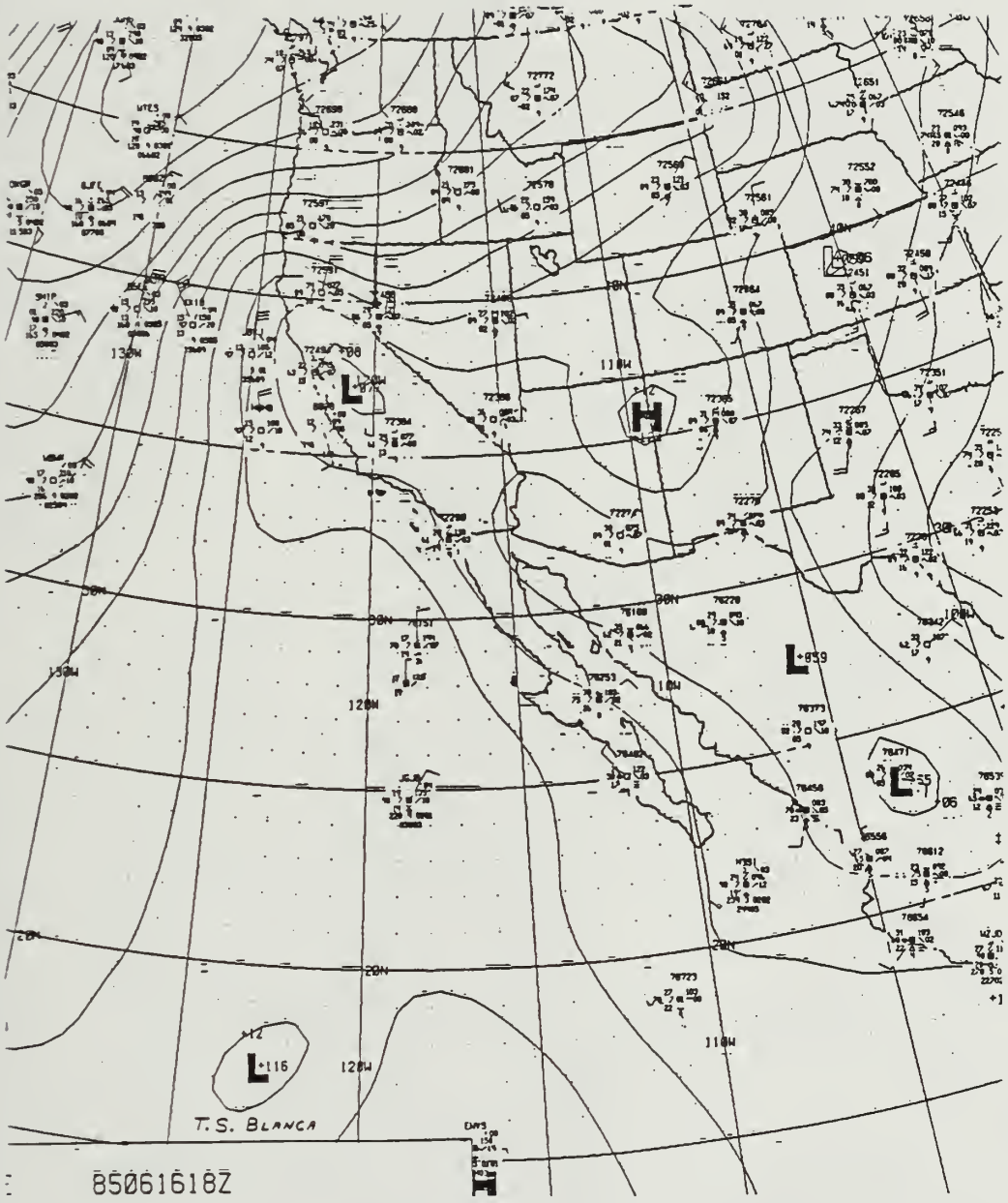

Fig. 16. Surface analysis of eastern Pacific for 1800 GMT 16 June 1985

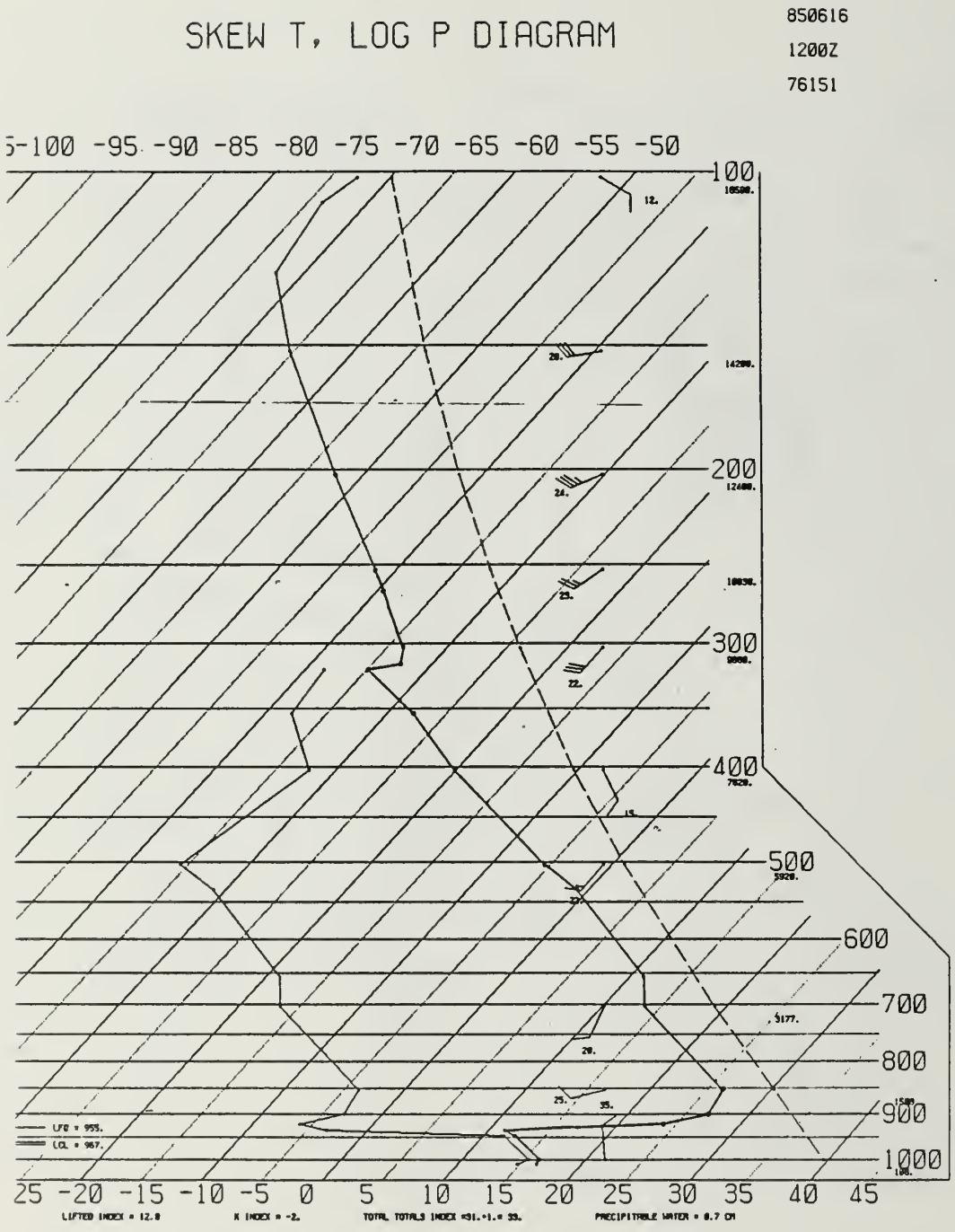

Fig. 17. Sounding for Guadalupe Island (76151) for 1200 GMT 16 June 1985

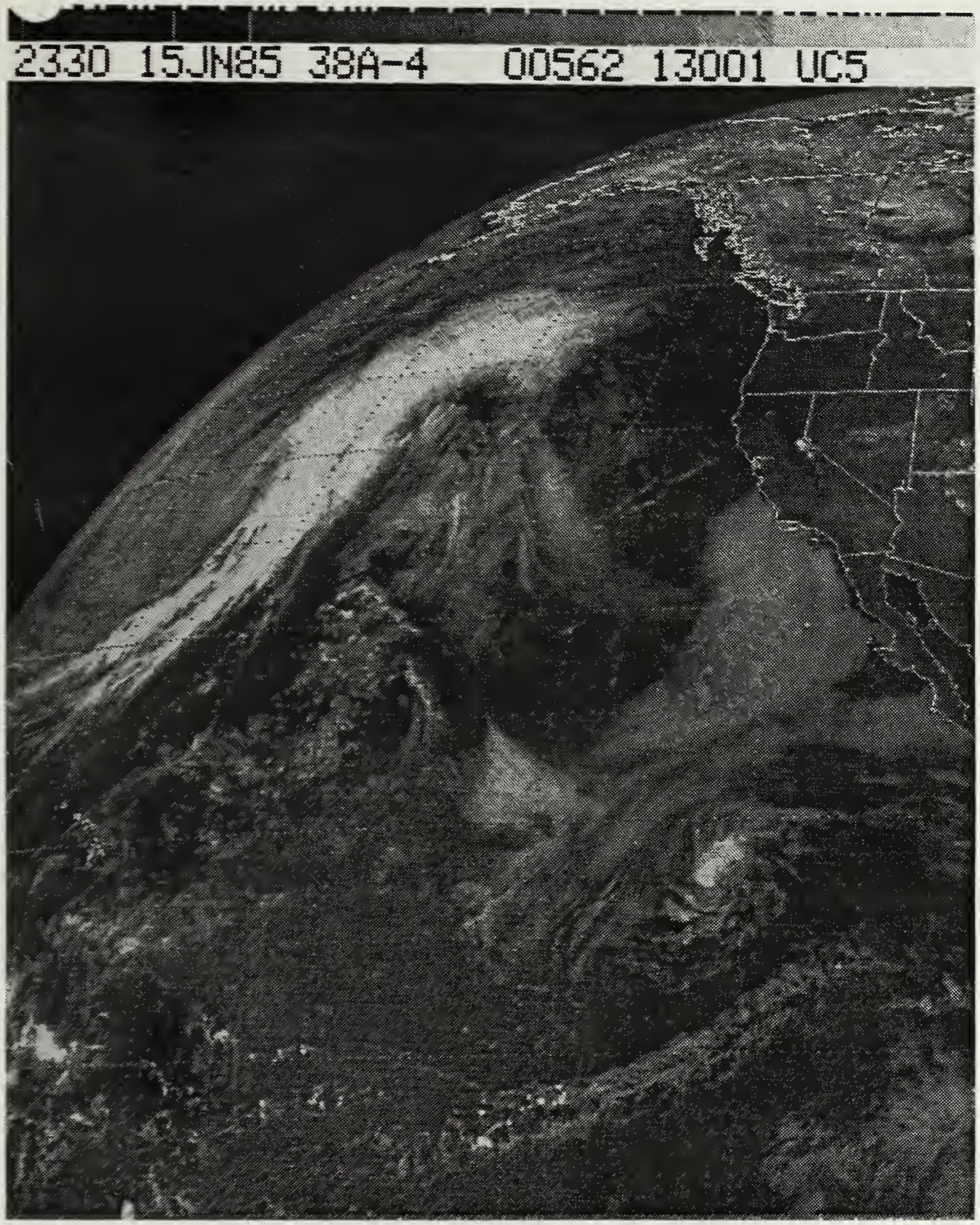

Fig. 18. 2330 GMT GOES visible image of 15 June 1985 before dry slot formation

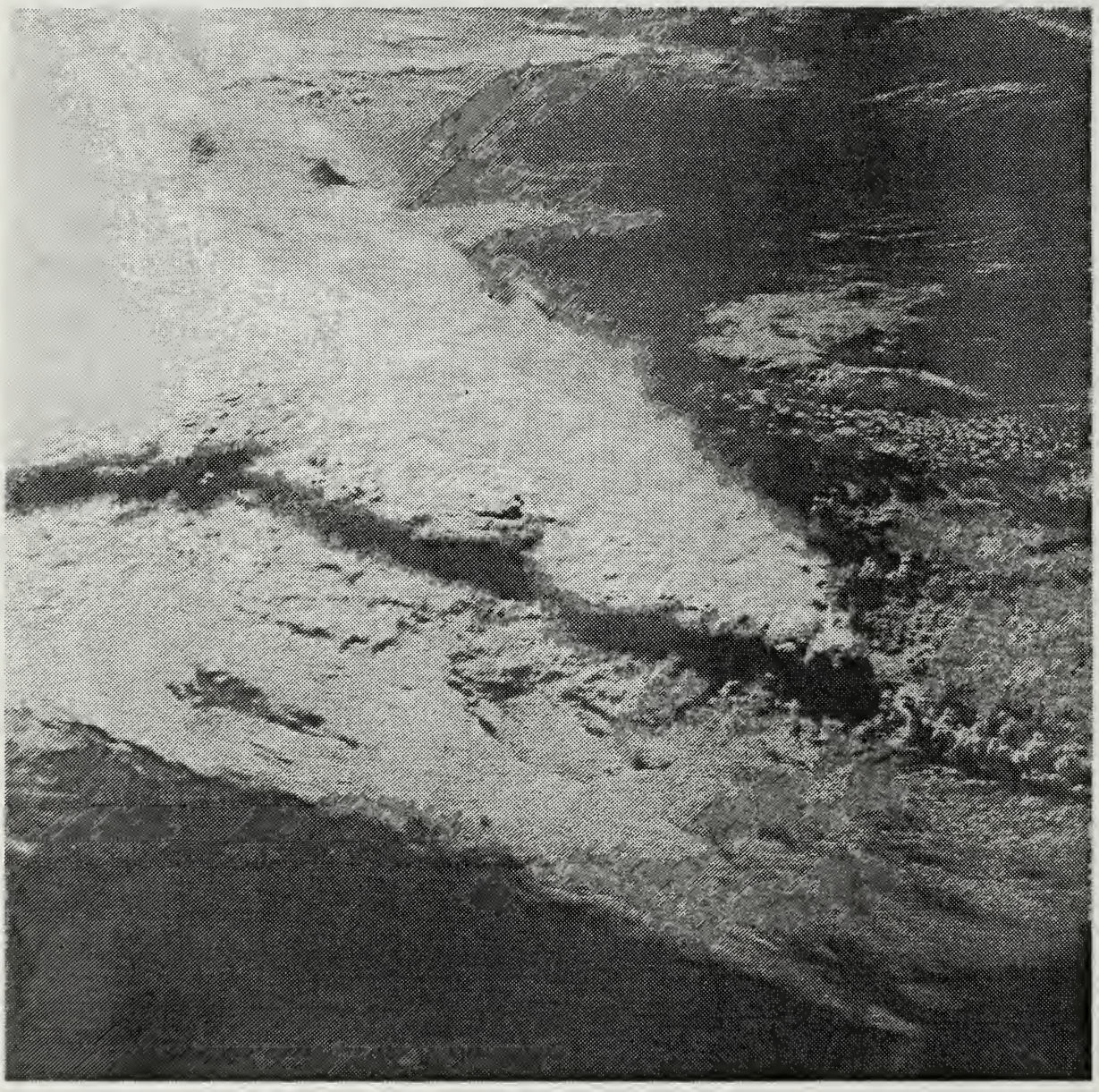

Fig. 19. Shuttle photograph (1338 GMT 9 April 1984) of enhanced-V cloud formation over Florida and the Gulf of Mexico (S13-392008)

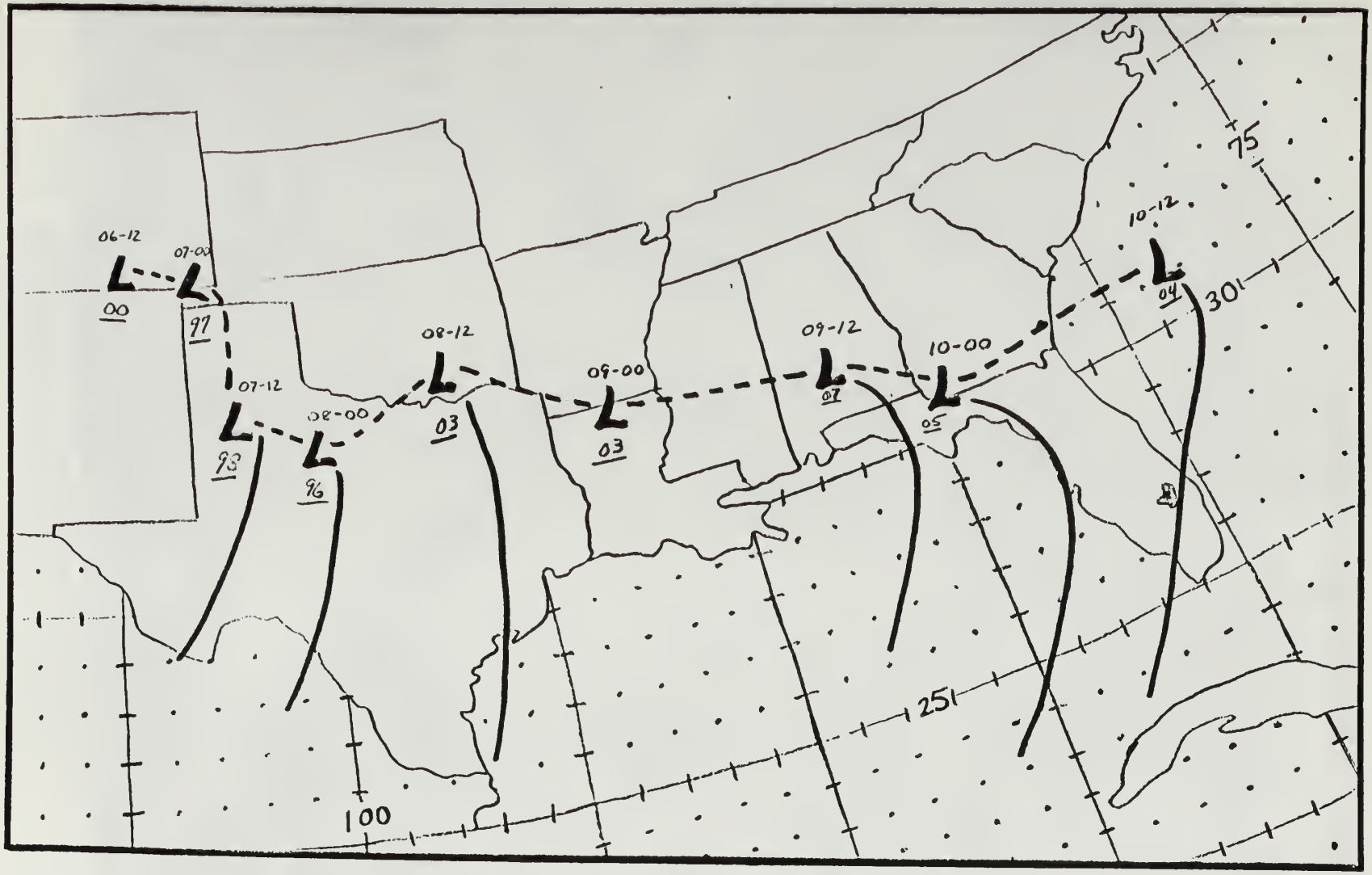

Fig. 20. Surface positions of low pressure center across southern states; 1200 GMT 6 April-1200 GMT 10 April

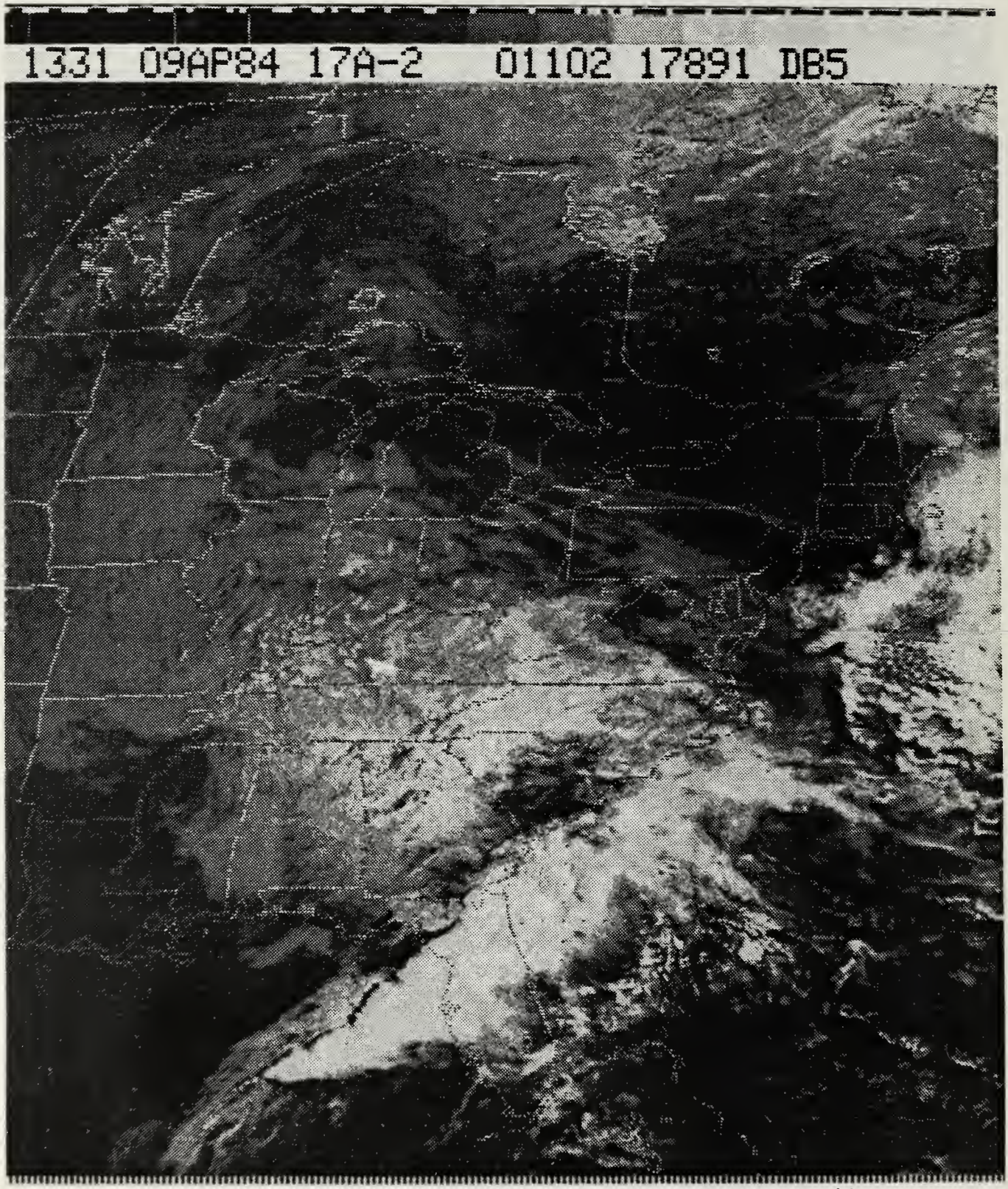

Fig. 21. 1331 GMT GOES visible image of 9 April 1984 with enhanced-V over Florida and the Gulf of Mexico

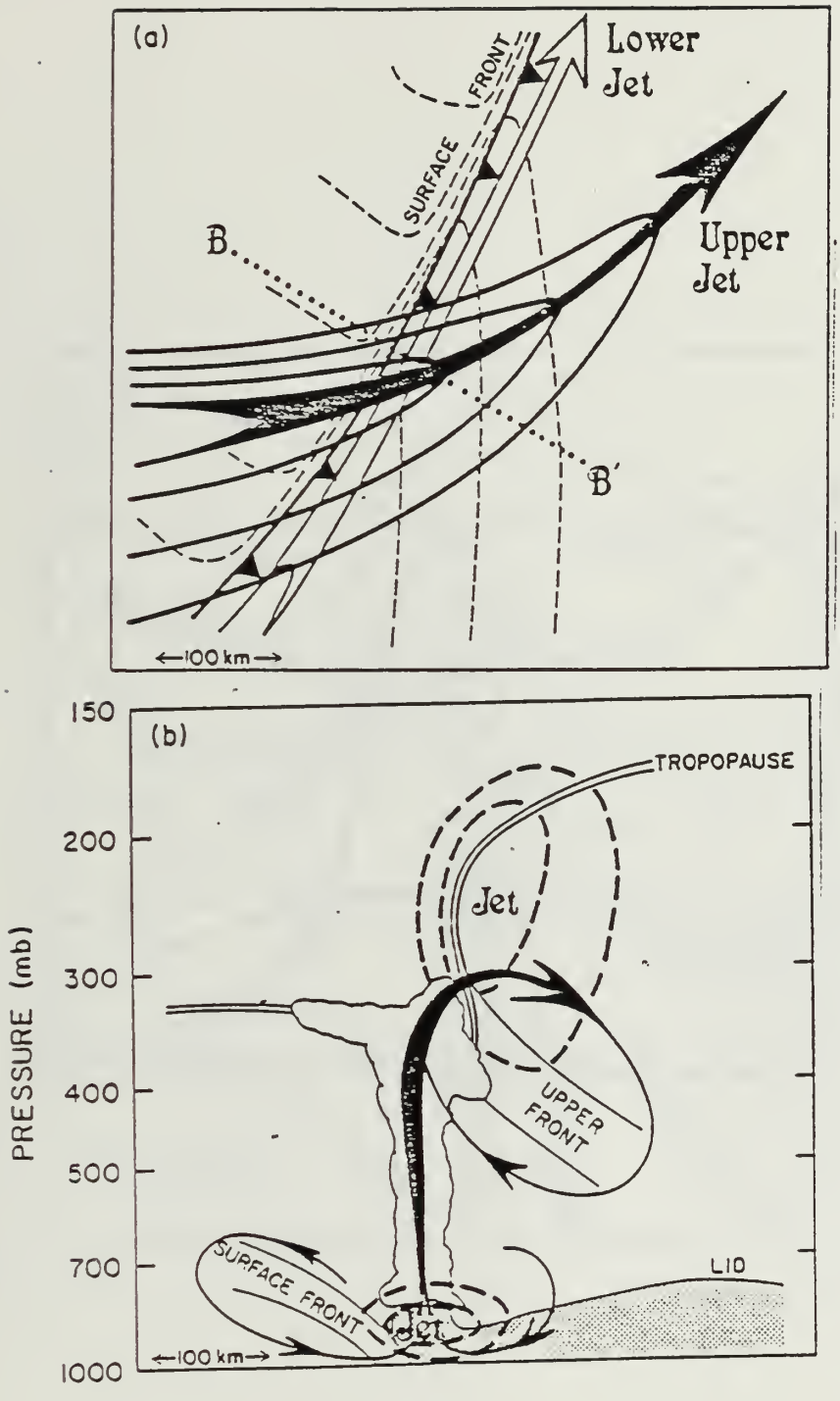

Fig. 22. Vertically coupled upper and lower-tropopheric jet front systems and their associated secondary circulations (Shapiro, 1983)

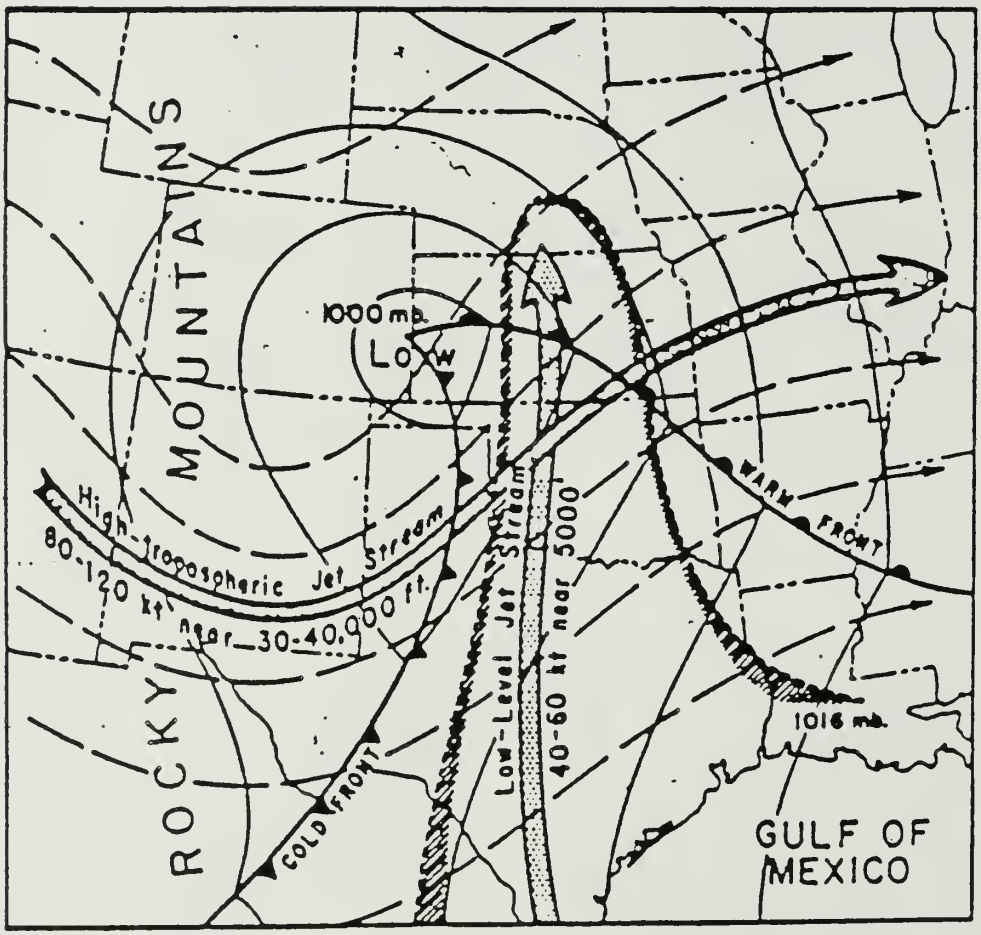

Fig. 23. Schematic features of a severe weather outbreak (Newton, 1967)

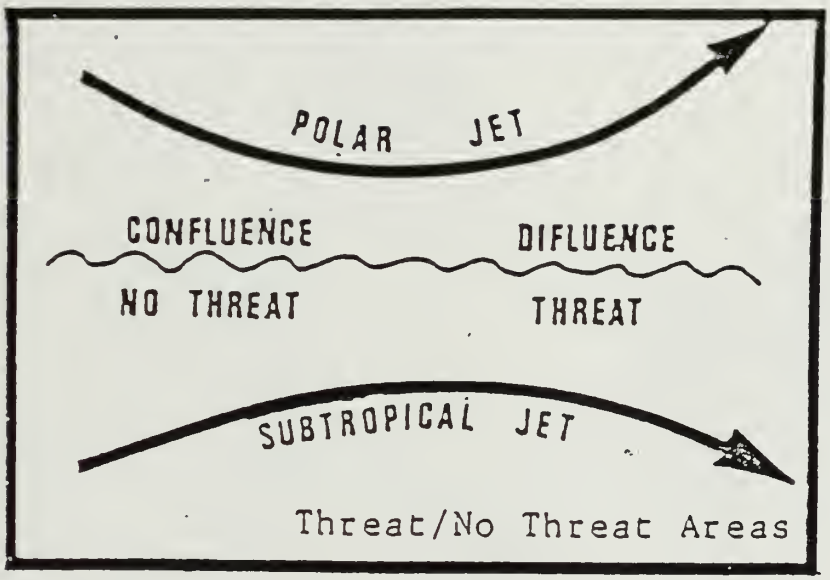

Fig. 24. Area of confluence (NO threat) and difluence (threat) in region where the polar and subtropical jets converge and then diverge (Wilderotter, 1981)

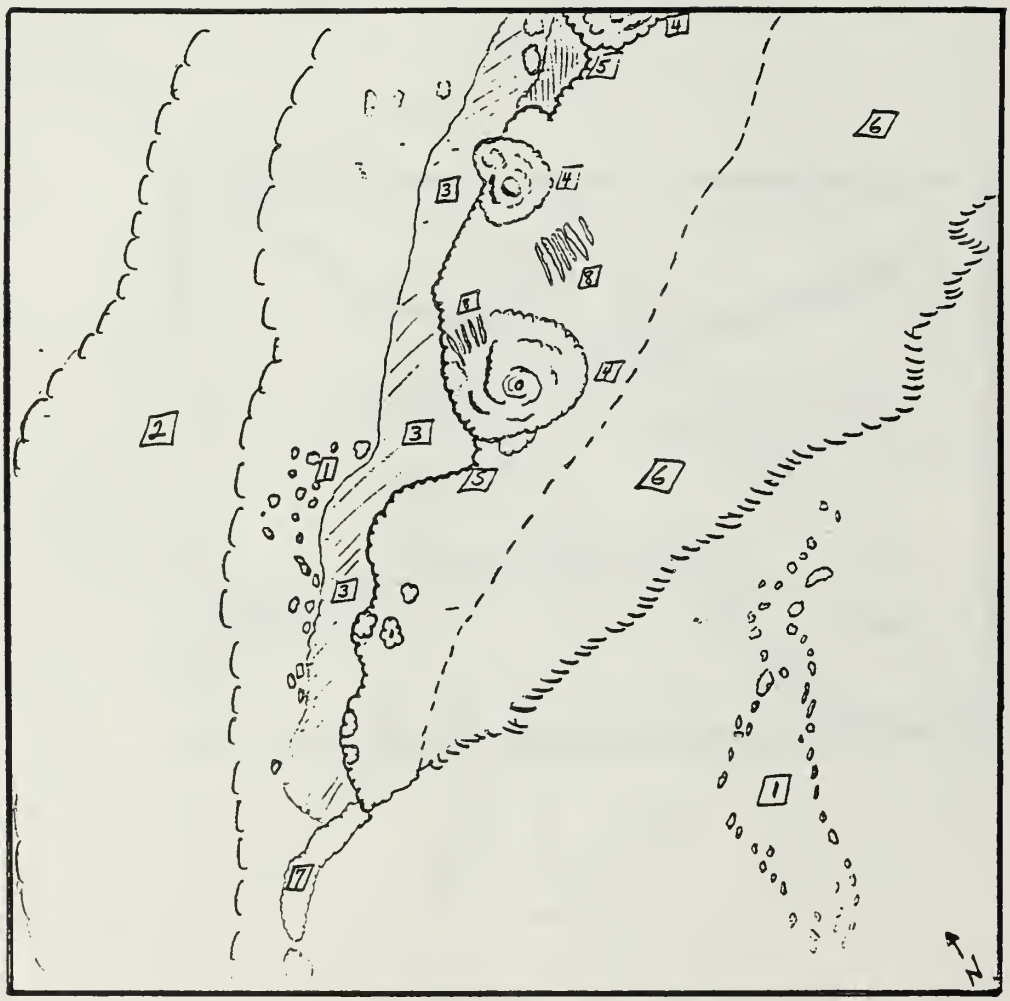

Fig. 25. Sketch of the eight features of the enhanced-V

Fig. 26. Shuttle photograph (1338 GMT 9 April 1984) of enhanced-V with 100 mm lens (S13-402134)

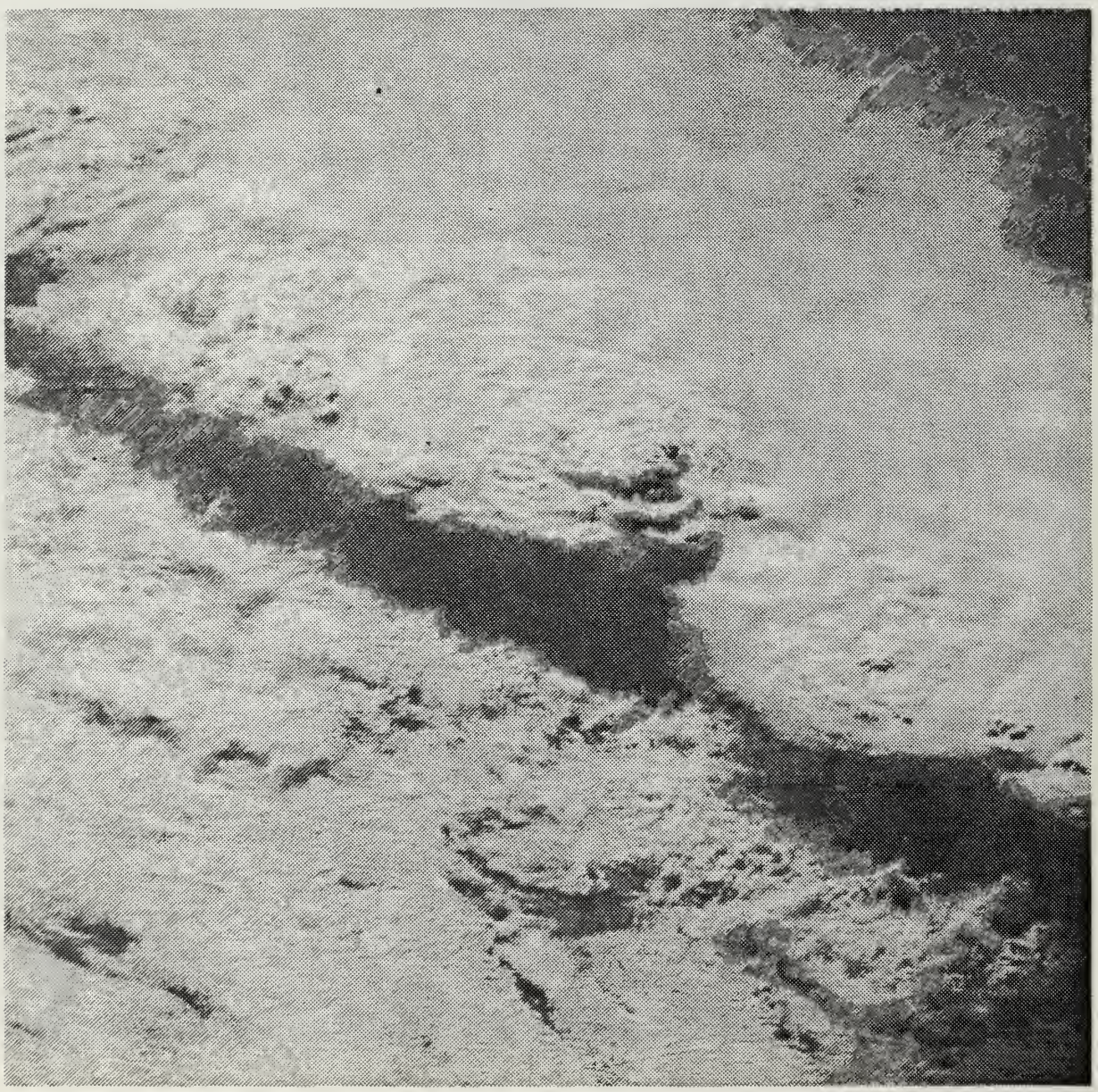

Fig. 27. Shuttle photograph (1338 GMT 9 April 1984) of enhanced-V with 250 mm lens (S13-392008)

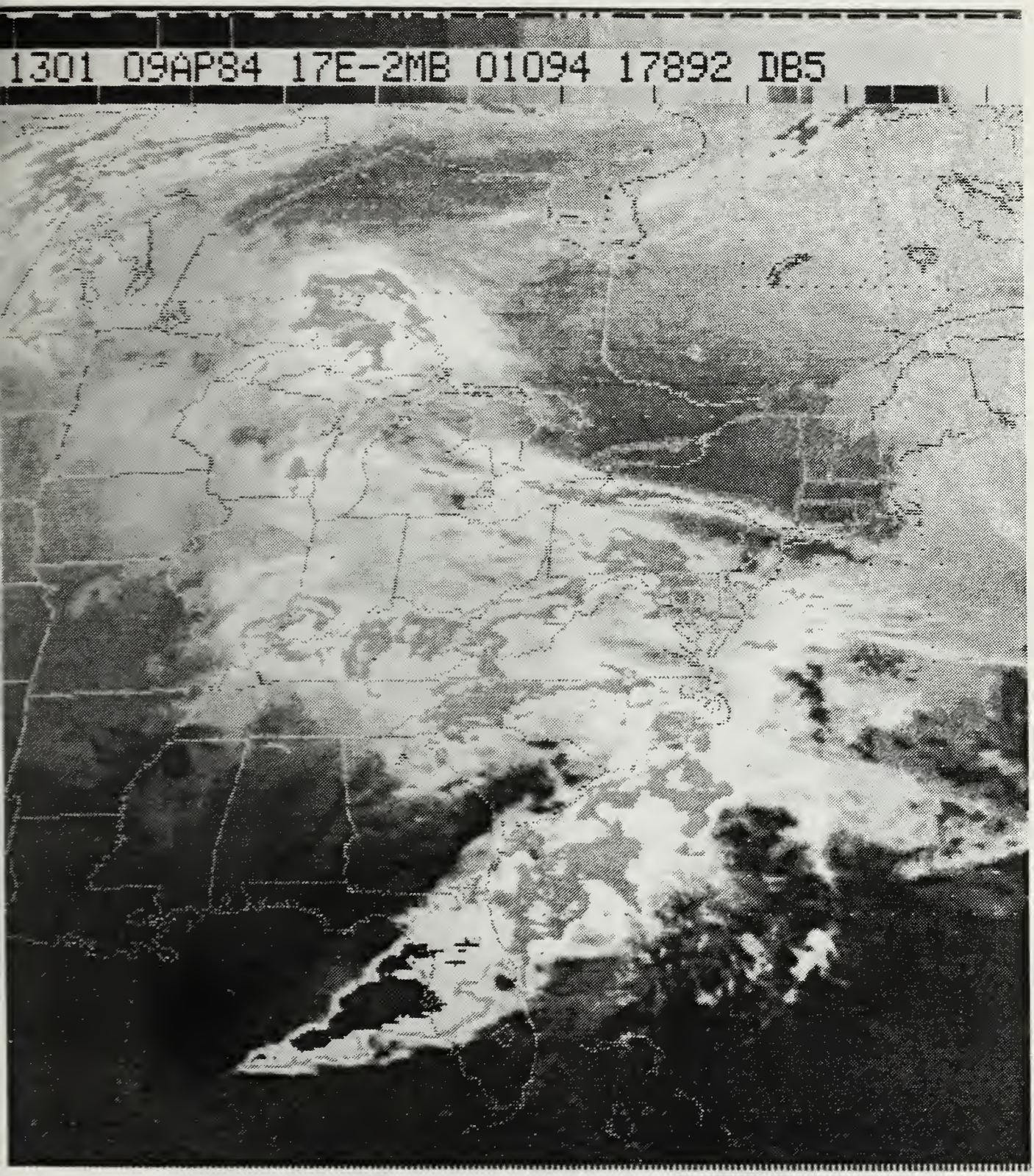

Fig. 28. 1301 GMT GOES enhanced infrared (MB) of 9 April 1984

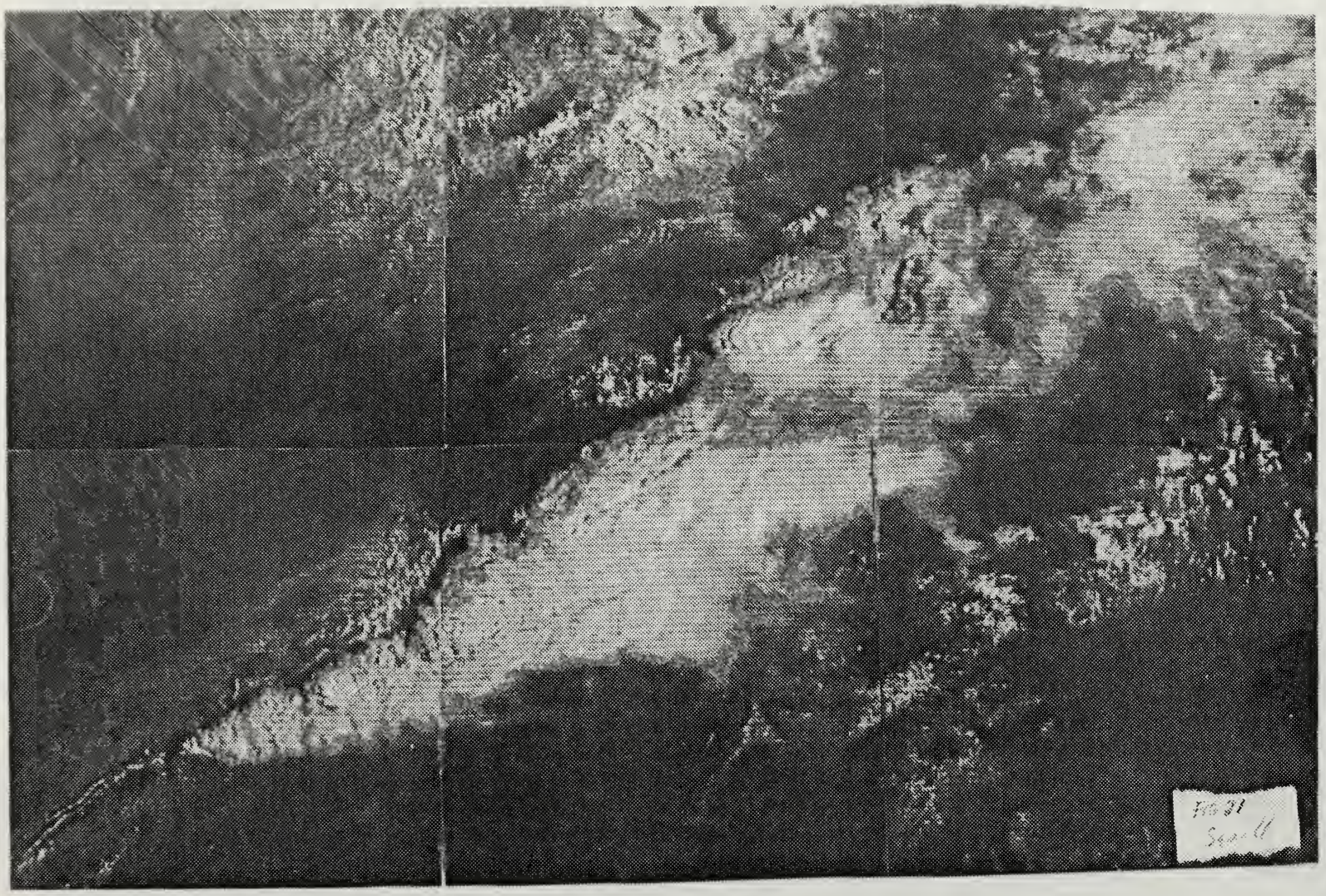

Fig. 29. 1331 GMT GOES visible image full resolution (1 km) of 9 April 1984

Fig. 30. 1338 GMT GOES enhanced infrared image (original colored) of 9 April 1984

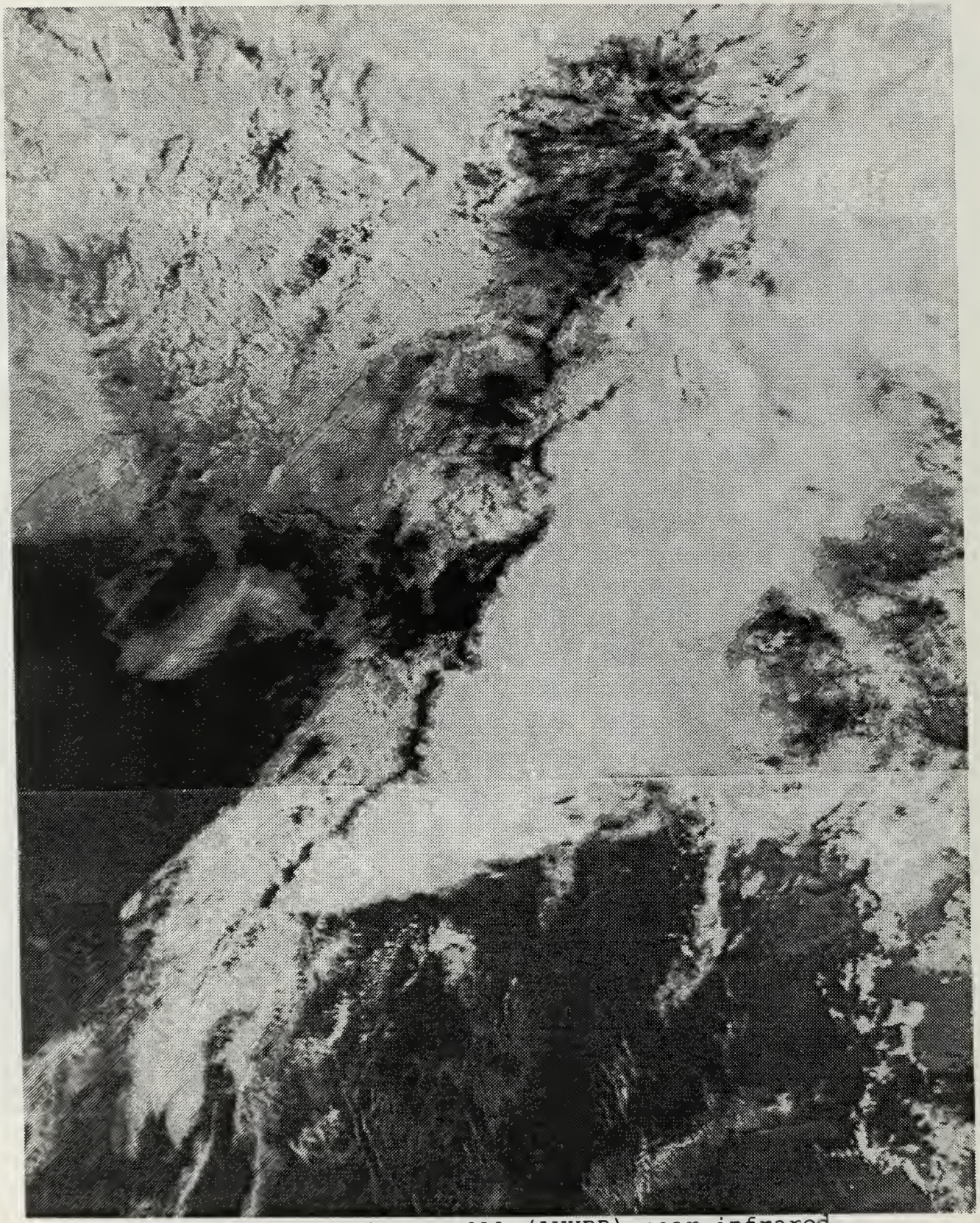

Fig. 31. 1336 GMT NOAA (AVHRR) near infrared (channel 2) image of 9 April 1984

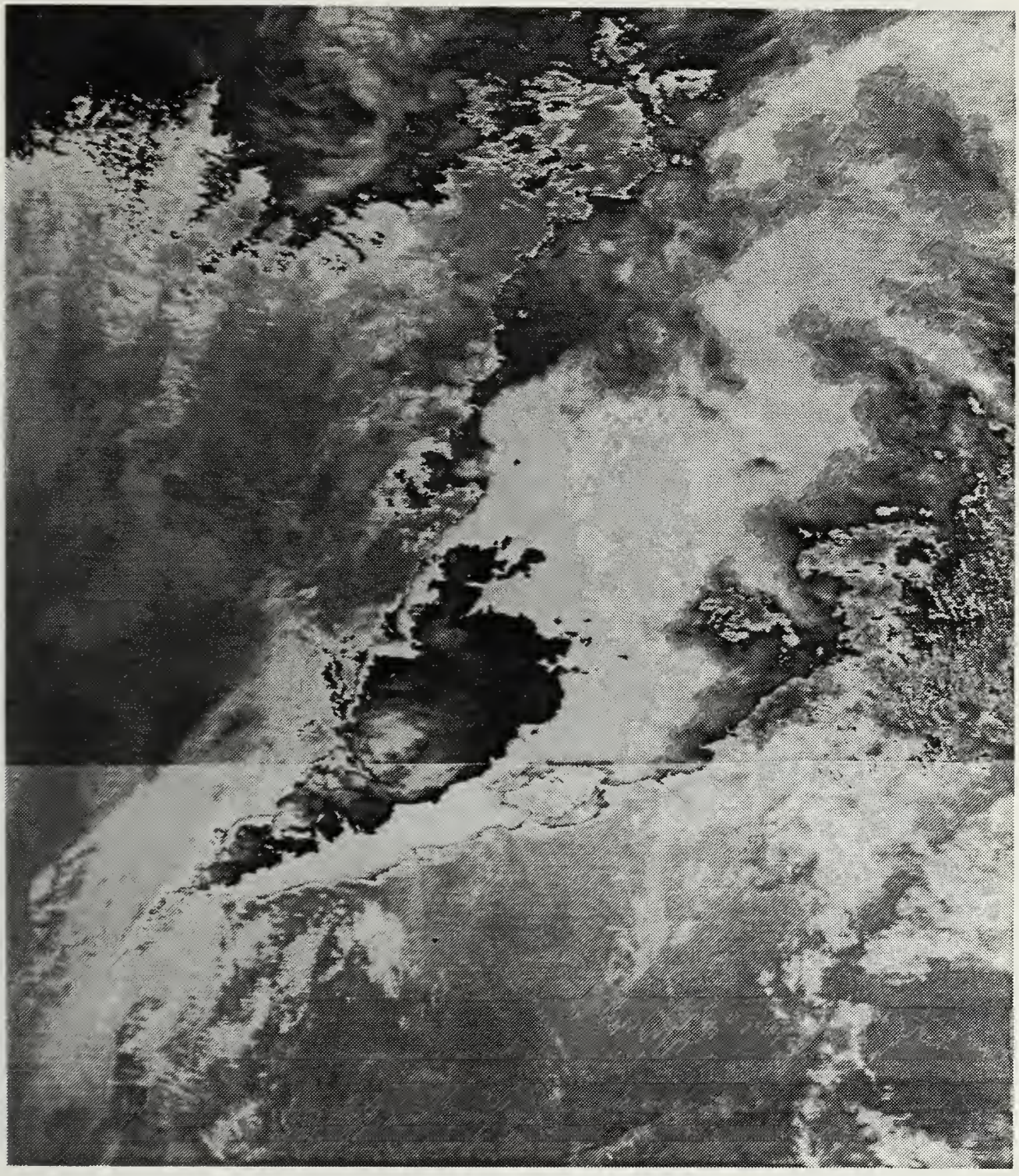

Fig. 32. 1336 GMT NOAA (AVHRR) enhanced infrared (channel 4) image of 9 April 1984

Fig. 33. 1336 GMT NOAA (AVHRR) visivle (channel 1) image of 9 April 1984

Fig. 34. 1336 GMT NOAA (AVHRR) enhanced infrared (original colored) image of 9 April 1984

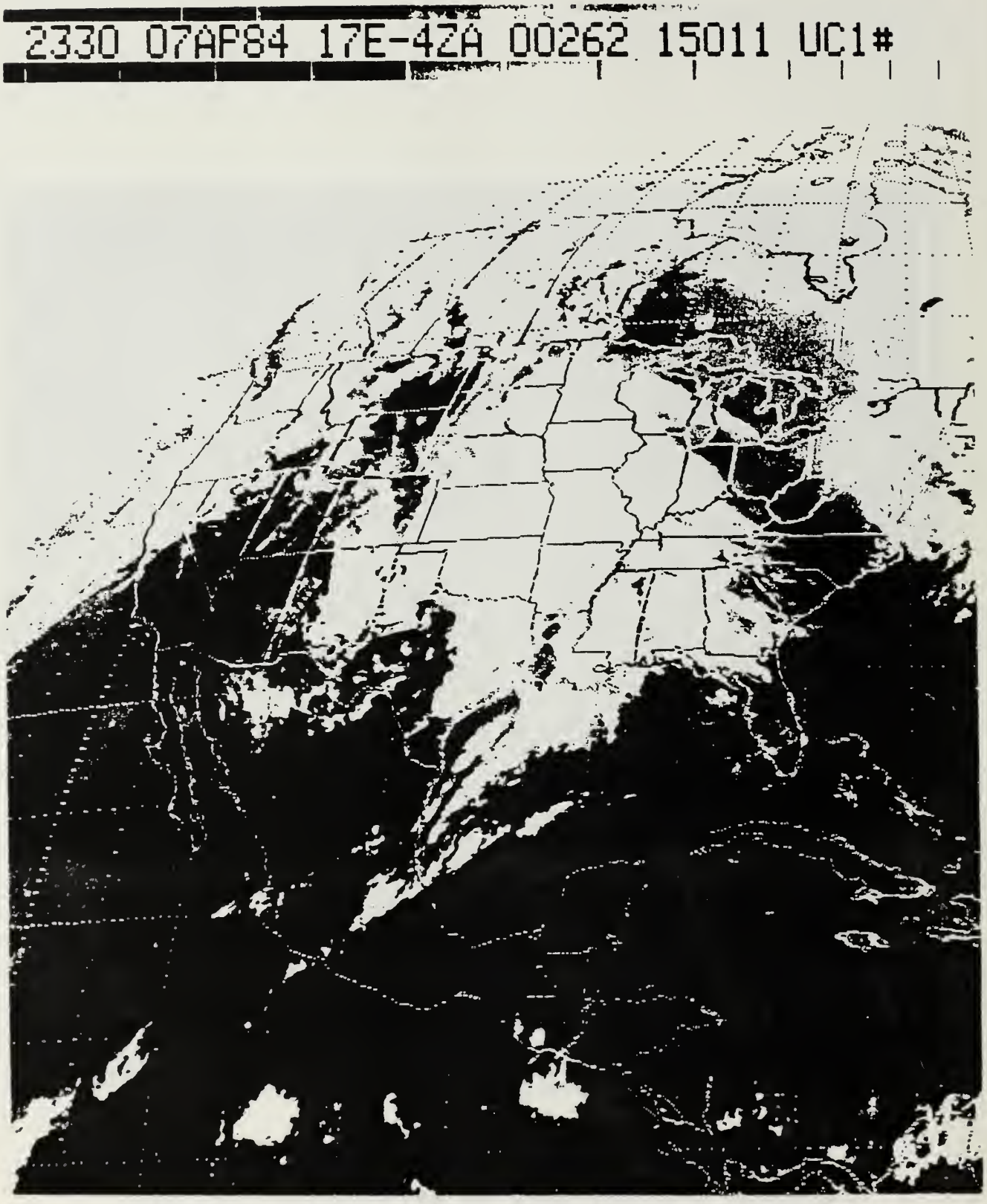

Fig. 35. 2330 GMT GOES infrared image of 7 April 1984 with enhanced-V over eastern Texas

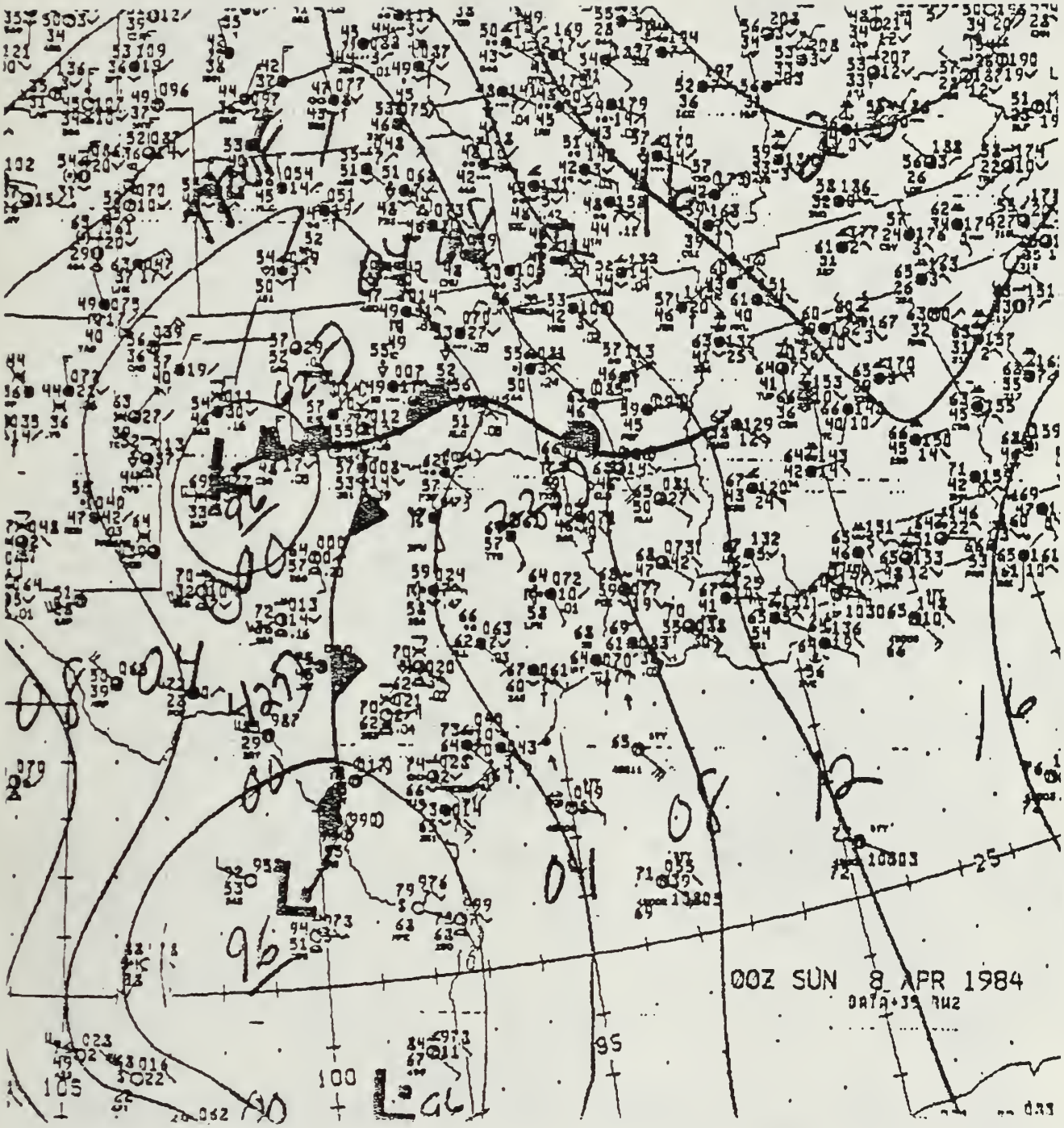

Fig. 36. NMC Surface Analysis, 0000 GMT 8 April 1984

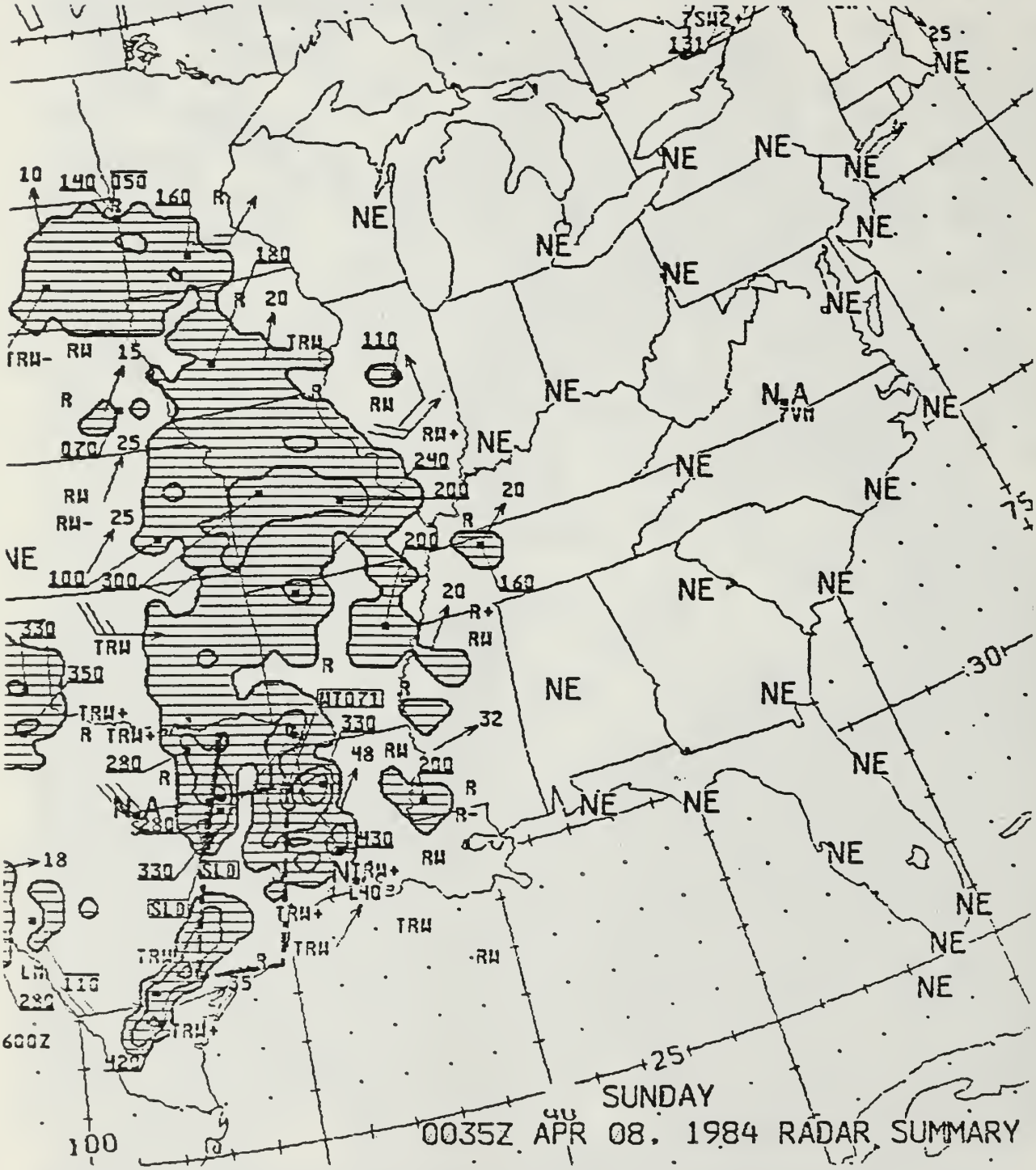

Fig. 37. NMC Radar Summary, 0035 GMT 8 April 1984

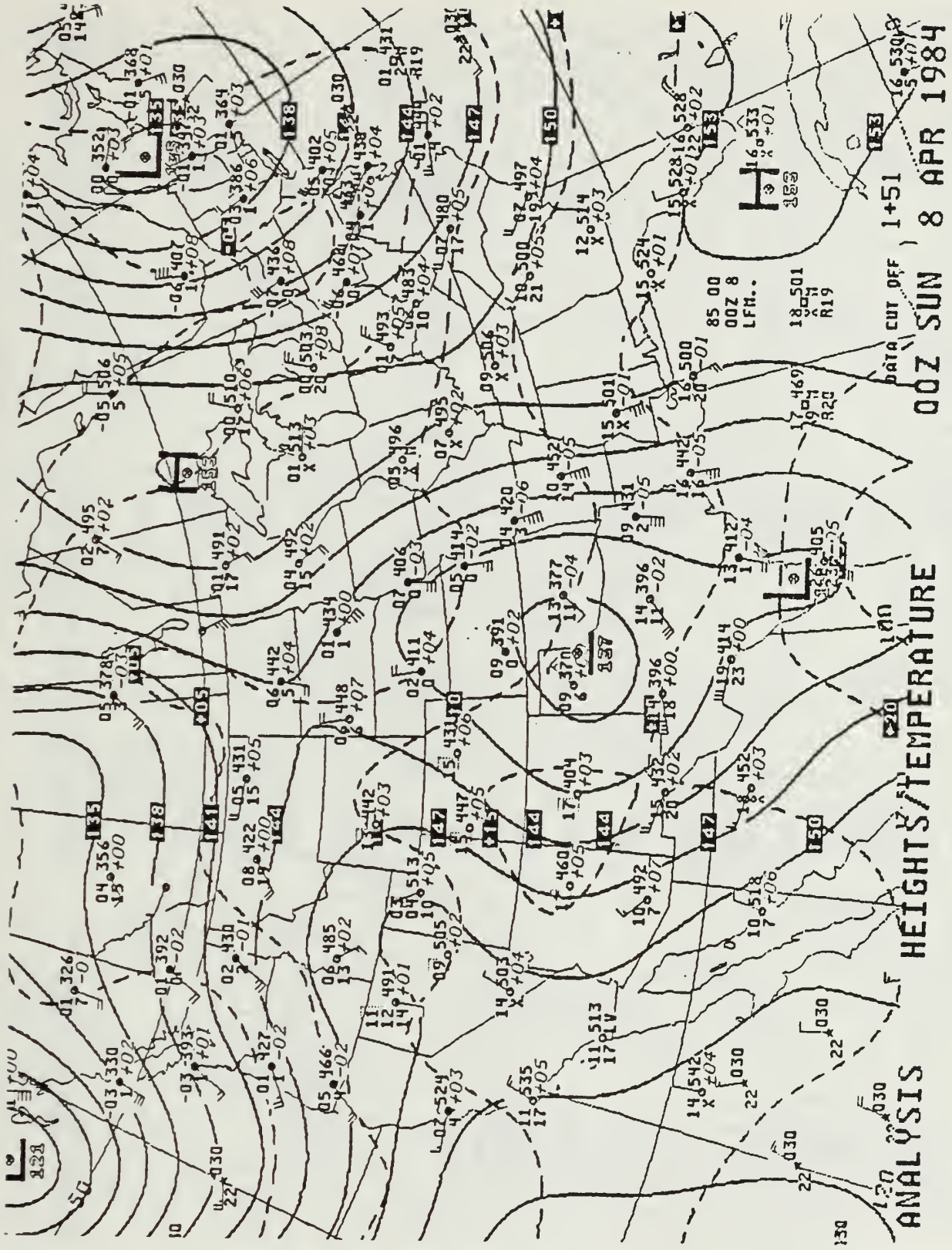

Fig. 38. NMC 850 mb Analysis with Heights/Temperature 0000 GMT 8 April 1984

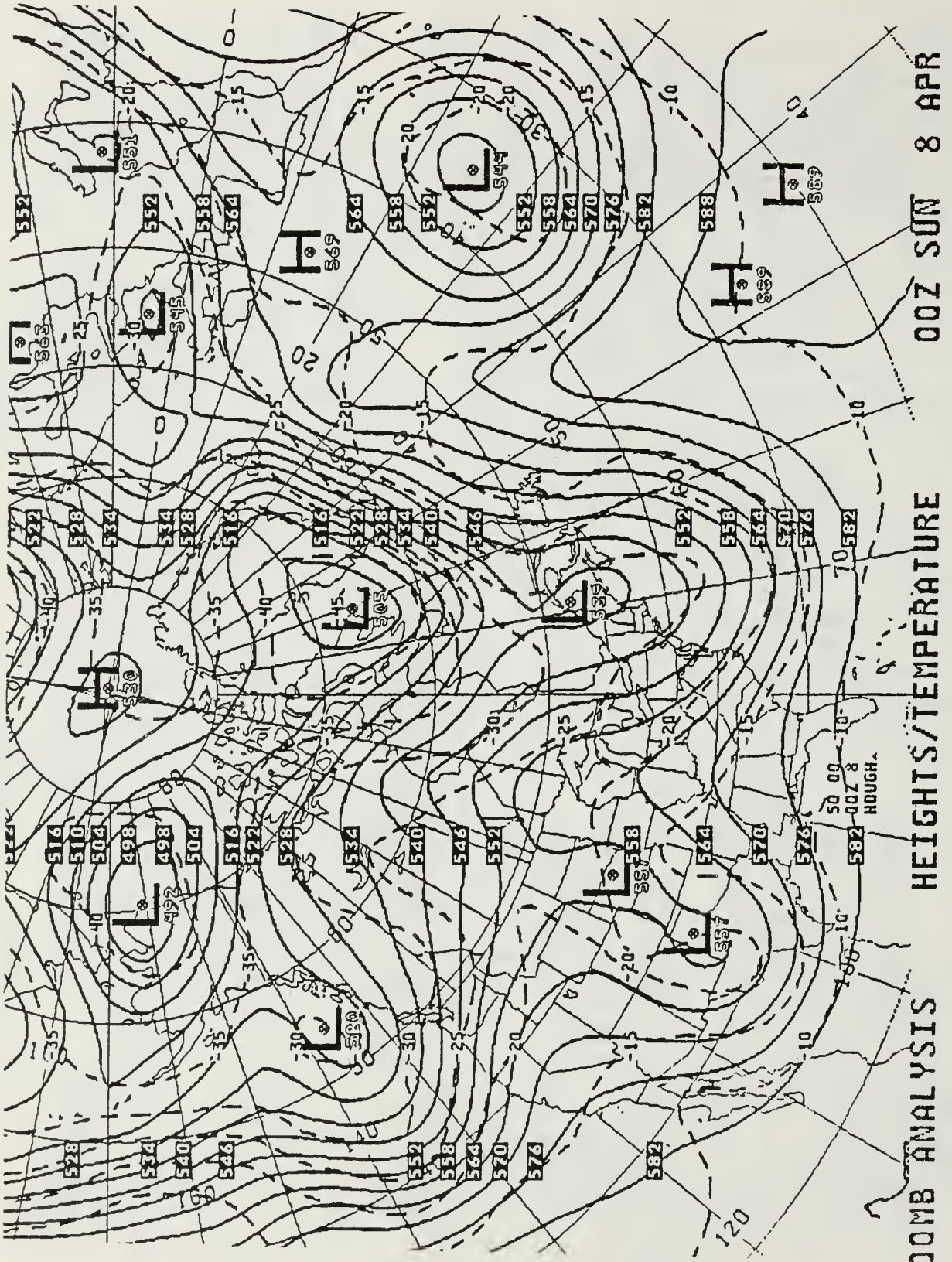

Fig. 39. NMC 500 mb Analysis with Heights/Temperature 0000 GMT 8 April 1984

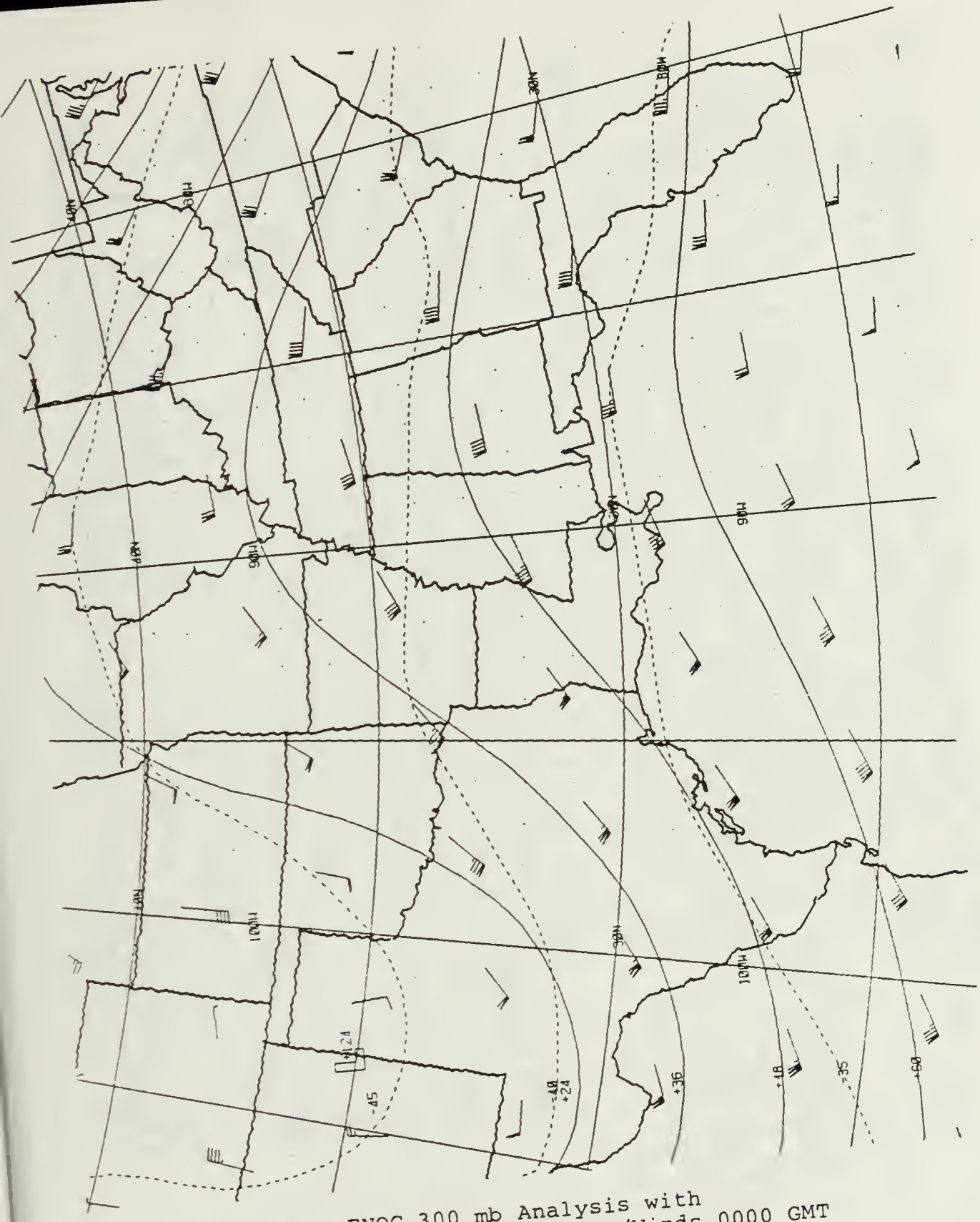

Fig. 40. FNOC 300 mb Analysis with Heights/Tmeperature/Winds 0000 GMT 8 APRIL 1984

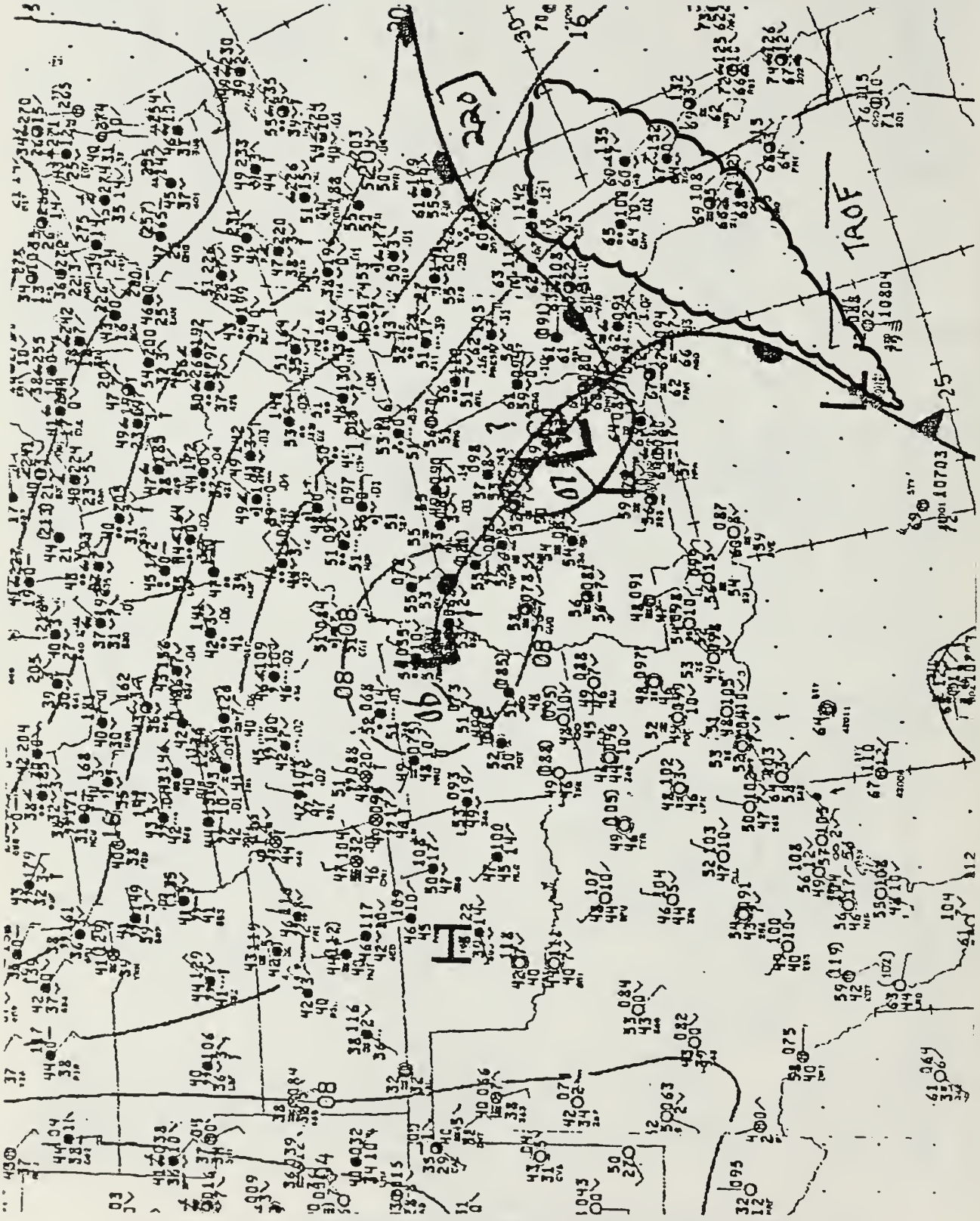

Fig. 41. NMC Surface Analysis, 1200 GMT 9 April 1984

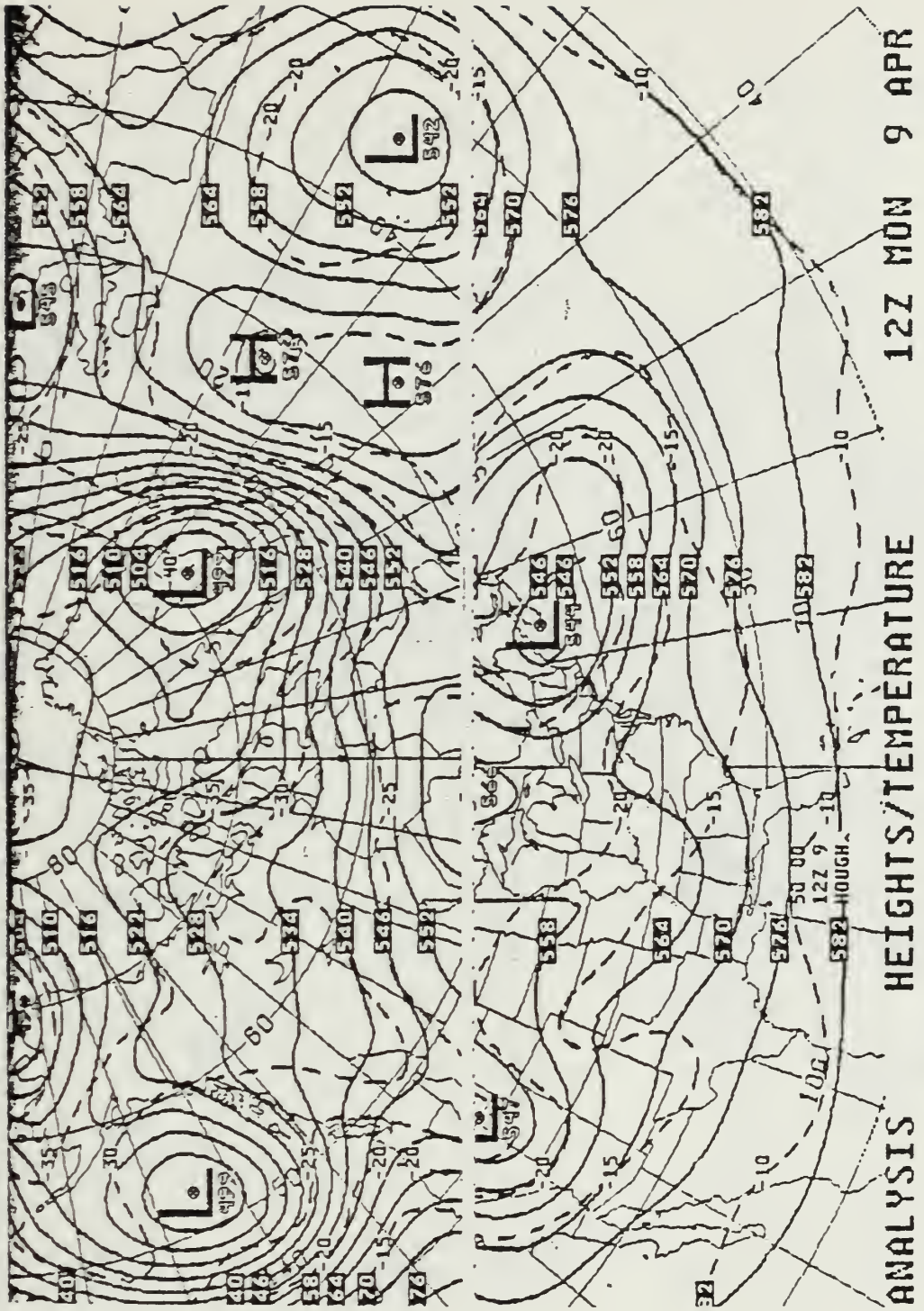

Fig. 42. NMC 500 mb Analysis with Heights/Temperature 1200 GMT 9 April 1984

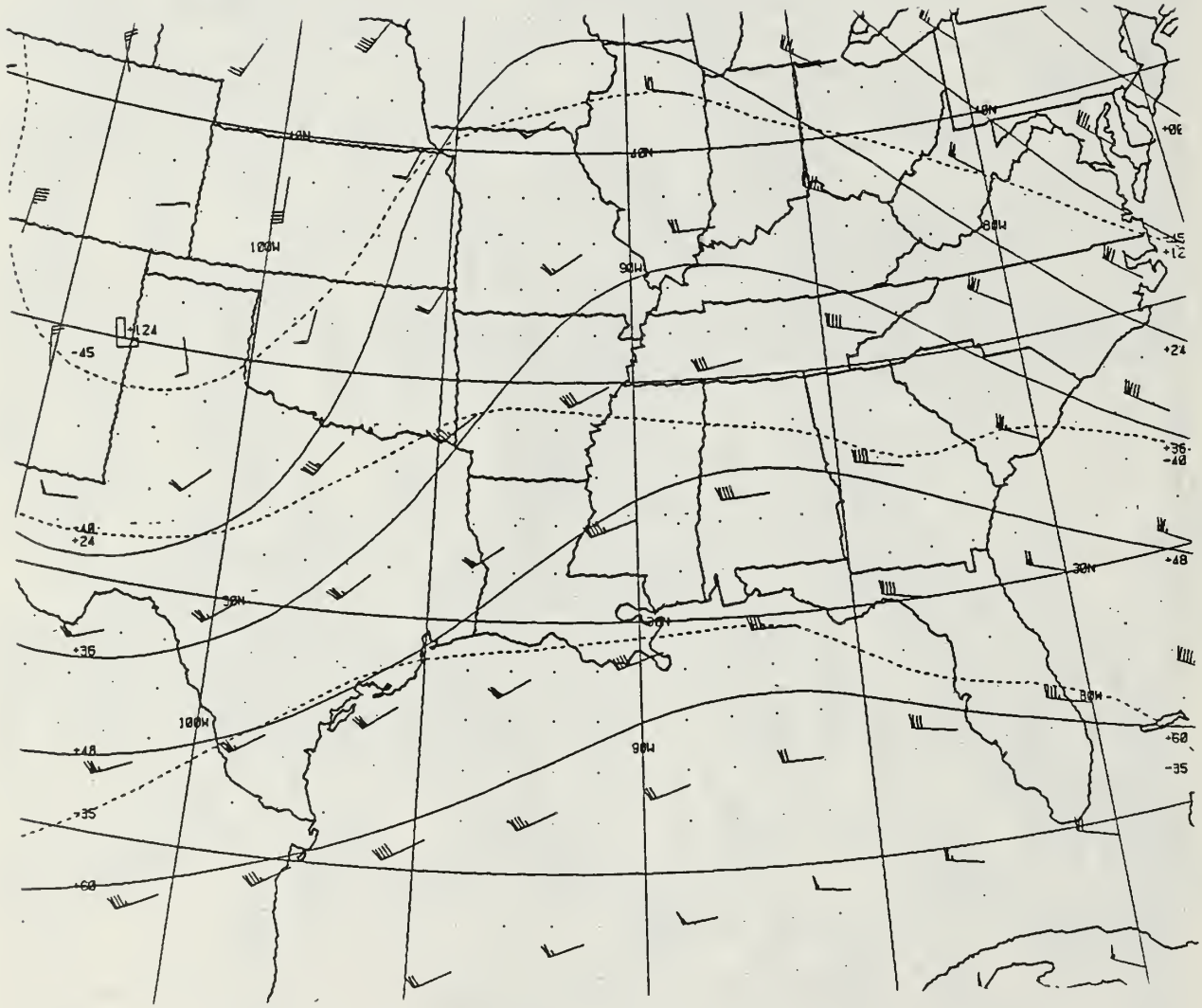

Fig. 43. FNOC 300 mb Analysis with Heights/Winds
1200 GMT 9 April 1984

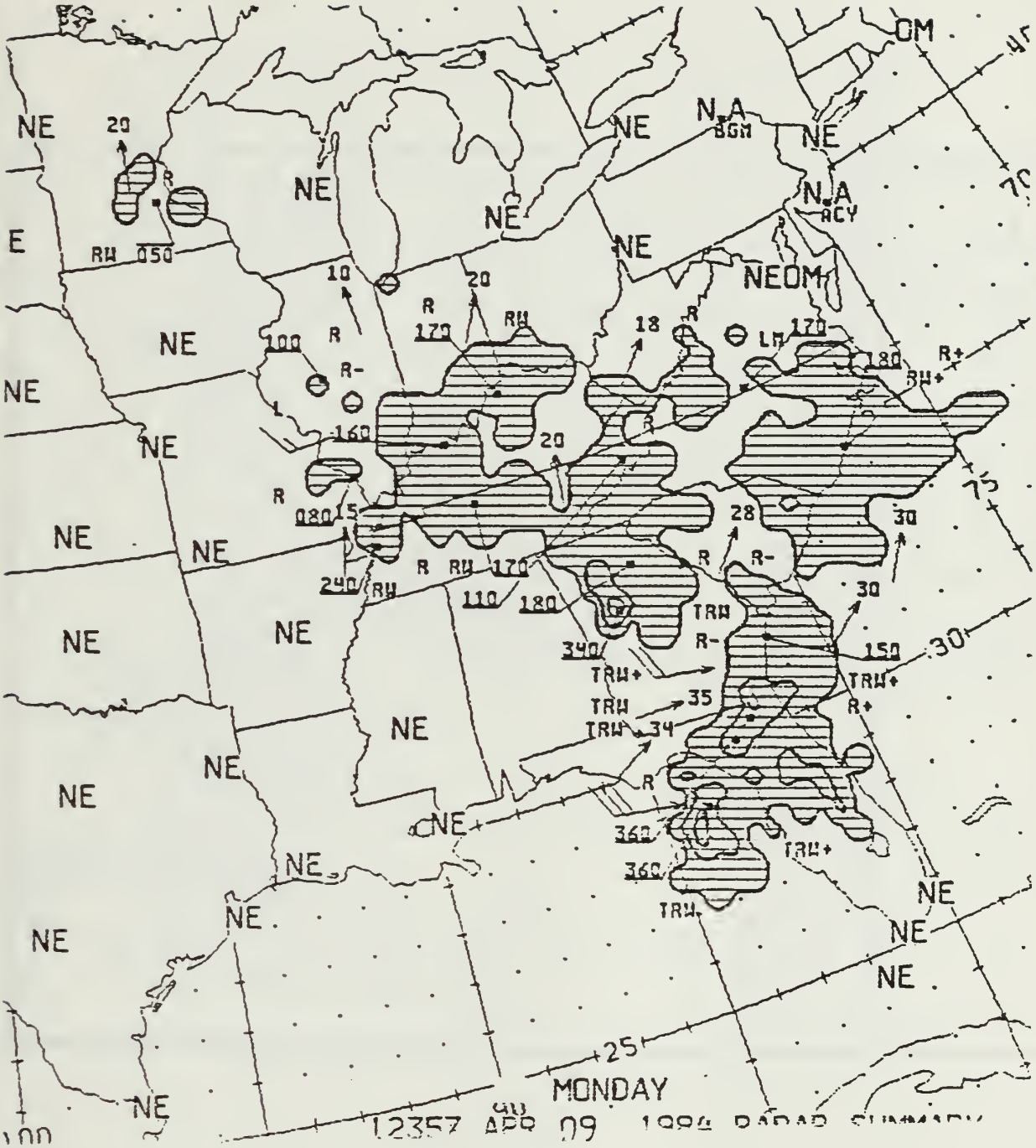

Fig. 44. NMC Radar Summary for 1200 GMT 9 April 1984

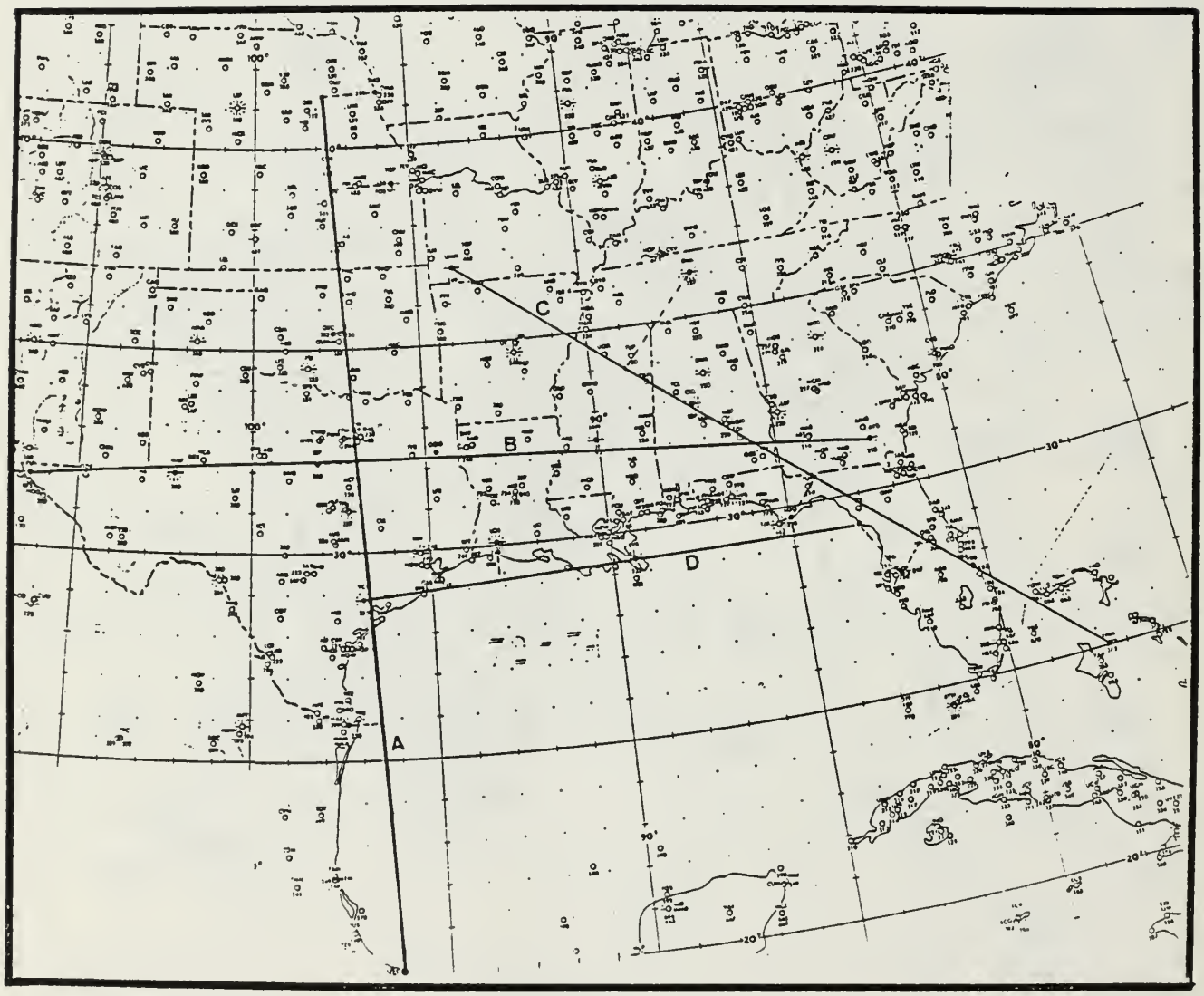

Fig. 45. Plot of sounding cross-sections over the southern U.S.

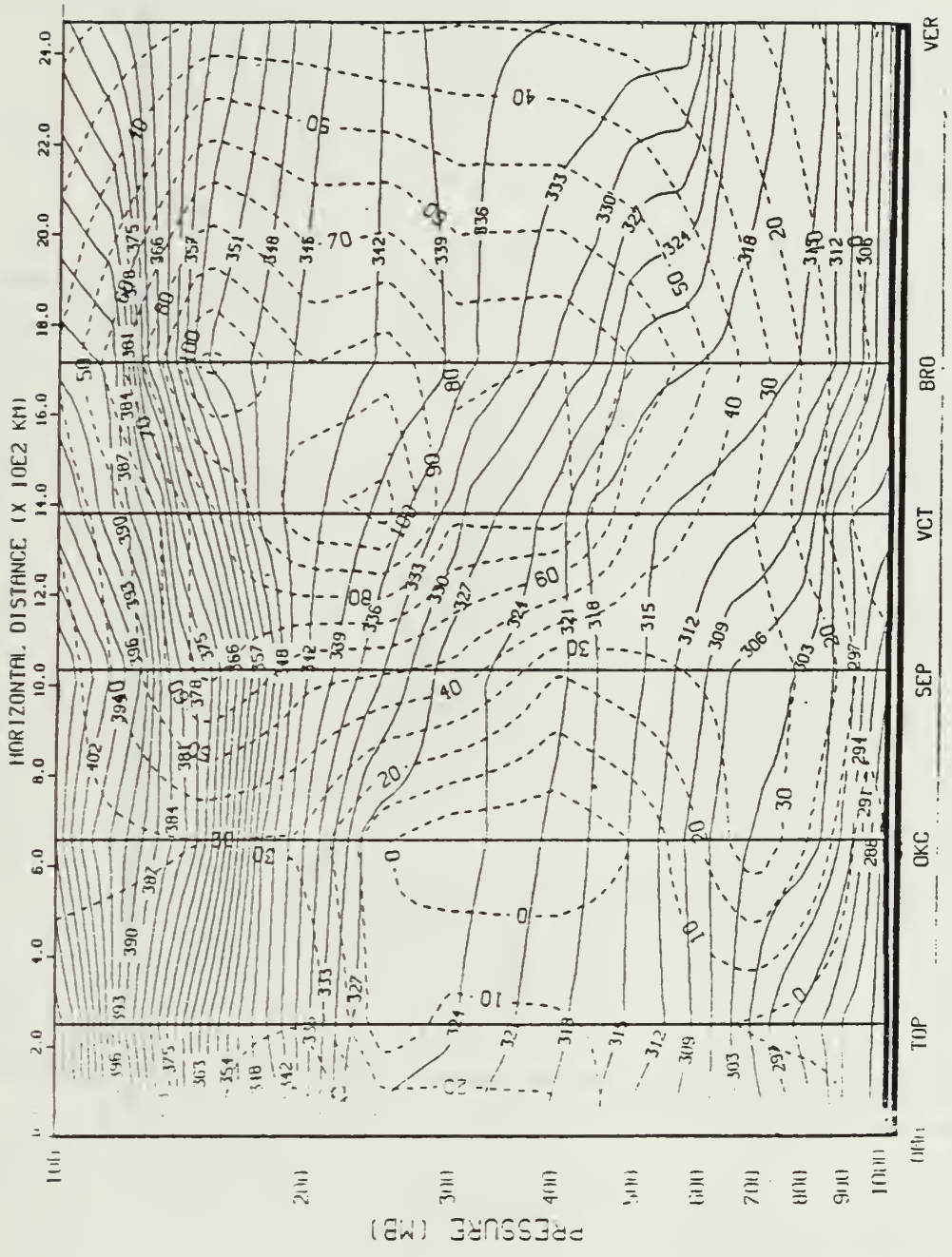

Fig. 46. North-South cross-section of isentropes/isotachs 0000 GMT 8 April 1984 for Omaha, NE (OMA) to Vera Cruz, Mexico (VER)

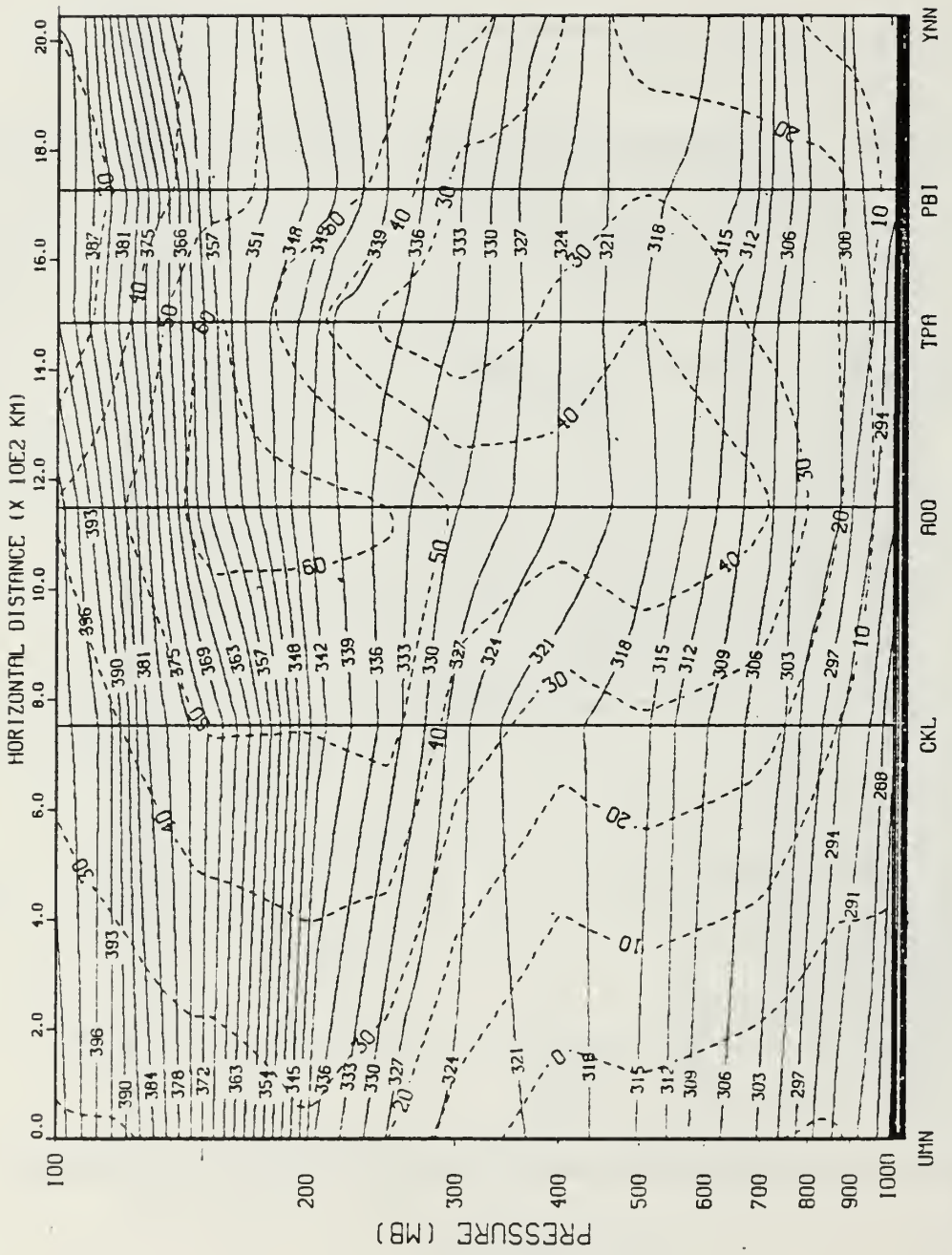

Fig. 47. North-south cross-section of isentropes/isotachs 1200 GMT 9 April 1984 for Monet, MO (UMN) to Bahamas (YNN)

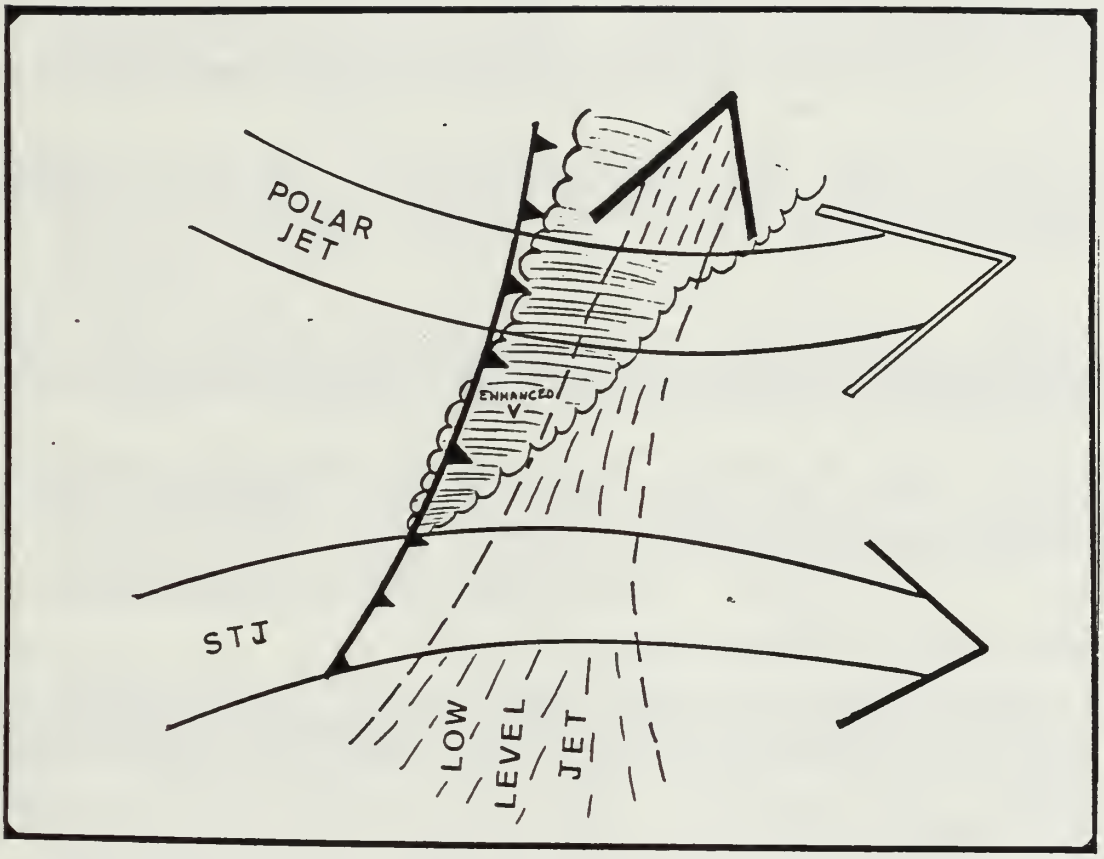

Fig. 48. Examples of the boundaries that define the enhanced-V

LIST OF REFERENCES

Anthes, R.S., 1983: Scientific and Technological Bases and Main Objectives, The National STORM Program. Univ. Corp. for Atmos. Res., Boulder, CO, 477 pp.

Bjerknes, J., 1951: Detailed Analysis of Synoptic Weather as observed from photographs taken on the Rocket Flights over White Sands New Mexico, July 26, 1948. Report No. P-887, The Rand Corp. 36 pp.

Bonner, W.D, 1968: Climatology of the low-level jet, Mon. Wea. Rev., **96**, 833-850.

Brandli, H.W., 1976: Satellite Meteorology. AWS-TR-76-264, Hq. Air Wea. Svc., Scott AFB, IL, 188 pp.

Clark, J.D., 1983: The GOES User's Guide. National Oceanic and Atmospheric Administration, Washington, D.C., 156 pp.

Courtois, M., and G. Weill, 1985: The SPOT satellite system. Monitoring Monitoring Earth's Ocean, Land, and Atmosphere from Space - Sensors, Systems, and Applications, AIAA, New York, NY, 493-523.

Cox, S.K., D.S. Mc Dougal, D.A. Randall, and R.A. Schiffer, 1987: FIRE - The first ISCCP regional experiment. Bull. Amer. Meteor. Soc., **68** 114-118.

Crowson, D.L., 1949: Cloud Observations from Rockets. Bull. Amer. Meteor. Soc., **30**, 17-22.

Fett, R.W., and W.A. Bohan, 1979: Navy Tactical Applications Guide, Vol. 2: Environmental Phenomena and Effects. NAVENVPREDRSCHFAC Applications Report 77-04. Naval Environmental Prediction Research Facility, Monterey, CA, 191 pp.

Fett, R.W., and W.A Bohan, 1986: Navy Tactical Applications Guide, Vol. 6: Tropical Weather Analysis and Forecast Applications. NAVENVPREDRSCHFAC Technical Report 86-02. Naval Environmental Predictiion Research Facility, Monterey, CA, 182 pp.

Fett, R.W., W.A. Bohan, J.J. Bates and S.L. Tipton, 1983: Navy Tactical Applications Guide - Operational Environmental Satellites. NAVENVPREDRSCHFAC Technical Report 83-02, Naval Environmental Prediction Research Facility, Monterey, CA, 70 pp.

Fett, R.W., and W.F. Mitchell, 1977: Navy Tactical Applications Guide, Vol. 1: Techniques and Applications of Image Analysis. NAVENVPREDRSCHFAC Applications Report 77-03. Naval Environmental Prediction Research Facility, Monterey, CA, 110 pp.

Fisher, M.G., 1986: Oceanographic Analysis of Sun Glint Images Taken on Space Shuttle Mission STS 41-G. M.S. Thesis, Naval Postgraduate Schl., Monterey, CA, 41 pp.

Gomberg, L., and S.M. McElroy, 1985: Remote sensing of the Earth with the Defense Meteorological Satellite. Monitoring Earth's Ocean, Land, and Atmosphere from Space - Sensors, Systems, and Applications, AIAA, New York, NY, 96-122.

Greaves, J.R. and W.E. Shenk, 1985: The Development of the geosynchronous weather satellite system. Monitoring Earth's Ocean, Land, and Atmosphere from Space-Sensors, Systems, and Applications, AIAA, New York, NY, 150-179.

Greenfield, S.M., 1956: Synoptic Weather Observations from Extreme Altitudes. The Rand Corporation, Paper P-761.

Homma, M., M. Minowa, M. Kobayaski and M. Harada, 1985: Geostationary Meteorological Satellite System in Japan. Monitoring Monitoring Earth's Ocean, Land, and Atmosphere from Space - Sensors, Systems, and Applications, AIAA, New York, NY, 570-588.

Honvault, C., 1985: The operational Meteosat program. Monitoring Earth's Ocean, Land, and Atmosphere from Space - Sensors, Systems, and Applications, AIAA, New York, NY, 483-492.

Johnson, D.S., and I.P. Vetlov, 1977: The Role of Satellites in WMO programmes in the 1980's. World Weather Watch - Report No. 36, World Meteor. Org., Geneva, Switzerland, 47 pp.

Kellogg, W.W., 1982: Early Satellite Program Developments. NASA Conference Publication 2257, NASA Washington, D.C., 101 pp.

Markley, D.R., 1986: Characteristics of Mesoscale Island Barrier Cloud Phenomena Observed in Satellite and Space Shuttle Imagery. M.S. Thesis, Naval Postgraduate Schl., Monterey, CA, 60 pp.

Maul, G.A., and M. McCaslin, 1977: An assessment of the potential contributions to oceanography from Skylab visual observations and hand-held camera photographs. Skylab Explores the Earth, NASA SP-380, eds. V.R. Wilmarth, J.L.Kaltenbach and W.B. Lenoir, NASA-Lyndon B. Johnson Space Center, Houston, TX, 517 pp.

McCann, D.W., 1981: The enhanced-V, a satellite observable severe storm signature. NOAA Tech. Memo NWS NSSFC-4, Nat. Wea. Svc., Wash., D.C., 31 pp.

McCann, D.W., 1983: The enhanced-V: a satellite observable severe storm signature. Mon. Wea. Rev., **111**, 887-894.

Meyer, W.D., 1985: The Defense Meteorological Satellite Program: A review of its impact. Monitoring Earth's Ocean, Land, and Atmosphere from Space - Sensors, Systems, and Applications, AIAA, New York, NY, 129-145.

NASA, 1966: Satellite Meteorology 1958-1964. NASA SP-96, National Aeronautics and Space Administration, Washington, D.C., 141 pp.

NASA, 1977: Skylab Explores the Earth. NASA SP-380, NASA Lyndon B. Johnson Space Center, Houston, TX, 517 pp.

NASA, 1982: Meteorological Satellites -- Past, Present, and Future, NASA Conference Publication 2227, AIAA 20th Aerospace Sciences Meeting, 11-14 January, Orlando, FL, 63 pp.

Nelson, R.M., 1986: Catalog of Space Shuttle Earth Observations Hand-Held Photography Space Transportaion System (STS) 5 Mission. JSC-20965, NASA-Lyndon B. Johnson Space Center, Houston, TX, 45 pp.

Newton, C.W., 1967: Severe convective storms. Advances in Geophysics, Vol. 12, Academic Press, 257-303.

Nowakowski, B.S., and W.F. Palmer, 1984: Catalog of Space Shuttle Earth Observations Hand-Held Photography Space Transportation System (STS) 41-C Mission. JSC-20056, NASA-Lyndon B. Johnson Space Center, Houston, TX, 46 pp.

Purdom, J.F., 1986: Satellite contributions to convective scale weather analysis and forecasting. Preprint-11th Conference Weather Forecast and Analysis, Amer. Meteor. Soc., Boston, MA, 295-313.

Reynolds, D.W., 1980: Observations of damaging hailstorms from geosynchronous satellite data. Mon. Wea. Rev., **108**, 337-348.

Rosenthal, J.S., and M. Lee, 1984: Tropical cyclone wakes across eastern North Pacific. Unpublished paper, Pacific Missile Test Center, White Sands, NM, 3 pp.

Schnapf, A., 1982: The development of the TIROS global environmental satellite system. Meteorological Satellites -Past, Present, and Future, NASA Conference Pub. 2227, NASA, Washington, D.C., 7-16.

Schnapf, A., 1985: The TIROS Meteorological Satellites--Twenty-five Years: 1960-1985. Monitoring Earth's Ocean, Land, and Atmosphere from Space - Sensors, Systems, and Applications, AIAA, New York, NY, 51-70.

Shapiro, M., 1983: Mesoscale weather in the United States-Review of regional phenomena. The National STORM Program, ed. R.A. Anthes, Univ. Corp. for Atmos. Res., Boulder, CO 477 pp.

Shenk, W.E. and R.J. Holub, 1971: An example of detailed cloud contouring from Apollo 6 photography. Bull. Amer. Meteor. Soc., **52**, 238.

Shenk, W.E., R.J. Holub and R.A. Neff, 1975: Stereographic cloud analysis from Apollo 6 photographs over a cold front. Bull. Amer. Meteor. Soc., **56**, 4-16.

Skaggs, R.H., 1967: On the association between tornadoes and 500 mb indicatiors of jet streams. Mon. Wea. Rev., **95**, 107-110.

Snow, J.W., and E.M. Tomlinson, 1987: Cloud population measurements using photographs taken from the Space Shuttle. Abstracts: Sixth Symposium Meteorological Observations and Instrumentation, Amer. Meteor. Soc., Boston, MA, 286-289.

Storm Data, 1984: Dept. of Commerce, NOAA EOIS/National Climactic Center, Ashville, NC, Vol. 22-No. 4, 21 pp.

Svetz, F.J., 1985: Use of Space Shuttle Photography in the Study of Meteorological Phenomena. M.S. Thesis, Naval Postgraduate Schl., Monterey, CA, 105 pp.

Uccellini, L.W., and D.R. Johnson, 1979: The coupling of upper and lower tropospheric jet streaks and implications for the development of severe convective storms. Mon. Wea. Rev., **107**, 682-703.

Vaeth, G.J., 1965: Weather Eyes in the Sky, America's Meteorological Satellites. New York, The Ronald Press Co., 124 pp.

Weber, E.M., and S. Wilderotter, 1981: Satellite interpretation. 3WW-TN-81-001 Technical Note, Third Wea. Wing, Offatt, NE, 95 pp.

Wexler, H., 1954: Observing the weather from a satellite vehicle. British Interplanetary Society, **13**, 280 pp.

Whitehead, V.S., I.D. Browne and J.G. Garcia, 1969: Cloud height contouring from Apollo 6 photography. Bull. Amer. Meteor. Soc., **50**, 522-528.

Whitney, L.F., 1986: Relationship of the subtropical jet stream to severe local storms. Satellite Imagery Interpretation for Forecasters - NAVEDTRA 40960, Naval Oceanography Command Facility, Bay St. Louis, MS, 612 pp.

World Meteorological Organization, 1975: Information on Meteorological Satellite Programmes Operated by Members and Organizations. World Weather Watch - Report No. 411, World Meteor. Org., Geneva, Switzerland, 86 pp.

INITIAL DISTRIBUTION LIST

		No. Copies
1.	Defense Technical Information Center Cameron Station Alexandria, VA 22304-6145	2
2.	Library, Code 0142 Naval Postgraduate School Monterey, CA 93943-5002	2
3.	Chairman (Code 63Rd) Department of Meteorology Naval Postgraduate School Monterey, CA 93943-5004	1
4.	Chairman (Code 68Tm) Department of Oceanography Naval Postgraduate School Monterey, CA 93943-5004	1
5.	Professor C. H. Wash (Code 63Wx) Department of Meteorology Naval Postgraduate School Monterey, CA 93943-5004	7
6.	Professor P. A. Durkee (Code 63De) Department of Meteorology Naval Postgraduate School Monterey, CA 93943-5004	1
7.	LT Randy J. Scanlon FLTASWTRACENLANT Norfolk Naval Base Norfolk, VA 23511	2
8.	Director Naval Oceanography Division Naval Observatory 34th and Massachusetts Avenue NW Washington, DC 20390	1
9.	Commander Naval Oceanography Command NSTL Station Bay St. Louis, MS 39522	1
10.	Commanding Officer Naval Oceanographic Office NSTL Station Bay St. Louis, MS 39522	1

11. Commanding Officer 1
Fleet Numerical Oceanography Center
Monterey, CA 93943

12. Commanding Officer 1
Naval Ocean Research and Development Activity
NSTL Station
Bay St. Louis, MS 39522

13. Commanding Officer 1
Naval Environmental Prediction Facility
Monterey, CA 93943

14. Chairman, Oceanography Department 1
U.S. Naval Academy
Annapolis, MD 21402

15. Chief of Naval Research 1
800 N. Quincy Street
Arlington, VA 22217

16. Office of Naval Research (Code 420) 1
Naval Ocean Research and Development Activity
800 N. Quincy Street
Arlington, VA 22217

17. Scientific Liason Office 1
Office of Naval Research
Scripps Institution of Oceanography
La Jolla, CA 92037

18. Commanding Officer 1
Naval Eastern Oceanography Center
Naval Air Station
Norfolk, VA 23511

19. Mr. Robert Fett 1
Naval Environmental Prediction Research Facility
Monterey, CA 93943

20. Air Weather Service Technical Library 1
Scott AFB, IL 62225-5000

21. Mr. and Mrs. James F. Scanlon 1
1040 Tobey Court
Schaumburg, IL 60193

18767

SCHOOL
A 93943-5002

Thesis
S24245 Scanlon
c.1 Mesoscale applications
of high resolution ima-
gery.

thesS24245
Mesoscale applications of high resolutio
3 2768 000 75399 0
DUDLEY KNOX LIBRARY